A geochemical profile through the Uitkomst Complex on the farm Slaaihoek, with special reference to the platinum-group elements and Sm-Nd isotopes

by

TAFADZWA EUPHRASIA SHARON GOMWE

Submitted in partial fulfillment of the requirements for the degree
MASTER OF SCIENCE
In the Faculty of Natural & Agricultural Science
University of Pretoria
Pretoria

Supervisor: Prof. W. D. Maier

February 2002

TABLE OF CONTENTS

ABSTRACT

The Uitkomst Complex is a mineralized, layered basic to ultrabasic intrusion, hosted by sedimentary rocks of the lower part of the Transvaal Supergroup. It is situated on the farms Uitkomst 541JT and Slaaihoek 540JT, about 25 km north of Badplass and 50 km east of the eastern limb of the Bushveld Complex in the Mpumalanga province of South Africa. The intrusion plunges between 8 to 10° to the northwest with an established length of 12 km and a total thickness of 850 m. It is divided into seven lithological Units (from base to top), the Basal Gabbro (BGAB), Lower Harzburgite (LHZBG), Chromitiferous Harzburgite (PCR), Main Harzburgite (MHZBG), Pyroxenite (PXT), Gabbronorite (GN) and Upper Gabbro units (UGAB).

A detailed petrographic and geochemical investigation of borehole core SH176, which provided a complete intersection of the Uitkomst Complex was carried out. The study shows that the Complex may have crystallized in a dynamic magma conduit setting. The whole rock geochemical trends indicate that there is a reversed fractionation in the basal portion of the Complex and a lack of fractionation in much of the MHZBG. Trace and REE variations show a decrease in concentration with height, contrary to what is expected of a progressively differentiating magma in a close system. Further, the platinum-group element concentration of the four basal units show no depletion with increasing height, suggesting that the individual units are not related to each other by means of *in situ* fractionation. Instead, a model whereby the individual units crystallized from distinct pulses of magma best explains the data.

By comparing Nd isotopes and ratios of highly incompatible trace elements like $[Th/La]_n$ and $[Sm/Ta]_n$ from the Uitkomst Complex and Bushveld Complex it is seen that the Uitkomst magmas are of a similar lineage as the B1 magma of the Bushveld Complex, supporting a genetic link between the two complexes. The upper portion of the Uitkomst Complex shows values more akin to B3 magmas indicating the possible presence of more than one type of magma.

Based on the available S isotope and trace element data, the sulphides of the Complex appear to have formed within the Complex, probably in response to contamination of the magma with dolomite. Entrainment of sulphides from depth is considered unlikely. The relatively low Cu/Ni ratios of the sulphides in the LHZBG, PCR and MHZBG (Cu/Ni 0.03 to 0.8) may be modeled by sulphide segregation from B1 magma and not from fractionation of sulphides that were later entrained in the streaming magma.

OPSOMMING

Die Uitkomstkompleks is 'n gemineraliseerde, gelaagde basiese tot ultrabasiese liggaam wat intrusief is in die sedimentêre gesteentes van die onderste deel van die Transvaal Supergroep. Dit is geleë op die plase Uitkomst 541JT en Slaaihoek 540JT, sowat 25km noord van Badplaas en 50km oos van die oostelike lob van die Bosveldkompleks in die Mpumalanga provinsie van Suid-Afrika. Die intrusie duik tussen 8 en 10° na die noordweste en het 'n bekende lengte van 12km en 'n dikte van 850m. Dit word onderverdeel in sewe litologiese eenhede (van onder na bo), die Basale Gabbro (BGAB), Laer Harzburgiet (LHZBG), Chroomryke Harzburgiet (PCR), Hoof Harzburgiet (MHZBG), Pirokseniet (PXT), Gabbronoriet (GN) en Boonste Gabbro (UGAB).

'n Gedetaileerde petrografiese en geochemiese ondersoek van gesteentekern uit boorgat SH176, wat 'n volledige interseksie van die Uitkomstkompleks verteenwoordig, toon aan dat die Kompleks moontlik gekristalliseer het in 'n dinamiese magmatoevoerkanaal. Daar is omgekeerde fraksionering in die basale deel van die Kompleks en 'n afwesigheid van fraksionering in die MHZBG. Die konsentrasie van platinumgroepelemente in die basale vier eenhede toon geen verarming met toenemende hoogte wat aandui dat die individuele eenhede nie aan mekaar verwant is deur *in situ* fraksionering nie. Die data word egter beste verduidelik deur 'n model waarin die individuele eenhede gekristalliseer het vanuit aparte magmapulse.

Deur vergelyking van Nd isotope en verhoudings van onversoenbare spoorelemente soos $[Th/La]_n$ en $[Sm/Ta]_n$ in die Uitkomstkompleks en die Bosveldkompleks kan daar gesien word dat die Uitkomstmagmas dieselfde oorsprong het as die B1 magma van die

Bosveldkompleks, dit ondersteun 'n genetiese verwantskap tussen die twee komplekse. Die boonste deelvan die Uitkomstkompleks toon waardes meer verwant aan die B3 magmas en dui op die moontlike teenwoordigheid van meer as een tipe magma.

Beskikbare S isotoop en spoorelement data dui daarop dat die sulfiedes van die Kompleks binne in die Kompleks gevorm het, waarskynlik as gevolg van kontaminasie van die magma met dolomiet. Vervoer van sulfiedes vanuit diepte word as onwaarskynlik beskou. Die relatiewe lae Cu/Ni verhoudings (0.03 tot 0.8) van die sulfiedes in die LHXBG, PCR en MHZBG dui daarop dat die sulfiedes fraksionering van monosulfied vaste oplossing ondergaan het gevolg deur fisiese skeiding van monosulfied vaste oplossing en gefraksioneerde sulfiedsmelt, met die laasgenoemde opgeneem deur magma wat deur die Kompleks gevloei het.

1. INTRODUCTION

1.1. Objectives of the study

A number of previous workers have suggested that the Uitkomst Complex formed in a dynamic magma conduit setting (Gauert *et al.*, 1995; Maier *et al.*, 1998). This suggestion was based largely on the tubular shape of the Complex, the lack of fractionation trends in the central harzburgitic portion of the Complex and the relatively large mass ratio of sulphides to silicates. Most recently, it has been established that the Uitkomst and Bushveld complexes are coeval and of a common magmatic lineage (De Waal *et al.*, 2001). The present work aims to test and constrain these hypotheses by means of a detailed petrographic and geochemical investigation of borehole SH176 that provides a complete intersection of the Complex. Previous studies either focused on selected portions of the Complex or compiled a composite intersection through the Complex based on a lithological correlation of several short boreholes along the plunge of the body (Gauert, 1998). The new trace element and isotope data will also significantly expand the existing database. The following points will be used as guidelines to constrain the formation of the Complex:

(a) The composition of olivines and the distribution of the platinum-group elements (PGE) can be used to determine whether the Complex crystallized from successive surges of magma flowing through a dynamic conduit or whether it represents a closed system. In the case of a dynamic conduit setting, successive lithological units may have undepleted Ni-PGE signatures. In the case of a closed system there should be a trend of progressive Ni-PGE depletion with height.

(b) Ratios of highly incompatible trace elements (for example: Th, Hf, REE, Nb, Ta, Zr and Y) and Sm/Nd isotopes may be used to determine whether the various lithological units of the Complex crystallized from magmas of different lineage as might be expected in a dynamic conduit system (e.g. Noril'sk and Voisey's Bay). These ratios will further be used to constrain whether any of the units has a similar lineage to the parental magmas of the Bushveld Complex.

(c) Comparison of the trace element and isotope characteristics of the sulphide

bearing samples with those of the country rocks can hopefully be used to determine if the sulphides segregated *in situ* due to localised contamination, or whether sulphide segregation occurred at depth, followed by entrainment of the sulphides and deposition in the Complex.

1.2. Regional geological setting

The Uitkomst Complex is a layered ultrabasic to basic intrusion with a $^{207}Pb/^{206}Pb$ zircon minimum estimate age of 2044 (+/-8) Ma (De Waal *et al.*, 2001). The Complex is situated in the Mpumalanga Province, about 25 km north of Badplaas (Fig. 1.1.) and about 50 km to the east of the eastern limb of the Bushveld Complex. The Uitkomst Complex concordantly intruded sedimentary rocks of the lower Transvaal Supergroup, with the Oaktree member forming its floor and the Lower Timeball Hill shale its roof (Fig. 1.2.(a)). Gauert *et al.* (1995) estimated that the Complex intruded the Transvaal Supergroup some 10 km below the level of the Bushveld Complex.

The Uitkomst Complex forms an elongate, tubular body with a relatively consistent lateral cross profile. The body forms three distinct troughs, a Deeper, Central and Upper Trough (Fig. 1.2.(b)). Near the base and the top there are significant sill-like lateral extensions of the intrusion (Von Scheibler *et al.*, 1995). Generally, the shape of the body is governed by the nature of the country rock in that the quartz-rich and dolomitic lithologies appear to be more resistant to thermal-chemical-mechanical erosion by the intruding magma than the shales. Some areas of the Complex are underlain by a "basal" shear zone that has been described as a pre-intrusive thrust zone in the country rocks extending laterally beyond the margins of the Complex (Gauert, 1998; Hornsey, 1999). Striations on the shear planes indicate a northwest-southeast movement (Gauert, 1998).

The total thickness of the Complex is about 860 m, but some 110 m of this consist of post-intrusive diabase sills. The intrusion plunges at an angle of about 8° to 10° to the northwest and is at least 12km long as established by boreholes on the farm Little Mamre (Fig. 1.1.) (De Waal and Gauert, 1997). To the southeast, the Complex is eroded and is overlain by a relatively thin gossaniferous cover of intrusive rocks (Gauert *et al.*, 1995).

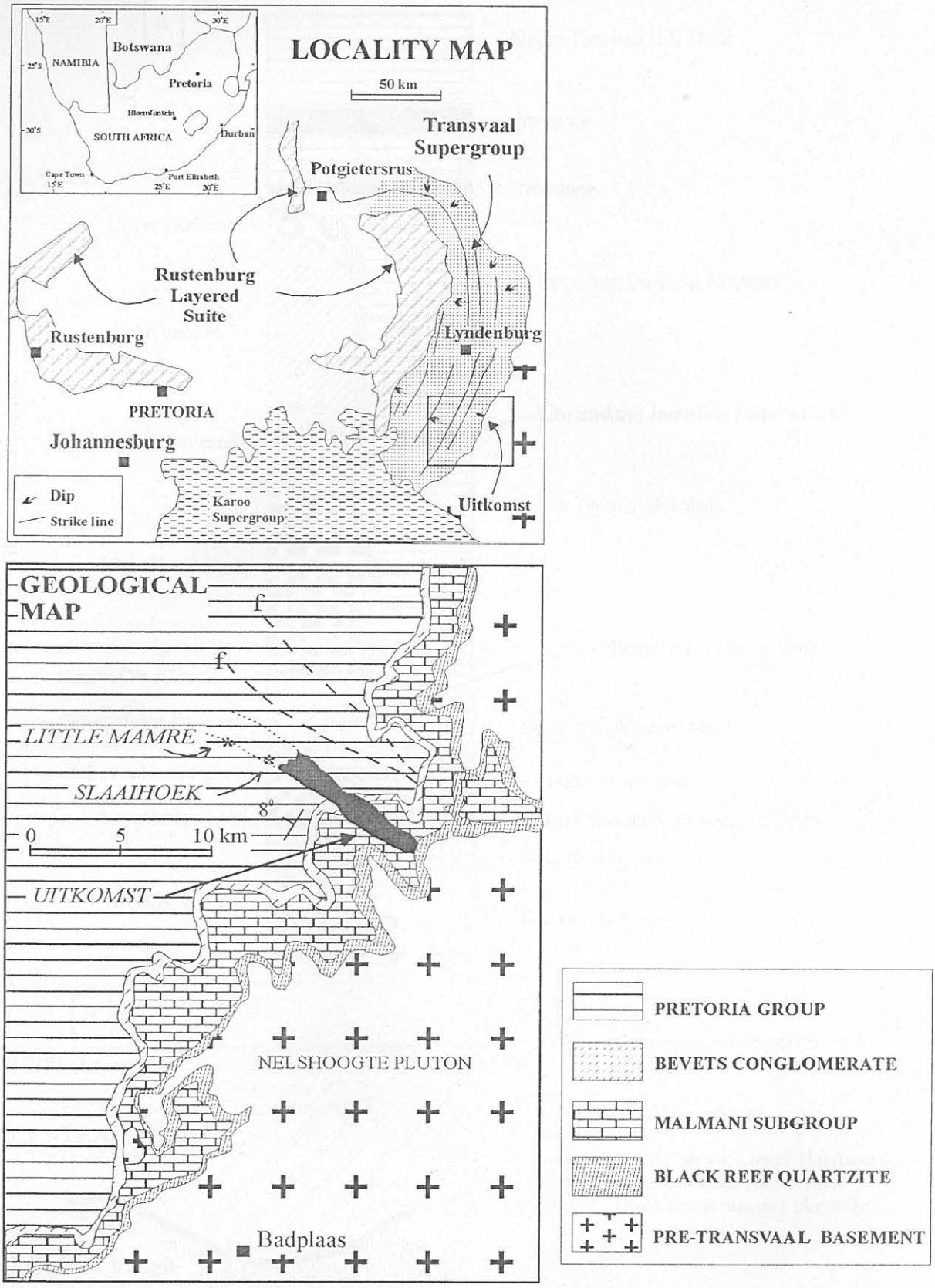

Fig 1.1. Locality and simplified geological map of the Uitkomst Complex (modified after Gauert (1997)).

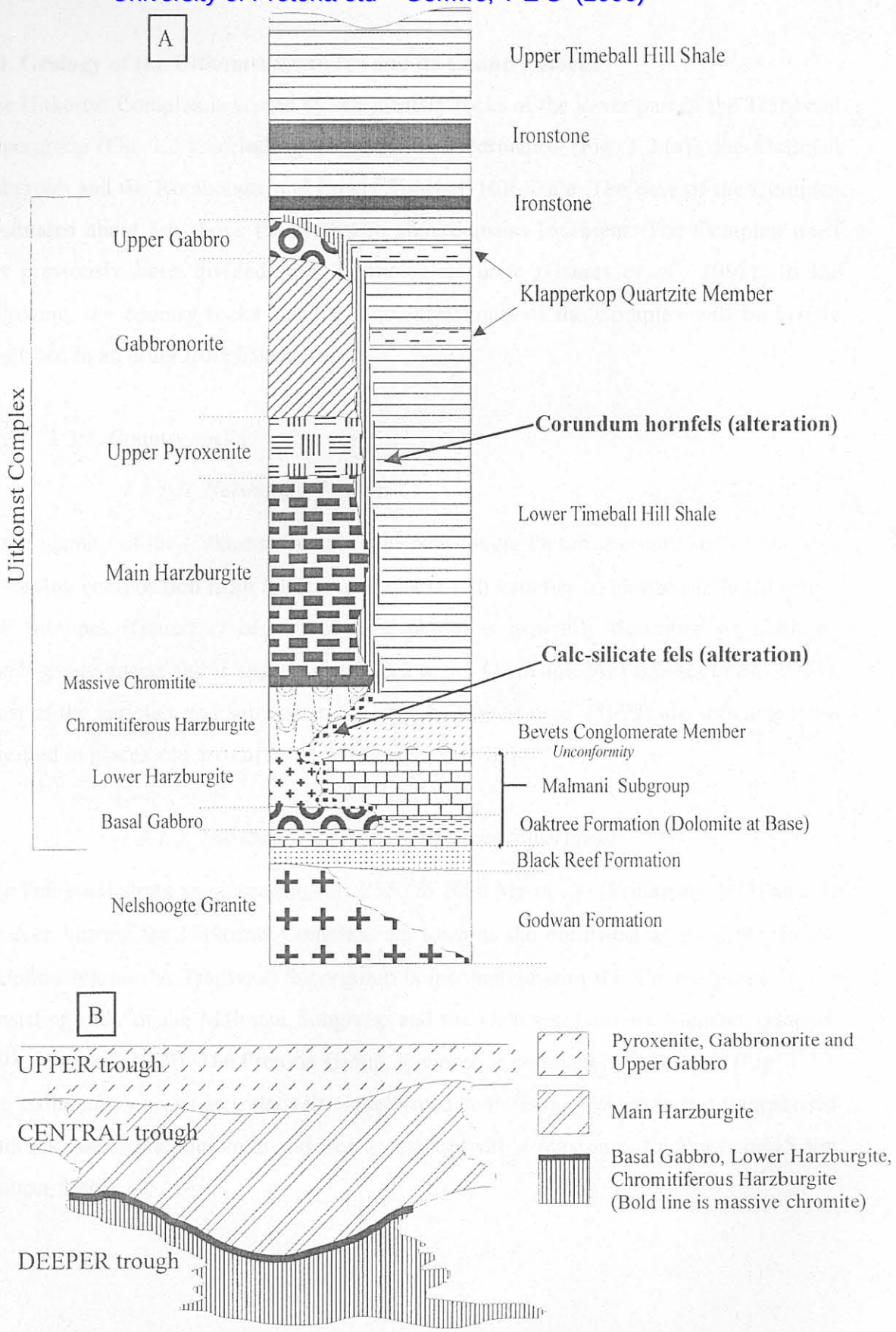

Fig.1.2. **A.** Schematic profile and contact relations of the Uitkomst Complex (after Hornsey, 1999; Gauert, 1998).
B. Cross section from Slaaihoek-Little Mamre boundary illustrating the trough-like nature of the Complex (from De Waal and Gauert, 1997).

1.3. Geology of the Uitkomst Complex and its Country Rocks

The Uitkomst Complex is hosted by sedimentary rocks of the lower part of the Transvaal Supergroup (Fig. 1.3.), including the Black Reef Formation (Fig. 1.2.(a)), the Malmani Subgroup and the Rooihoogte and Lower Timeball Hill Shale. The base of the Complex is situated about 5m above the Archaean granite-gneiss basement. The Complex itself has previously been divided into 7 lithological units (Gauert *et al.*, 1995). In the following, the country rocks and the lithological units of the Complex will be briefly described in an order from base to top.

1.3.1. Country rocks

1.3.1.1. Nelshoogte Pluton

In the vicinity of the Uitkomst Complex the Nelshoogte Pluton is comprised of gneisses of varying composition from feldspar and quartz-rich varieties to biotite and hornblende-rich subtypes (Gauert *et al.*, 1995). The pluton is generally described as a biotite trondhjemite gneiss and is approximately 3.2 to 3.5 Ga in age (Anhaeusser *et al.*, 1981). Most of the varieties and subtypes mentioned by Gauert *et al.* (1995) are sericitised and silicified in places and are cut by quartz and chlorite veins.

1.3.1.2. The lower part of the Transvaal Supergroup

The Transvaal strata are approximately 2550 to 2080 Ma in age (Eriksson, 1993) and, in the area hosting the Uitkomst Complex, dip towards the northwest at about 8°. In the Badplaas region the Transvaal Supergroup is incomplete with the Chuniespoort Group consisting only of the Malmani Subgroup and the Oaktree Quartzite Member (Gauert, 1998; Hornsey, 1999). The Pretoria Group, however, is completely developed (Fig. 1.3.). The sedimentary rocks are relatively undeformed comprising low-grade metamorphosed mudrock, sandstone, dolomite and iron formation with a maximum thickness of 15 km (Button, 1986).

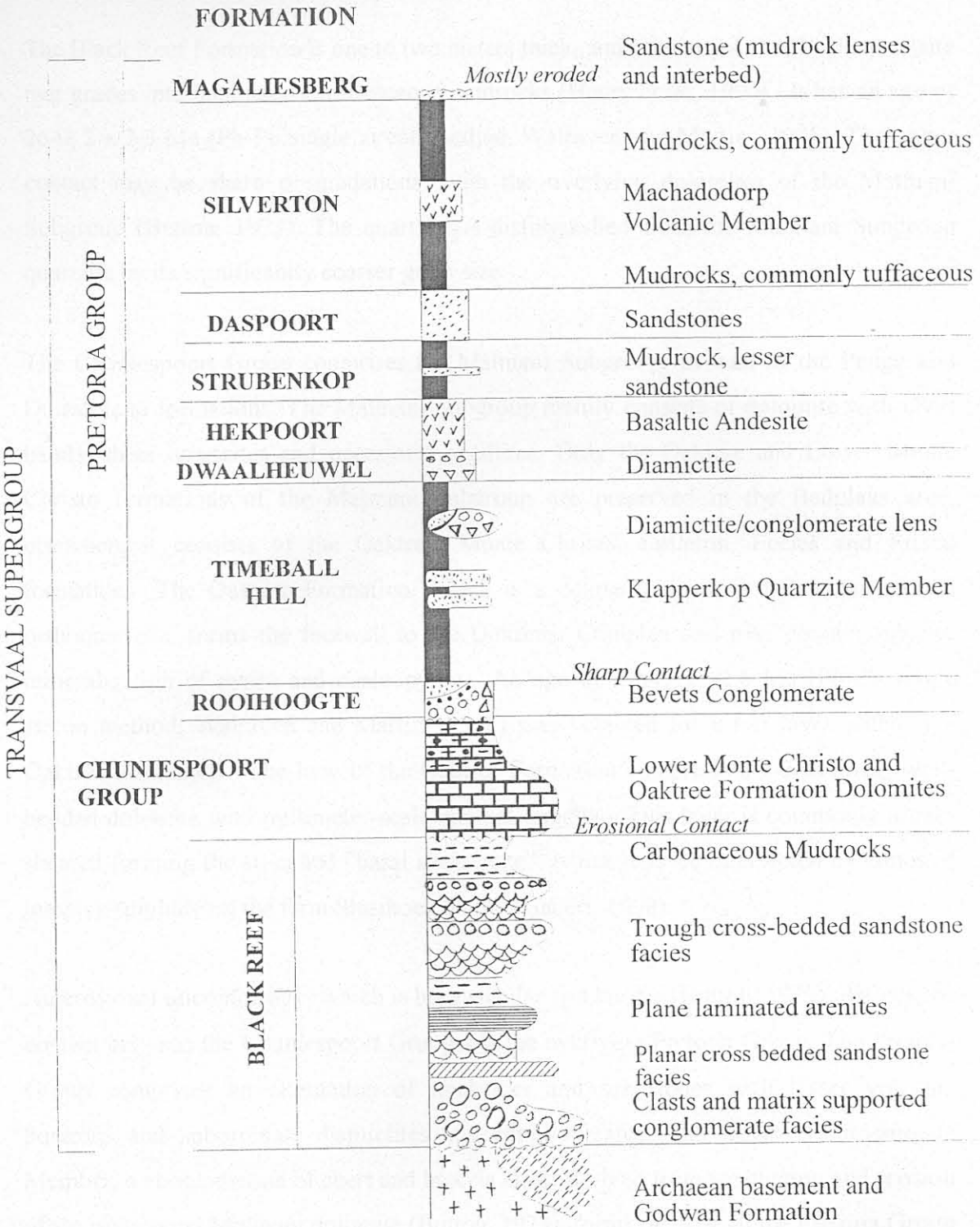

Fig.1.3. Simplified lithostratigraphy of the Eastern Transvaal basin. Vertical scale not proportional. Modified after Eriksson *et al.*, (1993).

The Black Reef Formation is one to two meters thick, and consists of an arkosic quartzite that grades into laminated carbonaceous mudrocks (Henry *et al.*, 1990). It has an age of 2642.2 ± 2.3 Ma (Pb-Pb single zircon method, Walraven and Martini, 1995). The upper contact may be sharp or gradational with the overlying dolomites of the Malmani Subgroup (Button, 1973). The quartzite is distinguished from the Malmani Subgroup quartzite by its significantly coarser grain size.

The Chuniespoort Group comprises the Malmani Subgroup, as well as the Penge and Duitschland formations. The Malmani Subgroup mainly consists of dolomite with chert bands, sheet quartzites and occasional argillites. Only the Oaktree and Lower Monte Christo formations of the Malmani Subgroup are preserved in the Badplaas area, elsewhere it consists of the Oaktree, Monte Christo, Littleton, Eccles and Frisco formations. The Oaktree Formation, which is a coarse grained, trough cross-bedded orthoquartzite, forms the footwall to the Uitkomst Complex and may contain stringer mineralization of pyrite and chalcopyrite. An age of 2 549.9 ±2.6 Ma (Pb-Pb single zircon method, Walraven and Martini, 1995) was obtained for a tuff layer within the Oaktree Formation. The base of the Oaktree Formation comprises a 2-3 m thick, well-bedded dolomite with millimeter-scale internal lamellae. This layer is commonly highly sheared forming the so-called "basal shear zone", which may be intersected by zones of massive sulphide on the farm Slaaihoek 540JT (Gauert, 1998).

An erosional unconformity, which is both angular and karstic (Button, 1973), defines the contact between the Chuniespoort Group and the overlying Pretoria Group. The Pretoria Group comprises an alternation of mudrocks and sandstones with lesser volcanic horizons and subordinate diamictites and conglomerates. The Bevets Conglomerate Member, a conglomerate of chert and breccia clasts derived from weathering and erosion of the underlying Malmani dolomite (Button, 1973), forms the base of the Pretoria Group in Mpumalanga. In general, the conglomerate consists of quartz clasts in a fine-grained matrix of clay minerals (Eriksson, 1988). However, at Uitkomst the Bevets Conglomerate consists of quartz gravel set in a dark quartzitic matrix (Hornsey, 1999) and is sharply overlain by the Timeball Hill Shale.

The roof of the Uitkomst Complex is situated within the Timeball Hill Formation, just above the Klapperkop Quartzite Member. The Timeball Hill Formation is divided into a lower and upper portion (Button, 1973; Eriksson, 1973). The Klapperkop Quartzite acts as a 10 m (Gauert, 1998) thick marker horizon separating the two portions of the Formation. The basal rocks of the Timeball Hill Formation are mainly carbonaceous mudrocks containing micro-algal fossils (Nixon *et al.*, 1988), with a poorly constrained age of 2224 ±21 Ma (Rb-Sr whole rock method, Burger and Coertze, 1976). They grade upwards into interbedded ferruginous mudrocks and fine-grained sandstones (Button, 1973; Eriksson, 1988). The Upper Timeball Hill Member comprises carbonaceous and ferruginous mudrocks locally enriched in pyrite (Eriksson, 1973). Ironstone is present as discrete beds within the Upper Timeball Hill Member. The shale becomes increasingly enriched in silt grading through ferruginous shale into oolitic ironstone.

1.3.1.3. Alteration of the Transvaal Supergroup by Intrusive Rocks

Within a contact zone of about 50 m surrounding the intrusion, the dolomites of the Malmani Subgroup have been transformed to a calc-silicate hornfels grading to a talc- and tremolite-bearing carbonate rock further from the contact. Dolomite xenoliths are common in the intrusion and are in some cases metamorphosed to skarns of diopside, epidote, calcite and tremolite. Extensive underground exposures of the dolomite and dolomitic xenoliths are exposed in the Nkomati Mine on the farm Slaaihoek 540JT. The Bevets conglomerate Member is transformed into a resistant fine-grained quartzite at the contact with the Uitkomst Complex. The pelitic roof rocks in contact with the Uitkomst Complex underwent medium to high-grade metamorphism, forming a 10-50 m thick rim of corundum-andalusite-hornfels.

1.3.2. The Uitkomst Complex

The Uitkomst Complex has been intruded by a large number of sills that constitute up to 10% of the total thickness of the Complex and are generally of a broadly concordant nature to the host rock lithologies. They probably represent several ages of intrusion (ref. in Hornsey, 1999). They are generally fine- to medium-grained and of gabbroic composition.

1.3.2.1. The *Basal Gabbro Unit* (BGAB)

This constitutes the base of the Uitkomst Complex and generally overlies the quartzitic floor rocks of the Oaktree Formation. In the Slaaihoek area this Unit overlies, and is deformed by, the basal shear zone. The BGAB is, on average, 5.6 m thick with a maximum thickness of about 15 m but it may also be absent in places. The width of the BGAB is relatively variable due to common sill-like offshoots. The rock type is a variably altered, equigranular, fine-grained gabbro with a distinct chill zone at the base and a gradational contact to the overlying unit. The BGAB is laterally more extensive than the overlying Lower Harzburgite Unit (Fig. 1.2.(a)).

1.3.2.2. The *Lower Harzburgite Unit* (LHZBG)

This forms the central portion of the deeper trough (Fig.1.2.(b)), but in places the LHZBG appears to have eroded the underlying BGAB to form the base of the Complex (Hornsey, 1999). The average thickness of the LHZBG is about 35 m with a maximum thickness of 90 m (Gauert *et al.*, 1995). The LHZBG is a relatively heterogeneous unit consisting mainly of poikilitic harzburgite, but locally including feldspathic lherzolite and feldspathic wehrlites (Gauert *et al.*, 1995). The most primitive rocks, i.e. the wehrlites, are the main sulphide bearing lithology (Hornsey, 1999). The LHZBG contains abundant xenoliths of dolomite and quartzite that may be up to tens of meters in diameter. Notably, the xenoliths appear to have experienced little rotation, as their layering is commonly sub-parallel to the igneous layering of the host rock.

1.3.2.3. The *Chromitiferous Harzburgite Unit* (PCR)

This forms the upper portion of the deeper trough (Fig.1.2.(b)), with an average thickness of 60 m (Gauert *et al.*, 1995), comprising abundant layers, lenses and schlieren of massive chromitite in a predominantly harzburgitic matrix. The chromitite becomes increasingly more massive towards the top of the Unit with a 0-15 m thick massive chromitite layer marking its upper contact. The silicate rocks are heavily altered to an assemblage comprising talc, carbonate, phlogopite, chlorite and serpentine.

1.3.2.4. The *Main Harzburgite Unit* (MHZBG)

This forms the central trough (Fig. 1.2.(b)), and is the thickest unit of the Complex at an average thickness of 330 m. The MHZBG is comprised of mainly harzburgite that locally grades into dunite. It lacks mineralization except for minor disseminated sulphides in the lowermost 10 m and some relatively thin horizons in its upper portion. There is a distinct macro layering on a centimeter to meter scale caused by modal and grain-size variations. The rocks are moderately altered to serpentine, but in most cases, relict olivine is preserved.

1.3.2.5. The *Pyroxenite Unit* (PXT)

This forms the lower part of the upper trough, extending laterally in the direction perpendicular to the plunge direction for about 1200 m. There is a gradational contact with the upper part of the Main Harzburgite Unit. The PXT is on average 60 m thick (Gauert *et al.*, 1995) and, according to Gauert (1998) can be subdivided into 3 sub-units i.e.:

- A lower olivine-orthopyroxenite portion,
- A central orthopyroxenite with minor accessory chromite and sulphide, and
- An upper norite to gabbronorite showing increasing amounts of plagioclase, clinopyroxene and minor quartz with height.

However, in the SH176 borehole intersection, orthopyroxenite grades very rapidly (over a distance of approximately 1 m) into gabbronorite of the overlying Gabbronorite Unit.

1.3.2.6. The *Gabbronorite Unit* (GN)

This Unit is approximately 250 m thick (Gauert *et al.*, 1995) forming the bulk of the upper trough. The GN may have sill-like lateral extensions of at least 1.4 km (Von Scheibler *et al.*, 1995). The Unit shows vertical compositional layering, with more melanocratic noritic and gabbronoritic rocks at the base grading into relatively leucocratic gabbros at the top. The uppermost 10 m are formed by diorite, which appears to intrude into the overlying Upper Gabbro Unit (PLATE 1).

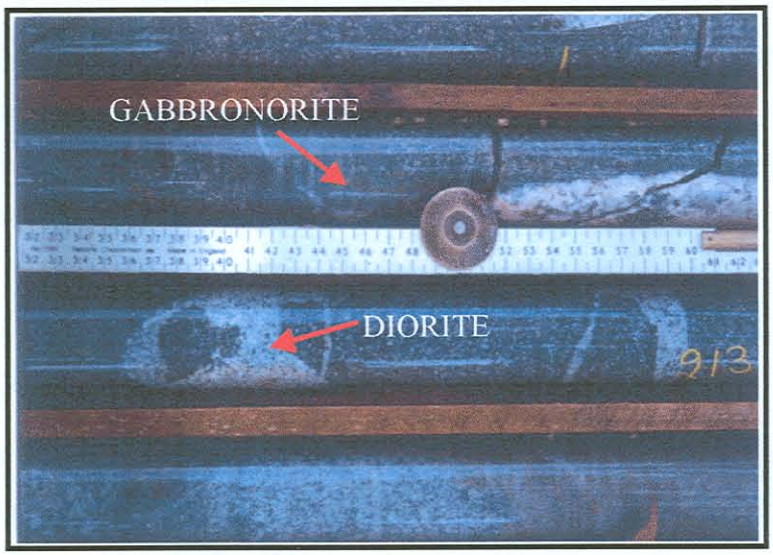

PLATE 1. Gabbronorite section near 123m showing diorite intrusion into gabbroic rock.

1.3.2.7. The *Upper Gabbro Unit* (UGAB)

This Unit constitutes the uppermost unit of the Uitkomst Complex with a thickness of approximately 50 m (Hornsey, 1999). The basal contact is intruded by diorite of the Gabbronorite Unit and the upper contact with the Timeball Hill Shale is distinctly chilled. The Unit grades from melanorite to gabbronorite at the top.

1.3.3. Sulphide mineralization

Sulphides occur within four lithostratigraphic units (Hornsey, 1999). These are (i) the Basal Mineralized Zone (BMZ) within the BGAB, (ii) the Main Mineralized Zone (MMZ) within the PXT, (iii) sulphide rich zones in the PCR (PCMZ) and (iv) several massive sulphide bodies (MSB) on the farms Slaaihoek and Uitkomst, stratigraphically situated in the footwall sediments to the Uitkomst Complex and within the basement granite gneiss. The MSB consists of three broadly lenticular bodies, predominantly of massive sulphide separated by other lithologies. The size of the deposit is about 500 by 200m with a maximum thickness of 20m (Hornsey, 1999). The sulphide mineralization is present as massive ore and stringers although the distinction between the two is governed by economic rather than geological parameters.

The sulphides consist mainly of pyrrhotite with lesser pentlandite, chalcopyrite, pyrite, magnetite and a range of PGE-bearing minerals (Theart and DeNooy, 2001). Both the MSB and MMZ are closely associated with numerous thrust faults and shear zones and with later intrusions of diabase sills. The sulphide bodies contain few xenoliths of country rock, except for in the marginal zones and where the sulphides intrude the basal Malmani dolomites.

1.3.4. Dolerite and Dykes

These make up about 13% of the total thickness of the Complex. They are composite in nature and are commonly concordant to their host. The basal sill, with a broadly uniform thickness of between 20 and 40m (20m in borehole SH176) is a fine-to medium-grained dolerite with a sharp contact to the massive sulphide and a 10-15cm chilled margin. The PCR contains about 57% of the total thickness of diabase sills, the MHZBG 30%, the GN 8% and the UGAB contains about 5%.

The sills are accompanied by faulting, the most persistent fault being represented by the Basal Shear Zone, a well-developed mylonitic talc-schist between 1 and 4m thick. This shear zone contains rare boudins of relatively undeformed country rock. Other shear zones throughout the Complex are about 20cm thick. Quartz veins and jogs are interspersed throughout the shear zones. Strike slip faults are also present with a general strike of 0.50 and 0.60^{0}N (Hornsey, 1999) and are characterized by 10-20cm thick zones of clay gouge. This faulting episode crosscuts all other structural features evident in the study area.

1.4. Methodology

Sixty half-core samples of borehole intersection SH176 were selected for petrographic and geochemical investigation. The interval between samples is on average about 20 m, depending on the degree of alteration. Highly altered, sheared or faulted rocks and diabase sills were avoided where possible and lithological contacts were always sampled where visible.

Polished thin sections were prepared from all samples and used for petrographic description. Mineral modes were determined for the relatively unaltered samples only using point counting. CIPW norms were calculated for all silicate rocks using MINPET (Mineralogical and Petrological Data Processing System version 2.02 by L.R. Richard). Forty of the 60 samples were investigated for olivine compositions (Li *et al*, 2002). The mineral chemistry of the samples was not determined, partly in view of the previous detailed mineral compositional study by Gauert (1998).

Quarter-core samples were crushed in a jaw-crusher and milled in a C-steel mill. To minimize possible PGE cross contamination during milling and crushing the samples were sorted prior to crushing; the magnetite rich samples were crushed first followed by samples with increasing sulphide content. Cleaning the mill between runs involved crushing one or more aliquots of clean quartz.

For X-Ray fluorescence (XRF) analysis the sample powders were dried at 100°C and then roasted at 1000°C to determine the absorbed water (H_2O^-) and the percentage loss on ignition (the volatile content of the samples), respectively. Major elements, except for Na_2O, were determined on fused beads, following the standard method used in the XRF laboratory of the University of Pretoria, as adapted from Bennett and Oliver (1992). The beads were made with one gram of sample powder together with about six grams of flux (Lithium Tetraborate) and a single crystal of Bromide as a non-wetting agent. The trace elements and Na_2O were analyzed on pressed powder pellets compacted at 5 kN. To increase their strength and stability the sample powders are pressed into aluminum cups. Less than 1 vol% of Mowail glue was used as a binder to the sample powder due to its low mass absorption coefficient (MAC), which, at these levels, results in no significant dilution. Sulphide-rich samples were not fully analyzed due to problems encountered during the preparation of fusion discs, i.e., sulphides can destroy the platinum crucibles. All whole-rock data are listed in Appendix II.

PGE and gold were determined by instrumental neutron activation analysis (INAA) after fire-assay collection of a Ni-sulphide bead at the University of Québec, Chicoutimi (UQAC). As an assessment of the accuracy of the analyses, results for the international standard SARM-7 are listed in Table 1. Platinum-group elements were also determined on the in-house standard AX90, and the relative standard deviations indicate precisions varying from 4 to 23% (Table 1). The PGE data are listed in Appendix II.

Sulphur contents were determined for all samples at UQAC by LECO titration. Thirty-eight selected samples were sent to the laboratories of Professor D. Reid at the University of Cape Town, for trace element analysis using Inductively Coupled Plasma-Mass Spectrometry (ICP-MS). Thirteen of these samples were additionally analyzed for Sm/Nd isotopes at the Hugh Allsopp Laboratories, University of the Witwatersrand. The author carried out the sample chromatography and Dr. S. Prevec carried out the electromagnetic analysis of the samples.

Table 1. Accuracy and precision of PGE analysis (values in ppb)

	1	2	3	4	5
Os	63(±7)	62	2.7	22.9	<0.5
Ir	74(±12)	74.5	2.75	4.8	<0.01
Ru	430(±57)	439	18	8.8	<1
Rh	240(±13)	232	10.3	6.8	<0.1
Pt	3740(±45)	3486	126	5.9	<2
Pd	1530(±32)	1551	305	4.3	<2
Au	310(±15)	332.9	4	13.1	0.3

1.International reference sample SARM-7; **2.** UQAC result of SARM-7; **3.** In-house standard run with every batch of 20 samples at UQAC (n=4); **4.** Relative standard deviation on in-house standard in %; **5.** Blank; results obtained when 50 g of reagent silica is used in place of sample.

2. PREVIOUS WORK

The Uitkomst Complex was first mentioned by Wagner in 1929 who described the intrusion as a "big sill of highly altered pyroxenite carrying platinum in association with magnetic iron sulphides". He proposed that the body was of Archaean age and possibly related to mafic rocks of the Barberton area. The sulphides, mainly pyrrhotite, pentlandite and chalcopyrite, were described as being "interstitial and molded on the silicates".

Kenyon *et al.* (1986) completed the first geochemical examination of the Complex concentrating on the chromitites from the ultramafic zone. Based on S/Se ratios they suggested that the main source of the sulphide mineralization was magmatic and that the Complex may have been emplaced by injection of different pulses of magma. The close spatial association of the sulphide mineralization with the dolomites of the Transvaal Sequence was explained by release from the dolomites of CO_2 on interaction with the magma. The resulting increase in oxygen fugacity along with the associated decrease in FeO resulted in sulphide supersaturation and sulphide segregation followed by chromite crystallization. The presence of numerous dolomitic xenoliths in the ultramafic rocks led Kenyon *et al.* (1986) to believe that the Uitkomst magmas thermally eroded the host Transvaal sedimentary rocks. Based on similarities in chromite composition Kenyon *et al.* (1986) postulated a genetic link between the Uitkomst Complex and the Bushveld Complex, a link that had earlier been proposed by Sharpe *et al.* (1981).

Allen (1990) suggested emplacement of the Complex by injection of three compositionally different pulses of magma. Her study was based on the farm Uitkomst, where the Upper Pyroxenite and Gabbronorite and Upper Gabbro Units are not exposed. Thus, she interpreted the Complex as an inverted fractionation sequence with the least differentiated peridotite zone at the top, the pyroxenite zone in the centre and the fractionated gabbro at the base. Sulphur isotopes of different rock units and sulphide minerals provided evidence for a sedimentary source for most of the sulphur, and thus the mineralization was interpreted to have formed due to contamination.

Strauss (1995) studied the whole rock and mineral chemistry of the Basal Gabbro on Slaaihoek 540JT, noting a similarity in geochemistry with the marginal rocks of the Muskox and Insizwa Complexes. Strauss (1995) observed a high Cu/(Cu+Ni) ratio of the Basal Gabbro and he attributed this to ore formation involving supercooling and country rock assimilation during emplacement of the Basal Gabbro.

Gauert *et al.* (1995) and Gauert (1998) carried out a comprehensive study of the Uitkomst Complex, looking at S isotopes, whole rock-and mineral chemistry of several boreholes along a strike length of 10 km. It was proposed that the Uitkomst Complex represented a magma conduit that crystallized in two stages (Fig. 2.). An early, relatively contaminated pulse of magma formed the Basal Gabbro, with the overlying Lower Pyroxenite representing a dense sulphide-rich highly contaminated cumulate rock. The bulk of the harzburgitic units are thought to have crystallized under open system conditions from magma that flowed through a magma conduit. The upper portions of the Complex crystallized to produce a normal fractionation sequence of the Upper Pyroxenite and Gabbronorite units in a closed system as a result of apparent deactivation of the conduit (Gauert *et al.*, 1995). The base of the closed system was placed about 75 m below the top of the Main Harzburgite Unit by De Waal *et al.* (2001). Gauert and co-workers did not distinguish the Upper Gabbro Unit from the Gabbronorite Unit. Based on S and Sr isotope studies of the Complex Gauert *et al.* (1995) suggested that the magmatic sulphur was contaminated by sedimentary sulphur, probably derived from the shales of the Timeball Hill Formation.

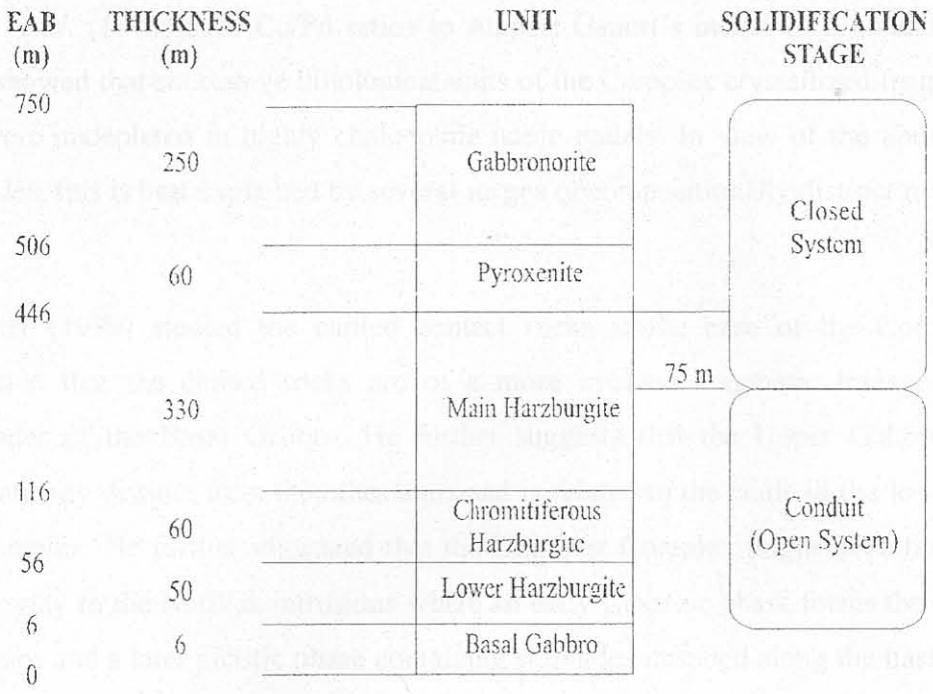

Fig.2. Lithological subdivision and solidification stages of the Uitkomst Complex (From Gauert *et al.*, 1995 and De Waal and Gauert, 1988). EAB indicates the mean elevation above the base of the intrusion and the thickness values are averaged. Vertical scale is approximate.

Gauert *et al.* (1995) and Gauert (1998) put forward three main arguments for the magma conduit model.

- The elongated tubular shape of the Complex.
- The large proportion of sulphides and chromite in relation to silicates within the basal units of the Complex, creating an apparent mass-balance problem. However, in view of the poorly known geometry of the Complex, this argument needs further constraint.
- Absence of a normal fractionation trend in the ultramafic rocks. A constant composition of the Main Harzburgite substantiates the existence of an infinite magma source. This would imply movement of large quantities of magma of constant composition through the conduit.

Maier *et al.* (1998) used Cu/Pd ratios to support Gauert's model of a conduit system. They showed that successive lithological units of the Complex crystallized from magmas that were undepleted in highly chalcophile noble metals. In view of the abundance of sulphides, this is best explained by several surges of compositionally distinct magmas.

Agranier (1999) studied the chilled contact rocks at the base of the Complex and suggested that the chilled rocks are of a more evolved magmatic lineage than the remainder of the Basal Gabbro. He further suggests that the Upper Gabbronorite is magmatically distinct from the other units and is related to the chills in the lower part of the Complex. He further suggested that the Uitkomst Complex might have formed in a similar way to the Noril'sk intrusions where an early gabbroic phase forms the top of the intrusions and a later picritic phase containing sulphides intruded along the base. Thus in the Uitkomst Complex the parental magma to the UGAB may have intruded first, forming chills around the intrusion. The Basal Gabbro magma may have intruded later, partially remelting the pre-existing chill, and created a gradual contact with it.

There have been two recent studies on the platinum group minerals of the Uitkomst Complex. Van Zyl (1996) noted four main minerals associated mainly with pyrrhotite. These are Kotulskite [Pd(Te,Bi)], Merenskyite [$(Pt,Pd)(Te,Bi)_2$], Stibiopalladinite [$(Pb,Cu)_5Sb_2$] and Sperrylite ($PtAs_2$). Theart and de Nooy (2001) studied the PGM in massive sulphides intruding the immediate floor rocks of Archaean basement gneiss. The PGM frequently occur as composite grains or aggregates and are preferentially associated with pyrrhotite (60%), pentlandite (20%), and chalcopyrite (6%). Thirteen percent of the PGM occur within silicate minerals and about 0.1% are hosted by magnetite. About 31% of the PGM are completely enclosed within the host mineral grain. Of these, about 80% (by mass) occur within pyrrhotite while 15% occur within chalcopyrite. The remaining 69% of the PGM occur along the grain boundaries between adjacent pyrrhotite grains or along boundaries between magnetite grains and surrounding pyrrhotite (Theart and de Nooy 2001). The main minerals include:

a. Merenskyite: (80% of all PGM.).

b. Michenerite: [PbBiTe] (5-10%).

c. Testibiopalladite: [PdTe(SbTeBi)] (5-10%).

d. Sperrylite: [$PtAs_2$] (5-10%).

e. Temagamite [Pd_3HgTe_3] (5-10%).

f. Gold [AuAg] (about 1%).

De Waal *et al.* (2001) conducted a $^{207}Pb/^{206}Pb$-age determination on clear zircon separates from the upper Gabbronorite Unit. This yielded an age of 2044 ± 8 Ma (concordant age) that is comparable to the $^{207}Pb/^{206}Pb$-age of Harmer and Armstrong (2000) for the Critical Zone of 2054.4 (±2.8). De Waal *et al.* (2001) also provided geochemical evidence that the parental magma of the Uitkomst Complex could be closely related to the B1 high-Mg andesite magma of the Bushveld Complex.

3. PETROGRAPHY

3.1. Basal Gabbro Unit

This Unit predominantly comprises phaneritic, equigranular to inequigranular rocks but has an aphanitic chilled margin (PLATE 2) at the base. Plagioclase (50-60 vol%) clinopyroxene (5-15 vol%) and orthopyroxene (10-20 vol%) are the major cumulus phases, with chromite comprising less than 1 vol%. The intercumulus phases make up between 5 and 10% of the rock and consist of quartz, mica (biotite and phlogopite), K-feldspar, magnetite, apatite, ilmenite and sulphides. These phases increase in abundance from the base to the top of the Unit. The rock may be classified as a gabbronorite (Le Maitre, 1989) which is consistent with the results obtained by De Waal *et al.* (1995), Gauert *et al.* (1995), and Strauss (1995).

Plagioclase occurs as euhedral and subhedral lath-like cumulus grains up to 4 mm in length, and as anhedral interstitial grains. The relative proportion of intercumulus grains increases towards the top of the Unit. The grains show characteristic polysynthetic albite and Carlsbad twinning and most have undergone extensive saussuritization.

The pyroxenes are euhedral, subhedral and anhedral, and occur as cumulus and intercumulus grains, with the cumulus mode being dominant. Clinopyroxene commonly displays exsolution blebs and lamellae of orthopyroxene.

Quartz, biotite, K-feldspar and apatite occur as late stage phases filling the interstices between plagioclase laths and pyroxenes. The biotite grains are reddish-brown in colour, possibly due to high titanium contents (Deer *et al.*, 1992).

Magnetite is present in two main forms, as discrete anhedral grains and as spongiform or skeletal grains (see plate in section on Gabbronorite Unit). The latter grains generally increase in abundance with height. The abundance of the discrete grains tends to be directly proportional to the concentration of sulphide in the rock. The anhedral grains typically contain inclusions of ilmenite and globular pyrrhotite.

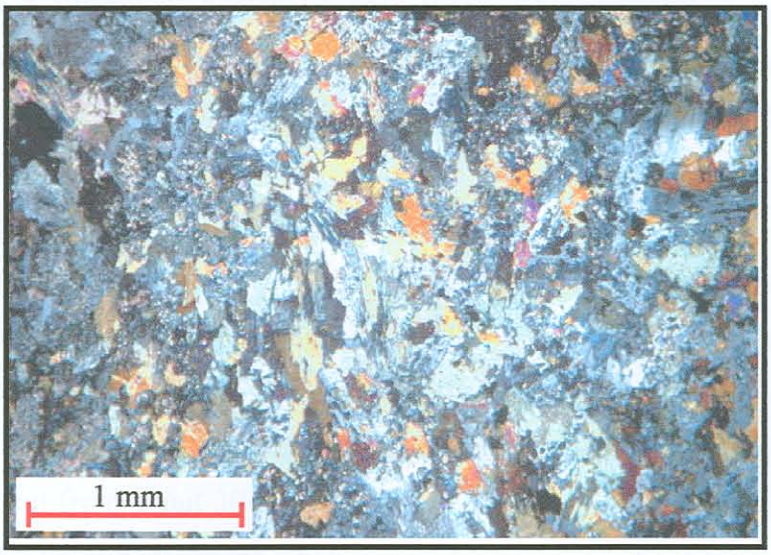

PLATE 2. Basal Gabbro chilled margin SH176 UP 60

Disseminated sulphides occur throughout the Unit, as discrete blebs and as fillings of interstices although Gauert (1998) reported that the basal part of the BGAB is essentially sulphide free. Chalcopyrite (about 50%) is the most abundant sulphide followed by pyrrhotite (about 40%) and then pentlandite (about 10%). Two types of pentlandite were identified. A flame-like exsolution variety and granular inclusions within pyrrhotite, particularly near fractures and grain boundaries between pyrrhotite and chalcopyrite. The former is more abundant than the latter.

Alteration

Secondary hydrothermal alteration of the Unit led to widespread reconstitution of the rocks, resulting in the formation of amphibole, chlorite, carbonate and epidote. Plagioclase is commonly partially altered to saussurite, a fine-grained aggregate of epidote group minerals, albite, sericite and other minerals (Deer *et al.*, 1992). Pyroxene alteration may be pervasive with complete pseudomorphic replacement of the pyroxenes by amphibole. Two types of amphibole were identified i.e. hornblende and acicular tremolite-actinolite. Phlogopite-biotite displays reaction rims of chlorite and calcite as well as occurring as rims attached to corroded grains of clinopyroxene.

3.2. Lower Harzburgite

The LHZBG is lithologically the most heterogeneous Unit of the Uitkomst Complex comprising a variety of ultramafic rock types. The main lithology is a poikilitic harzburgite with variable amounts of chromite and intercumulus plagioclase. Local varieties include feldspar-bearing lherzolite grading to sulphide-rich wehrlites and websterite.

The contact with the underlying BGAB is gradational, characterized by an increase in ferromagnesian minerals, including olivine. The latter phase comprises, on average, about 45 vol% of the LHZBG, but is rare in the BGAB. The major cumulus phases in the LHZBG are (i) olivine which generally increases in abundance from the base to the top of the Unit from about 30 to 45 vol%, (ii) orthopyroxene which varies from 10 to 30 vol% and (iii) clinopyroxene which ranges from zero to about 10 vol%, but broadly increases in abundance from the base to the top. Postcumulus phases are, in decreasing abundance, plagioclase, biotite and K-feldspar. Feldspar makes up about 20 vol% of the rock at the base decreasing to 10 vol% near the top. Biotite ranges from 5 to 10 vol% increasing gradually with height. Sulphides are concentrated within wehrlites (on average about 4 vol%), which occur predominantly in the central portion of the Unit. In general, the sulphide content increases from about 3 vol% at the base to about 4 vol% in the wehrlites and then decreases to about 2 vol% towards the top of the Unit. The chromite content increases marginally with height from less than 1 vol% to about 1 vol%.

The rocks are medium-grained throughout the Unit. Olivine is generally subhedral and equigranular ranging in size from 1 mm to 3 mm. Smaller olivine grains may occur as chadacrysts within clinopyroxene in which case they are relatively less altered than the larger cumulus grains. Towards the top of the Unit alteration is more pervasive, with "islands" of remnant olivine being surrounded by serpentine. Orthopyroxene occurs as euhedral to subhedral grains commonly showing clinopyroxene exsolution blebs and lamellae where the orthopyroxene grains are larger than 1 mm. The exsolution features are most prevalent in the feldspar-bearing lherzolite.

Clinopyroxene is present either as a cumulus phase, forming oikocrysts up to 4 mm in size, or as exsolution lamellae in orthopyroxene. Occasionally, smaller clinopyroxene grains may be strongly embayed and rimmed by hornblende.

Sulphides occur as discrete grains less than 1 mm in size or as net-textured aggregates. Some larger sulphide blebs of up to 1 mm in size may also be present. The main sulphides, in decreasing abundance, are pyrrhotite (approximately 60 vol%), chalcopyrite (approximately 30 vol%) and pentlandite (less than 10 vol%), with lesser pyrite and millerite (approximately 1 vol% in total). Generally, the sulphide grain boundaries are intergrown with acicular serpentine (PLATE 3 A). Pyrrhotite is commonly rimmed by secondary magnetite (PLATE 3 B). Chalcopyrite occurs as subhedral prismatic grains associated with pyrrhotite and as fracture fillings within orthopyroxene grains. It is relatively more enriched in the websterite than the wehrlite. Pentlandite occurs at the grain boundaries of pyrrhotite and as flame lamellae within pyrrhotite. Pyrite occurs as euhedral and subhedral grains within pyrrhotite (PLATE 3 B and C) and as discrete grains interstitial to silicates and chromite. It is most abundant in the sulphide-rich wehrlites. Millerite forms anhedral aggregates in pyrite exhibiting undulose extinction.

Disseminated chromite occurs as discrete euhedral and subhedral grains (less than 50 μm) or as partially annealed aggregates. The chromite is generally hosted by clinopyroxene, and more rarely by orthopyroxene. Fractures within chromite grains are commonly filled with magnetite.

PLATE 3

A. **LHZBG, SH176 UP56.** Intergrowth between pentlandite (PENT) and silicates.

B. **LHZBG, SH176 UP56.** Magnetite alteration rim around pyrrhotite (PO). Euhedral pyrite and subhedral chalcopyrite are enclosed in pyrrhotite. Note exsolution flame of pentlandite.

C. **LHZBG, SH176 UP56.** Subhedral pyrite grains enclosed in pyrrhotite (PO).

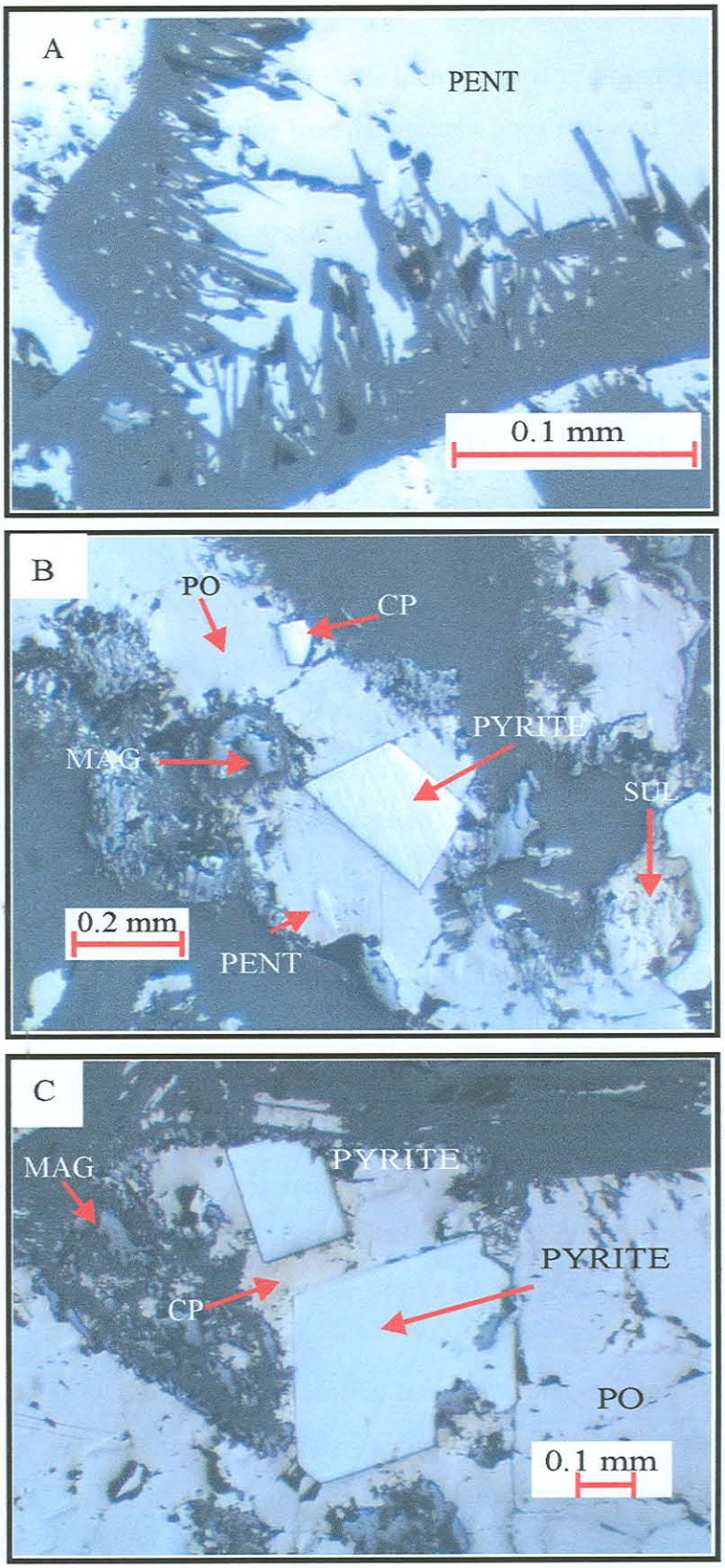
A
PENT
0.1 mm
B
PO
CP
PYRITE
MAG
SUL
0.2 mm
PENT
C
MAG
PYRITE
PYRITE
CP
PO
0.1 mm

PLATE 3

Alteration

Pervasive alteration throughout the Unit made identification of primary phases difficult in some sections. The olivine grains have commonly been replaced by chrysotile and lizardite with magnesite or magnetite and carbonate present at the center of the pseudomorphosed grain (PLATE 4). During alteration of olivine, serpentine, brucite and magnetite are produced along with talc and magnesite, according to the following equations (Deer *et al.*, 1992):

$$2Mg_2SiO_4 + 3H_2O \rightarrow Mg_3Si_2O_5(OH)_4 + Mg(OH)_2$$

Forsterite — Serpentine — Brucite

$$Mg_3Si_2O_5(OH)_4 + 3CO_2 \rightarrow Mg_3Si_4O_{10}(OH)_2 + 3MgCO_3 + H_2O$$

Talc — Magnesite

The olivine of the Uitkomst Complex contains some iron (Fe^{2+}) and this forms magnetite ($Fe^{2+}Fe_2^{3+}O_4$) during serpentinization, which is associated with the other alteration minerals of olivine.

Both orthopyroxene and clinopyroxene have been replaced by chlorite-tremolite and phlogopite, with phlogopite dominating in the core of the grains. Two juxtaposed varieties of chlorite could be distinguished, one being enriched in iron with distinct green-brown pleochroism and the other being reddish-brown in colour and displaying weak pleochroism. Chlorite is a common constituent of igneous rocks in which they have usually been formed by hydrothermal alteration of primary ferromagnesian minerals (Deer *et al.*, 1992). Phlogopite occurs as a result of continuous reactions

involving some or all of muscovite, chlorite, quartz and plagioclase. Amphibole occurs in association with biotite as irregular grains, occasionally forming rims around sulphide grains. Pentlandite is partially replaced by creamy-blueish violarite along fractures. Where the rock alteration assemblage is dominated by talc, worm-like aggregates of millerite within pyrite are observed characterized by strong anisotropism from yellow to light blue.

PLATE 4

LHZBG, SH176 UP56. Altered olivine grains embedded in massive sulphide. Grains have been pseudomorphically replaced by magnetite, lizardite and chrysotile. The top photomicrograph was taken in cross-polarized light, the bottom photomicrograph was taken in plane-polarized light.

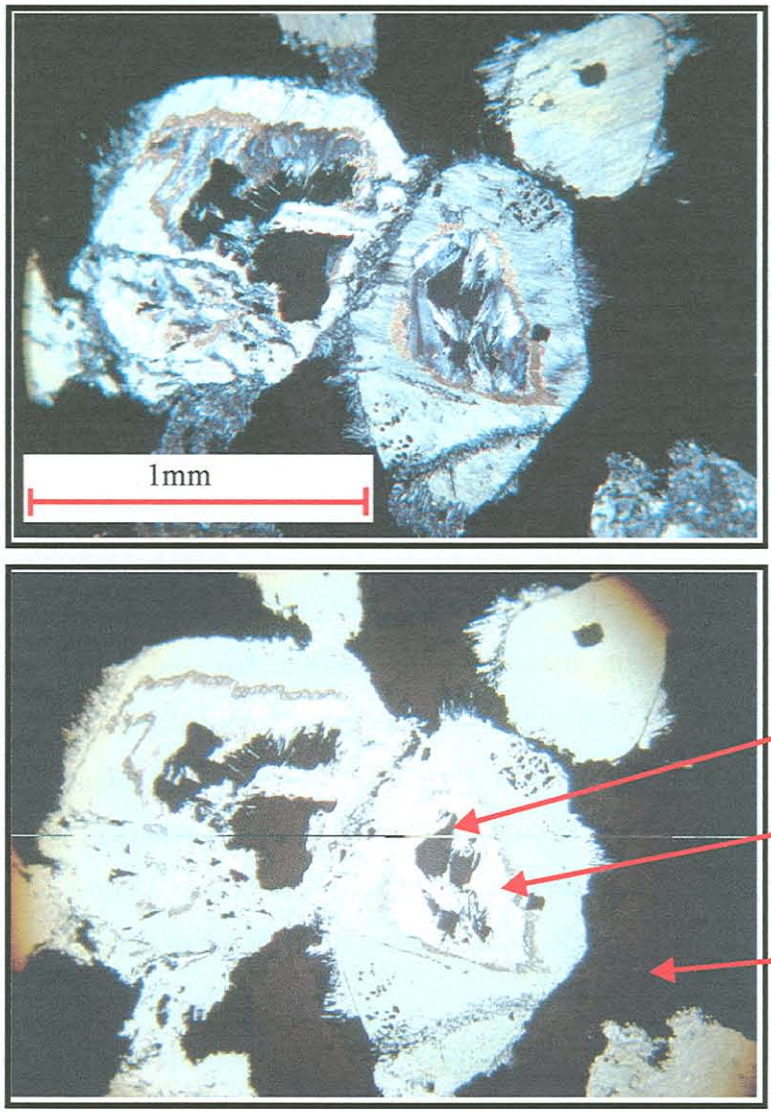

PLATE 4

3.3. Chromitiferous Harzburgite Unit

This Unit comprises equigranular and inequigranular rocks with olivine, chromite and orthopyroxene as major cumulus phases. There is a gradational basal contact with the LHZBG that is marked by an increasing olivine content from about 45 vol% to 60 vol%. Orthopyroxene averages 20 vol%, and the chromite content is greater than or equal to 10 vol%. Clinopyroxene averages about 2 vol% except for the base of the Unit where it may reach up to 20 vol% of the rock. Interstitial minerals, in decreasing abundance, are sulphides, plagioclase, muscovite, phlogopite and amphibole. Plagioclase, muscovite and phlogopite together make up less than 5 vol% of the rock with sulphides between 1 and 5 vol%, decreasing in abundance with height. The grain sizes vary between 3-4 mm for orthopyroxene, about 1 mm for the olivine and plagioclase, less than 1 mm for the remaining interstitial phases and between 50-500μm for chromite.

Olivine grains are subhedral equigranular with smaller grains near the base being enclosed by clinopyroxene. There is a gradual increase in olivine with height.

Chromite occurs as euhedral and subhedral disseminated grains that are largely interstitial to olivine and pyroxenes. Aggregates of chromite may be partially annealed or cemented by magnetite (see plates in section on MHZBG). A massive chromitite layer about 40 cm in thickness marks the boundary with the overlying MHZBG Unit. Within the layer, chromite grains are strongly brecciated along fractures that are dominantly oriented parallel to the sub-horizontal layering of the Complex.

Clinopyroxene occurs as oikocrysts enclosing olivine, as interstitial fillings as well as occasional exsolution lamellae in orthopyroxene. Cumulus clinopyroxene is rare. Orthopyroxene occurs as anhedral grains. Anhedral plagioclase fills interstices. Subhedral and anhedral biotite, phlogopite and amphibole also occur as interstitial phases.

Sulphide minerals are disseminated throughout the Unit. In decreasing abundance they consist of pyrrhotite, chalcopyrite, pentlandite, pyrite and millerite (similar relative proportions as in the LHZBG). Pyrrhotite occasionally displays exsolution of flame-like and granular pentlandite (PLATE 5 A). The finer grains are skeletal in morphology and tend to be intergrown with secondary silicate minerals. Chalcopyrite may be associated with pyrrhotite, occurring as anhedral grains juxtaposed with pyrrhotite (PLATE 5 B). Veinlets of chalcopyrite and millerite usually occur adjacent to or within chrysotile veins. Some magnesite veins contain remobilized sulphide grains indicating the secondary nature of part of the mineralization. The sulphide assemblage associated with chromitite layers usually consists of blebby aggregates of pentlandite, pyrrhotite and chalcopyrite. Net-textured and cusp shaped sulphides draped around cumulus chromite grains are also common textural features in the chromitite layers.

Alteration

Serpentine, amphibole, chlorite, calcite, phlogopite and muscovite occur as alteration products replacing olivine, orthopyroxene and clinopyroxene. Magnetite occurs as discrete grains occasionally surrounded by rims of lizardite and chrysotile and as veinlets within the serpentine in olivine grains. Serpentine occurs as fibrous masses that may show intergrowths with sulphides. The sulphides are commonly partially replaced by violarite and secondary magnetite. Secondary phlogopite plume aggregates may embay sulphide grain boundaries (see plates in section on LHZBG).

PLATE 5

A. **PCR, SH176 UP51.** Pyrrhotite (PO) showing flame exsolution lamellae of pentlandite (PENT). Note replacement of pyrrhotite by magnetite.

B. **PCR, SH176 UP51.** Chalcopyrite (CP) intergrown with pyrrhotite, also present are chromite and magnetite grains.

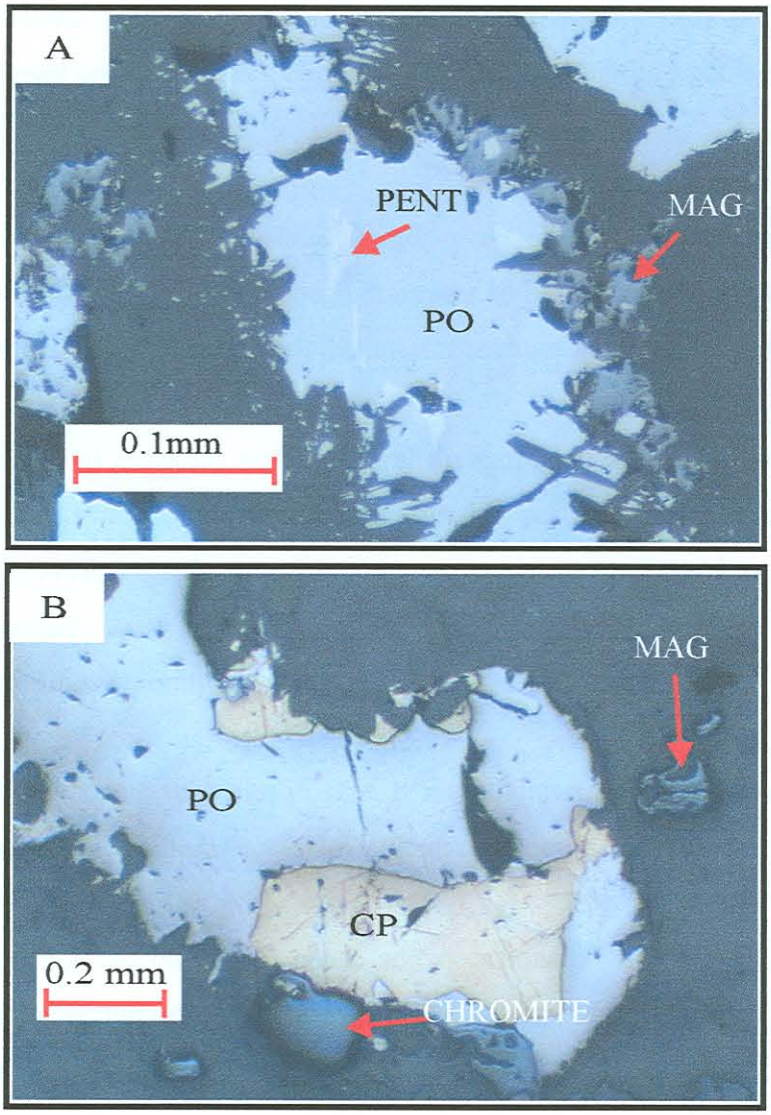

PLATE 5

3.4. Main Harzburgite Unit

This Unit is lithologically the most homogeneous of the Complex comprising essentially a poikilitic harzburgite (PLATE 6 A). Olivine and chromite are the main cumulus phases. Olivine averages between 65 and 70 vol% increasing towards the top. Chromite ranges between 1 and 5 vol% (PLATE 6 B). Oikocrystic orthopyroxene decreases from about 20 vol% near the base to about 15 vol% near the top. Minor intercumulus phases are plagioclase, clinopyroxene and amphibole making up between 5 and less than 10 vol% of the rock.

Olivine occurs mainly as 0.5 to about 2 mm sized chadacrysts enclosed in large oikocrysts of orthopyroxene. There does not appear to be a systematic change in size (between <1 and 2 mm) of olivine from the interior to the margin of oikocrysts.

Chromite is present as euhedral and subhedral disseminated grains hosted mainly by orthopyroxene. The grains are generally equigranular, partially annealed or cemented by magnetite (PLATE 7) and may also form vein aggregates. The chromite content marginally decreases with height through the Unit. A selvage of phlogopite occasionally surrounds chromite crystals.

Orthopyroxene may be up to 4 mm in size. It rarely shows clinopyroxene exsolution lamellae, but commonly contains accessory euhedral chromite.

Plagioclase occurs as an interstitial phase and occasionally as corroded or partially resorbed inclusions within orthopyroxene grains. These grains could be relicts of earlier cumulus plagioclase (Eales *et al.*, 1991).

Rare clinopyroxene is present as oikocrysts or as interstitial fillings as well as occasional exsolution lamellae in orthopyroxene. Cumulus clinopyroxene is rare. Some of the clinopyroxene may be rimmed by amphibole.

Sulphides are mainly pyrrhotite (70%) with lesser pentlandite (<30%) and minor chalcopyrite (about 1 to 2%). The sulphides occur as finely disseminated grains. The

grain size and concentration of the sulphides decreases with height. The sulphide grains are commonly very finely intergrown with serpentine and phlogopite grains.

Alteration

Alteration of this Unit increases with depth resulting in almost complete serpentinization of olivine near the base of the Unit. Magnetite and magnesite are common within the serpentinized zone along with lizardite, chrysotile and talc. Secondary amphibole (largely hornblende) is pervasive as a result of alteration of the pyroxenes.

PLATE 6

A. and B. **MHZBG, SH176 UP36**. Partially serpentinized olivine chadacrysts within orthopyroxene. Chromite and sulphide grains are disseminated in orthopyroxene.

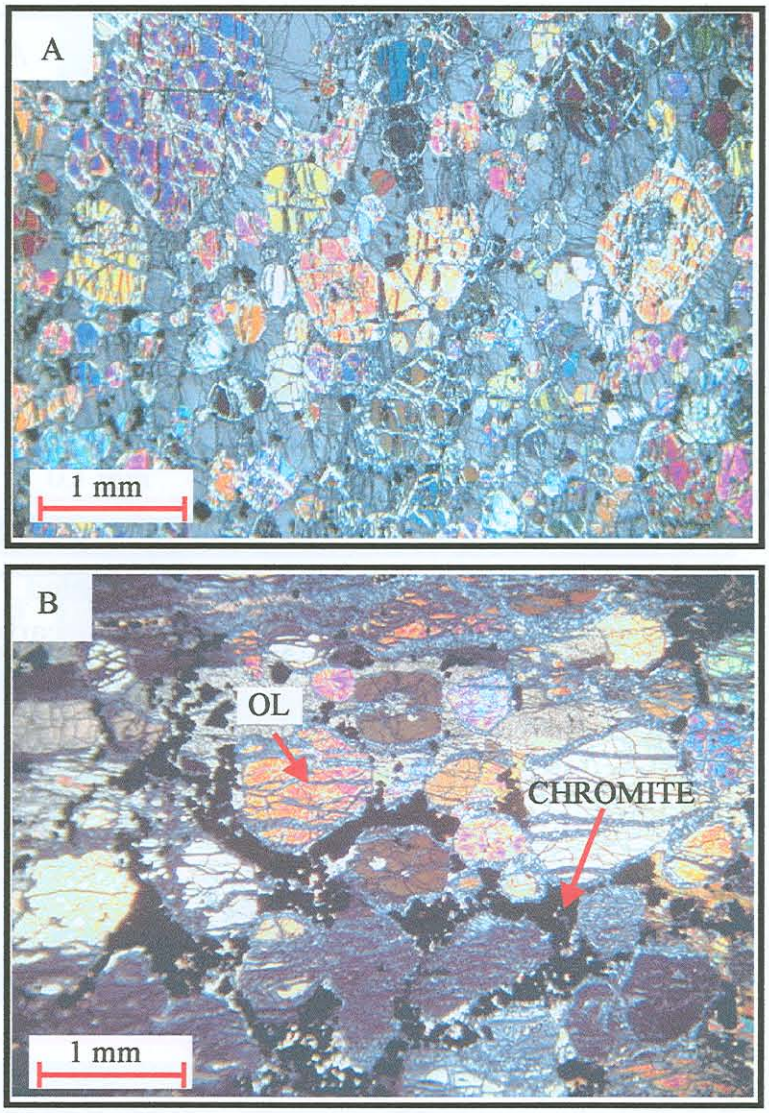

PLATE 6

PLATE 7

A. **MHZBG, SH176 UP51**. Partially annealed euhedral and subhedral chromite grains. C = Remnants of carbon coating for electron microprobe analyses.

B. **MHZBG, SH176 UP46**. Chromite grains annealed with magnetite.

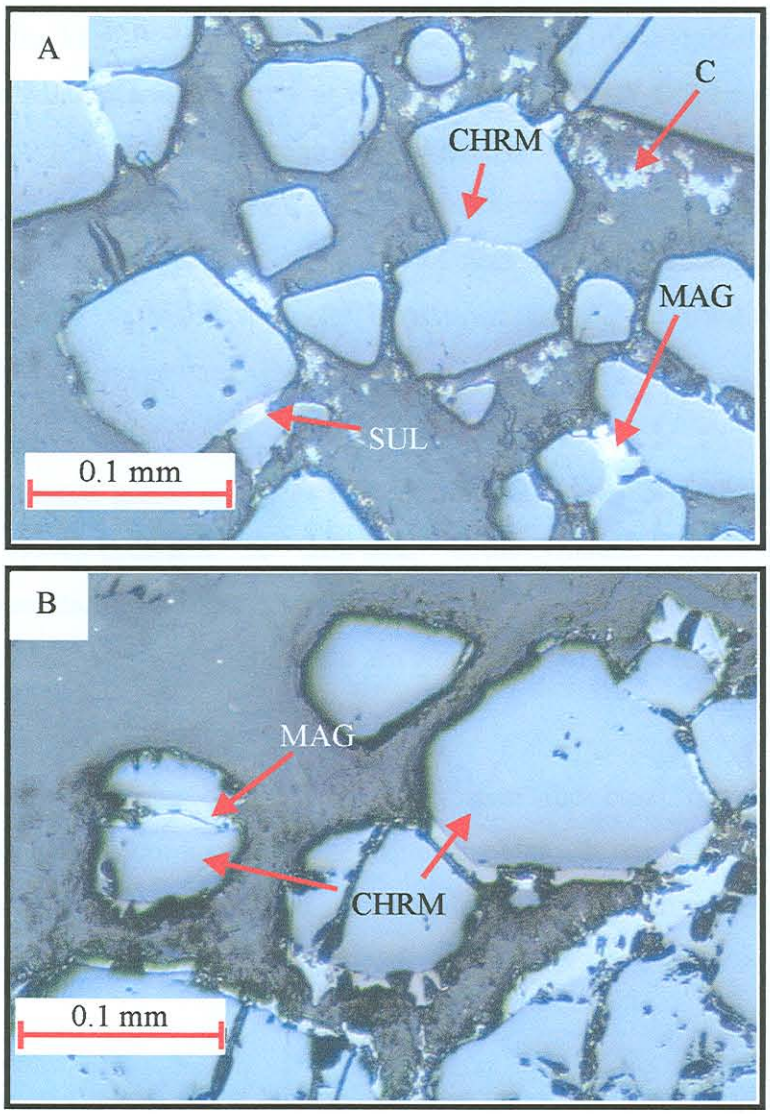

PLATE 7

3.5. Pyroxenite Unit

Orthopyroxene is the major cumulus mineral in the PXT, amounting to over 80 vol% of the rock (PLATE 8 A and B). Olivine, chromite and clinopyroxene (approximately 5 vol%) are locally present. Post-cumulus phases are, in order of decreasing abundance, plagioclase clinopyroxene, mica (phlogopite), amphibole and quartz. The basal contact of the PXT with the MHZBG is gradational over 1-2 m, with olivine rapidly decreasing from 65% in the MHZBG to 35 vol% at the base of the PXT. Olivine continues to decrease markedly in abundance through the remainder of the PXT and is essentially absent in the upper portion of the PXT. Plagioclase increases with height from about 10 vol% at the base to over 50 vol% at the top contact with the Gabbronorite Unit. It attains cumulus status within a relatively narrow noritic 1-2 m transition interval between the PXT and the overlying GN.

Cumulus orthopyroxene grains are generally subhedral equigranular with crystal habits varying from stubby-prismatic to lath-like. Orthopyroxene commonly shows clinopyroxene exsolution lamellae approximately parallel to (100). These lamellae tend to disappear towards the crystal margins and are generally rare at the base of the Unit.

Accessory euhedral chromite occurs particularly near the basal contact with the MHZBG and is much less common near the top of the Unit. It may be enclosed by any of the post cumulus phases as well as cumulus olivine. Orthopyroxene grains containing chromite are rare.

Within the norites at the top of the Unit, plagioclase generally forms oikocrysts with a maximum size of 5 mm enclosing orthopyroxene. In the orthopyroxenite, plagioclase occurs as small intercumulus grains. Some orthopyroxene grains in the norite contain ovoid plagioclase inclusions that are partially embayed.

Clinopyroxene is mainly present as oikocrysts, as interstitial fillings or as exsolution lamellae in orthopyroxene. Cumulus clinopyroxene is rare (but see Plate 8 B).

Amphibole (mainly hornblende) occurs interstitial to orthopyroxene in the pyroxenite. Mica is an abundant accessory or minor phase, associated with quartz in the orthocumulate pyroxenites. The interstitial quartz grains show no strained extinction. Other accessory minerals present are phlogopite, discrete anhedral magnetite grains surrounded by rims of phlogopite, and green actinolite. Magnetite occurs as anhedral grains with ilmenite and sulphide inclusions (PLATE 8 C).

Finely disseminated sulphides appear to be confined or concentrated towards the base of the Unit. Pyrrhotite is the most abundant sulphide followed by lesser pentlandite and minor chalcopyrite. Pyrrhotite is generally globular with flame-like exsolution zones of pentlandite. Overall, the sulphides fill the interstices together with biotite, plagioclase and quartz. In some instances, pentlandite occurs as finely disseminated grains within fractures of olivine and intergrown with serpentine.

Alteration

This is the least altered Unit of the Complex, but some of the orthopyroxene may be rimmed by an alteration halo of tremolite, phlogopite and fuchsite (a chromium muscovite). Some clinopyroxene grains display rims or patches of amphibole, evidence for interaction with late stage fluids.

PLATE 8

A. **Upper PXT Unit, SH176 UP26**. Norite.

B. **PXT central portion, SH176 UP30.** Pyroxenite.

C. **PXT, SH176 UP21.** Anhedral magnetite grain with (faint) exsolution lamellae of ilmenite and globule of sulphur.

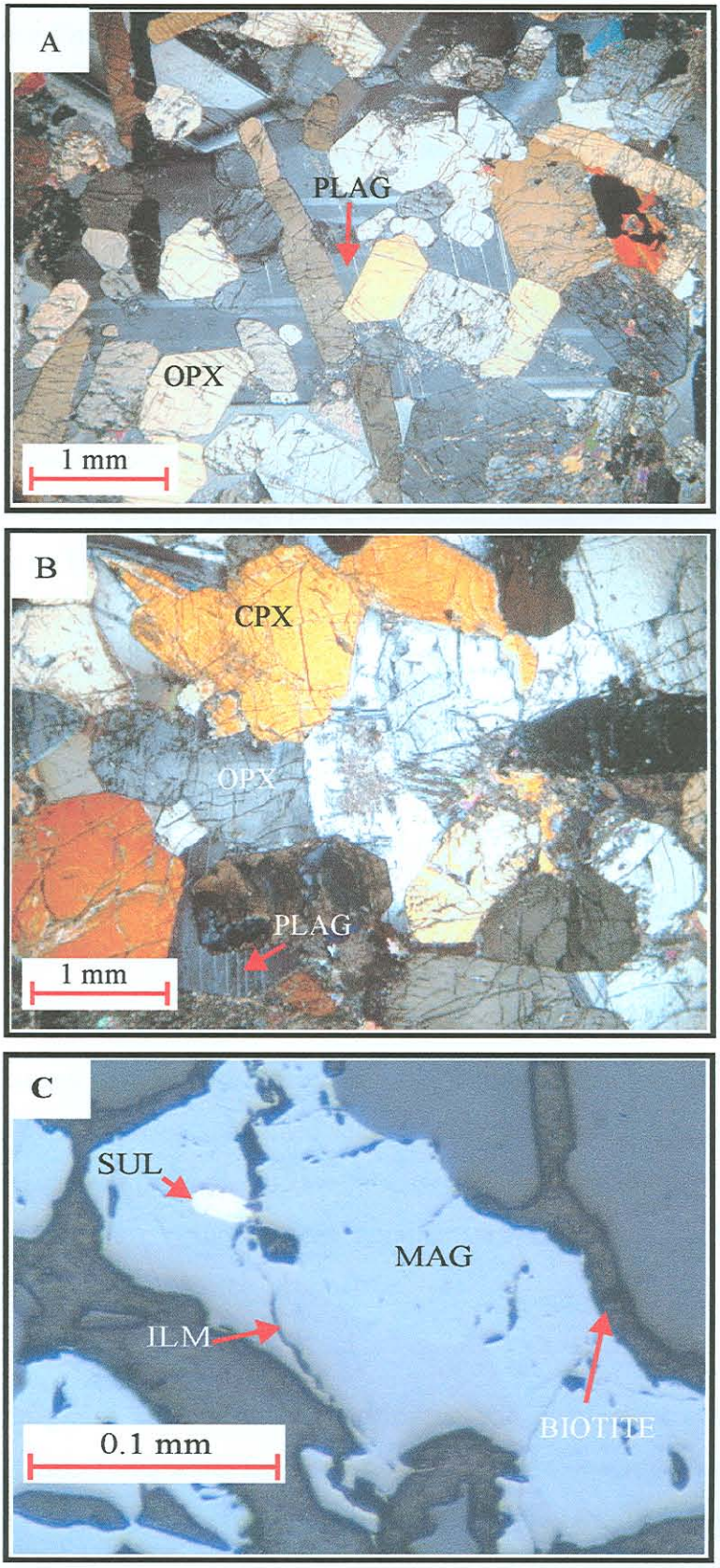

PLATE 8

3.6. Gabbronorite Unit

This Unit is essentially composed of fine to coarse-grained equigranular gabbronoritic to gabbroic rocks with minor norites and diorites. The contact with the PCR is gradational. The primary igneous lithology of the GN Unit is a plagioclase-pyroxene-hornblende rock with interstitial phlogopite, biotite, hornblende, quartz, apatite and opaque minerals. Plagioclase constitutes between 50 and 60 vol% of the rock. Generally, clinopyroxene increases with height whilst orthopyroxene decreases. Thus the base of the GN consists of a medium-grained norite with an intergranular texture (PLATE 9 A) becoming more gabbronoritic with height. At the top of the Unit, gabbro and diorite is developed. Biotite-phlogopite is ubiquitous throughout the Unit occurring in concentrations up to 10 vol% with hornblende, quartz, apatite and opaque minerals making up to 5 vol% in parts of the Unit.

Cumulus plagioclase grains average between 2 and 3 mm in length, reaching 5 mm in exceptional cases. Plagioclase additionally occurs within interstices and as subhedral to anhedral inclusions in clinopyroxene at the base of the Unit (PLATE 9 A). In some cases there is a sub-grain development of plagioclase grains, possibly in response to deformation of the grains (PLATE 9 B).

Clinopyroxene ranges from 1 to 2 mm in size and orthopyroxene grains are usually about 1 mm in size or less. Coarse-grained anhedral clinopyroxene occurs as oikocrysts hosting up to 1 mm sized plagioclase grains and as exsolution lamellae of orthopyroxene. Anhedral orthopyroxene grains may contain inclusions of clinopyroxene and, to a lesser degree, plagioclase.

Biotite-phlogopite grains are interstitial to pyroxene and plagioclase and are often associated with (titano-) magnetite, forming a rim around the magnetite grains. Primary hornblende occurs as stubby to long prismatic crystals in the GN. Towards the top of the Unit hornblende mainly occurs as an alteration mineral. The primary hornblende is normally zoned, being more blue-green and sodic around the outer rim. This could be an indication of a change in fluid composition during cooling of the magma and

crystallization of hornblende. Interstitial quartz grains increase in abundance with height to approximately 25 vol% in the diorite at the top of the Unit. Apatite occurs as elongate to prismatic grains increasing in abundance towards the top of the Unit.

Opaque minerals comprise magnetite, ilmenite and sulphides with a combined concentration of less than 1 vol%. There is a slight increase in the grain size of the sulphides with height. Magnetite tends to be enclosed by biotite or phlogopite throughout the Unit (PLATE 9 C). The least altered rocks have interstitial sulphides together with biotite, hornblende and quartz. The sulphides appear to have been vein remobilized in the more altered rocks, being associated with the secondary hornblende and with magnetite. The main sulphides present are pyrrhotite, pentlandite and chalcopyrite.

Alteration

Amphibolitization of the orthopyroxene and clinopyroxene is extensive with secondary hornblende making up to 10 vol% of the rock. Chlorite dominates the centers of the pseudomorphosed grains. There is an increase in abundance of hornblende with height, which indicates a strong overprint of hydrothermal alteration of the top portion of the Unit, with the base being least altered.

PLATE 9

A. **Base of GN, SH176 UP25**. Gabbronorite, plagioclase (PLAG) laths enclosed in clinopyroxene (CPX). Note corona of hornblende (HNBL) around orthopyroxene (OPX). The plagioclase is partially saussuritized.

B. **GN, SH176 UP22**. Gabbronorite showing a weak preferred orientation of the plagioclase laths. Quartz (QTZ) is also present. Note plagioclase subgrain development in the center of the photo.

C. **GN, SH176 UP18**. Magnetite grain (light grey in colour) showing skeletal texture. The matrix is mainly biotite.

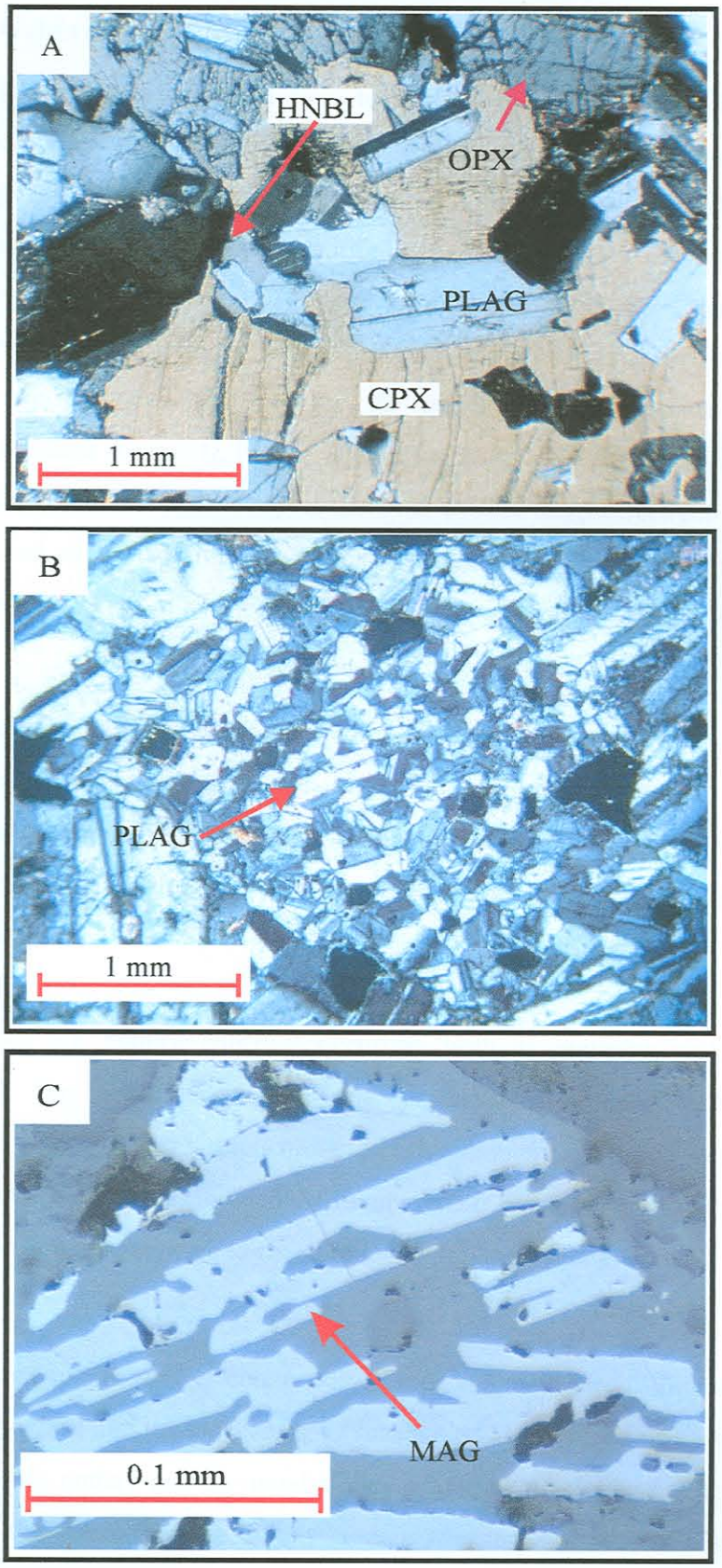

PLATE 9

3.7. Upper Gabbro

This Unit is composed mainly of fine- to medium-grained equigranular and seriate gabbroic rock. Closer to the roof contact the rocks become finer grained with long acicular plagioclase crystals (up to 5 mm) dominating the assemblage (PLATE 10 A). An up to 2 m thick aphanitic chilled margin containing composite inclusions of quartz (PLATE 10 B) that are possibly derived from the Klapperkop Quartzite Member characterizes the contact with the roof rocks. Plagioclase (40-60%), orthopyroxene (25-40%) and clinopyroxene (5-10%) are the major cumulus phases in the Unit. Intercumulus phases are quartz, biotite, apatite and zircon. Quartz ranges between 5 and 10 vol%, increasing towards the top of the Unit. Biotite ranges between 2 and 5 vol% with apatite and zircon making up between 1 and 2 vol%. Disseminated sulphides, less than 1 mm in size, occur in an irregular manner and make up less than 1 % of the rock.

Plagioclase occurs as lath-like cumulus- and anhedral interstitial grains. At times, the cumulus laths reach up to 3 mm in length with no preferred orientation. Occasionally, smaller radiate grain aggregates of alkali feldspar are observed, mainly towards the top of the Unit (PLATE 10 A). Many of the grains show Carlsbad twinning and partial saussuritization.

The pyroxenes are mainly anhedral occurring both as cumulus and intercumulus phases, with the cumulus mode being dominant. Orthopyroxene shows the characteristic pink to green pleochroism of hypersthene with no visible sign of exsolution lamellae of clinopyroxene. Clinopyroxene decreases gradually with height whereas orthopyroxene appears to remain broadly constant in abundance.

Quartz, biotite, apatite and zircon occur as late stage phases filling the interstices between plagioclase and the pyroxenes. Quartz grains are rounded or irregular in shape and may slightly embay and surround stubby grains of plagioclase. The quartz grain inclusions in the aphanitic zone usually contain intergrowths of apatite and inclusions of zircon (PLATE 10 B). Biotite displays light brown to dark brown pleochroism, and

increases in abundance with height. Apatite occurs as small colourless, subhedral (acicular), crystals within feldspar, quartz and other interstitial phases.

The sulphides are mainly pyrrhotite with minor chalcopyrite and pentlandite. Pyrrhotite occurs as finely disseminated grains, commonly less than 50 μm in size, but occasionally reaching up to 1 mm. Pyrrhotite occasionally shows globular and flame-like inclusions of pentlandite.

Alteration

Secondary hydrothermal alteration is pervasive throughout the Unit forming amphibole, alkali feldspar, chlorite and epidote. Plagioclase is altered to sericite, epidote and saussurite. Pyroxene is altered to amphibole. As in the alteration assemblage of the BGAB two types of amphibole are observed i.e. hornblende and actinolite tremolite.

PLATE 10

A. **UGAB, SH176 UP 2**. Elongated plagioclase laths and radial alkali feldspar. Matrix contains plagioclase, orthopyroxene, clinopyroxene, hornblende and biotite. Some of the plagioclase laths are saussuritized.

B. **UGAB, SH176 UP1**. Chilled margin, containing quartz grain aggregates. Note growth of needle-like grains of apatite along grain boundaries.

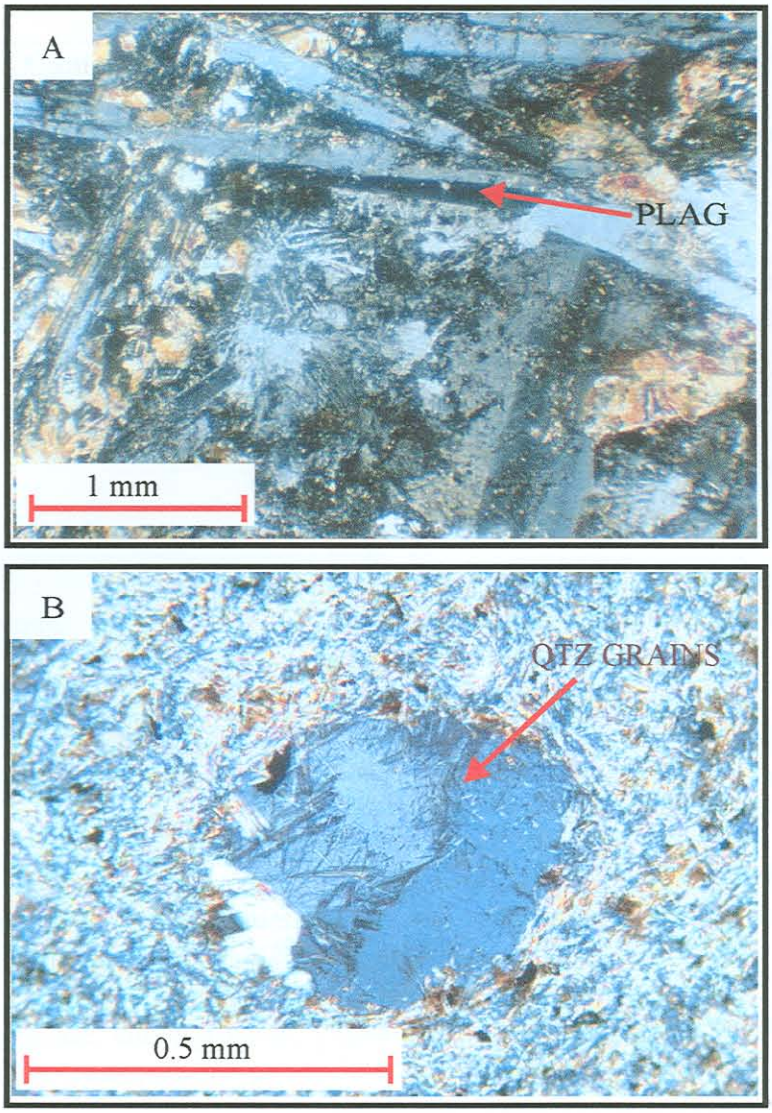

PLATE 10

3.8. Summary

The major-, intercumulus-, and alteration mineralization of the Uitkomst Complex is summarized in Table 2.

Table 2. Cumulus, intercumulus and alteration minerals in the different lithological units

Unit	Main Cumulus Minerals	Intercumulus and Alteration Minerals
UGAB	Plagioclase, orthopyroxene, clinopyroxene.	Quartz, biotite, apatite, zircon, pentlandite, chalcopyrite. Amphibole (hornblende and tremolite-actinolite, chlorite, carbonate, epidote, sericite, saussurite.
GN	Plagioclase, orthopyroxene, clinopyroxene, hornblende.	Phlogopite, biotite, hornblende, quartz, apatite, magnetite, chlorite, sulphides. Amphibole, chlorite.
PXT	Orthopyroxene, olivine, chromite.	Plagioclase, clinopyroxene, mica (phlogopite), amphibole, quartz, pyrrhotite, pentlandite, chalcopyrite. Tremolite, phlogopite, fuchsite, amphibole.
MHZBG	Olivine, orthopyroxene, chromite.	Plagioclase, clinopyroxene, amphibole, pyrrhotite, pentlandite, chalcopyrite. Serpentine, magnetite, lizardite, chrysotile, talc, hornblende.
PCR	Olivine, chromite, orthopyroxene, sulphides.	Sulphides, plagioclase, muscovite, phlogopite, amphibole. Serpentine, amphibole, chlorite, calcite, phlogopite, muscovite, violarite
LHZBG	Olivine, orthopyroxene, clinopyroxene, sulphides, chromite.	Biotite, K-feldspar. Chrysotile, lizardite, magnetite, magnesite, chlorite, tremolite-actinolite, phlogopite, millerite, amphibole, violarite.
BGAB	Plagioclase, clinopyroxene, orthopyroxene, chromite.	Quartz, mica, K-feldspar, magnetite, ilmenite, chalcopyrite, pyrrhotite, pentlandite. Amphibole (hornblende and tremolite-actinolite, chlorite, carbonate, epidote, saussurite, calcite.

4. WHOLE ROCK GEOCHEMISTRY

4.1. Introduction

Sixty samples from all major rock units have been analysed for major and selected trace elements by XRF at the University of Pretoria, using an ARL 8420 wavelength dispersive spectrometer. Analytical procedures are given in Appendix I and the analyses are listed in Appendix II. Thirty-six samples were analysed for additional trace elements, including REE, by ICP-MS at the University of Cape Town. Sulphur was separately determined for all samples by LECO – titration at the University of Quebec at Chicoutimi. Copper was determined by atomic absorption and the PGE were determined by INAA, all at the University of Quebec at Chicoutimi. This chapter presents the major and trace element data to ascertain effects of alteration, the crystallisation trends with the aid of variation diagrams and the overall mineral distribution throughout the Complex.

4.2. The Effects of Alteration on Major-, Trace- and Rare Earth Element Concentration

It has been pointed out in the previous chapter that many of the rocks of the Uitkomst Complex are highly altered. The alteration may overprint the original geochemical signatures of the rocks and thereby render the determination of the genesis of the Complex and its mineralization difficult. It is therefore important to determine which of the analysed elements behaved in a mobile manner during alteration.

Zirconium has been shown to be relatively immobile during alteration and high-grade metamorphism, for example in the Sao Francisco craton of Brazil (Figueiredo, 1980). Thus, incompatible elements that have remained immobile during alteration should correlate closely with Zr. Most of the REE have apparently remained immobile (e.g. La, Yb, Lu) as is evidenced by their good positive correlation with Zr (Fig. 4.1. (a)). Elements that show a poor correlation with Zr, for example Rb, Th (Fig. 4.1. (b)), P, Ti, K (Fig. 4.2.) and, to a lesser extent, Na (not shown) and Eu (Fig. 4.1. (a)) may have been affected by

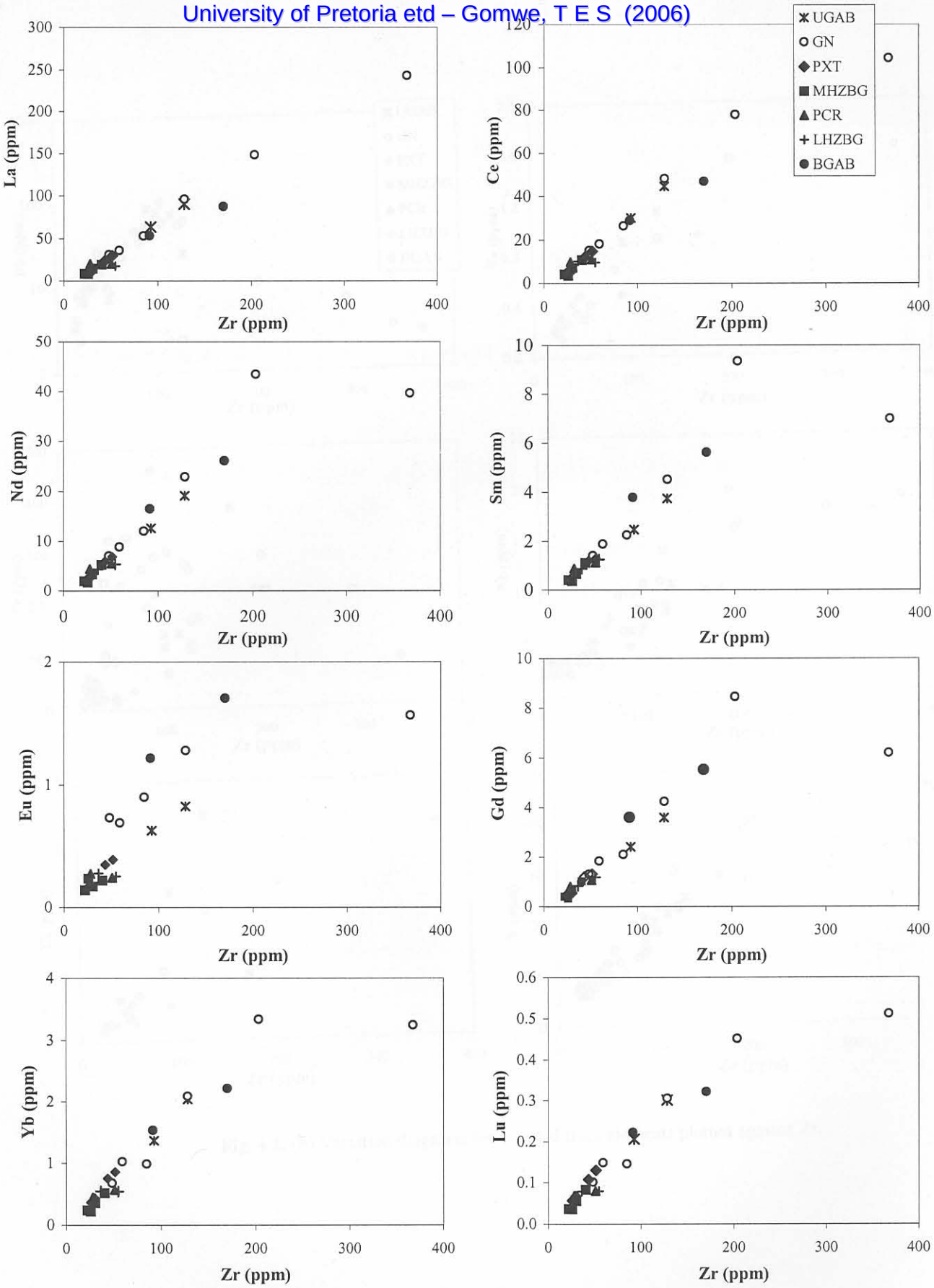

Fig. 4.1. (a) Variation diagrams of selected REE versus Zr

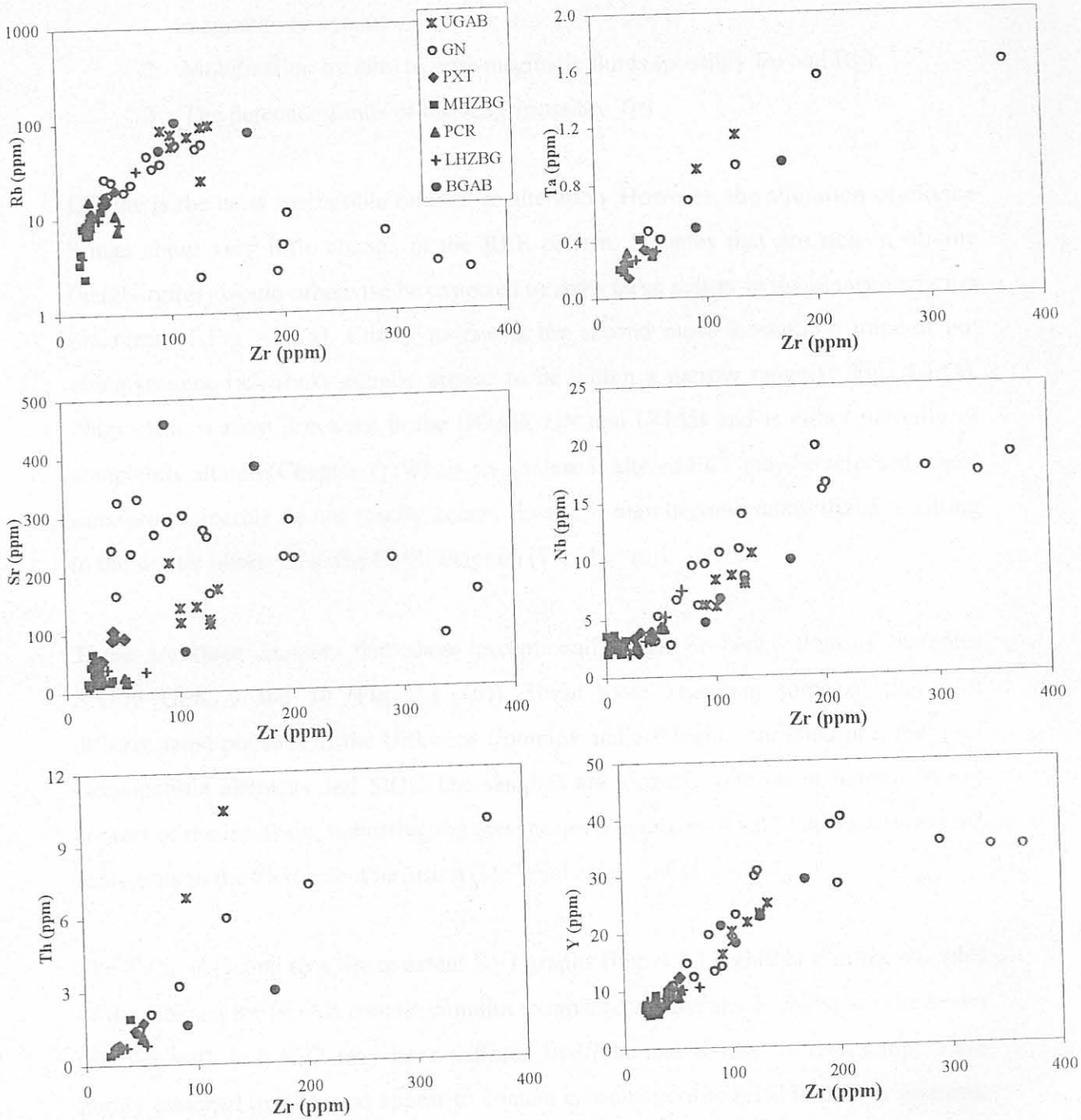

Fig. 4.1. (b) Variation diagrams for selected trace elements plotted against Zr.

1. The intermittent appearance or disappearance of a cumulus phase e.g. magnetite or apatite.
2. Mobilization by late- to post-magmatic fluids (possibly Eu and Rb).
3. The detection limits of the XRF (possibly Th).

Olivine is the most susceptible mineral to alteration. However, the alteration of olivine brings about very little change in the REE pattern. Samples that are rich in olivine (harzburgites) would otherwise be expected to show large scatter in the binary variation diagrams of Fig. 4.1.(a). Clinopyroxene is the second most susceptible mineral but clinopyroxene-rich rocks equally appear to be within a narrow range in Fig. 4.1.(a). Plagioclase is most prevalent in the BGAB, GN and UGAB and is either partially or completely altered (Chapter 3). When plagioclase is altered Eu^{2+} may be released, since saussurite minerals do not readily accept Eu and it may become remobilized resulting in the scatter observed in the Eu/Zr diagram (Fig. 4.1. (a)).

There are three samples that show exceptionally high Zr concentrations (samples SH176 UP8, 9 and 10 (Fig. 4.1. (b)). These rocks represent some of the most differentiated portions of the Uitkomst Complex and are highly enriched in a range of incompatible elements and SiO_2. The samples are located some 60 m below the top contact of the intrusion, indicating the presence of a highly evolved "sandwich horizon" analogous to the Skaergaard intrusion (De Waal *et al.*, 2001).

The TiO_2, P_2O_5 and to a lesser extent K_2O graphs (Fig. 4.2.) highlight that the samples of the GN and the BGAB contain cumulus magnetite, apatite and K-feldspar. The seven samples with low K_2O may have suffered hydrothermal K-loss. A few samples are highly enriched in P_2O_5 and appear to contain cumulus apatite (visible in thin sections, Chapter 3). Notably, they are not particularly SiO_2 or Zr-enriched, indicating that cumulus apatite appeared before zircon.

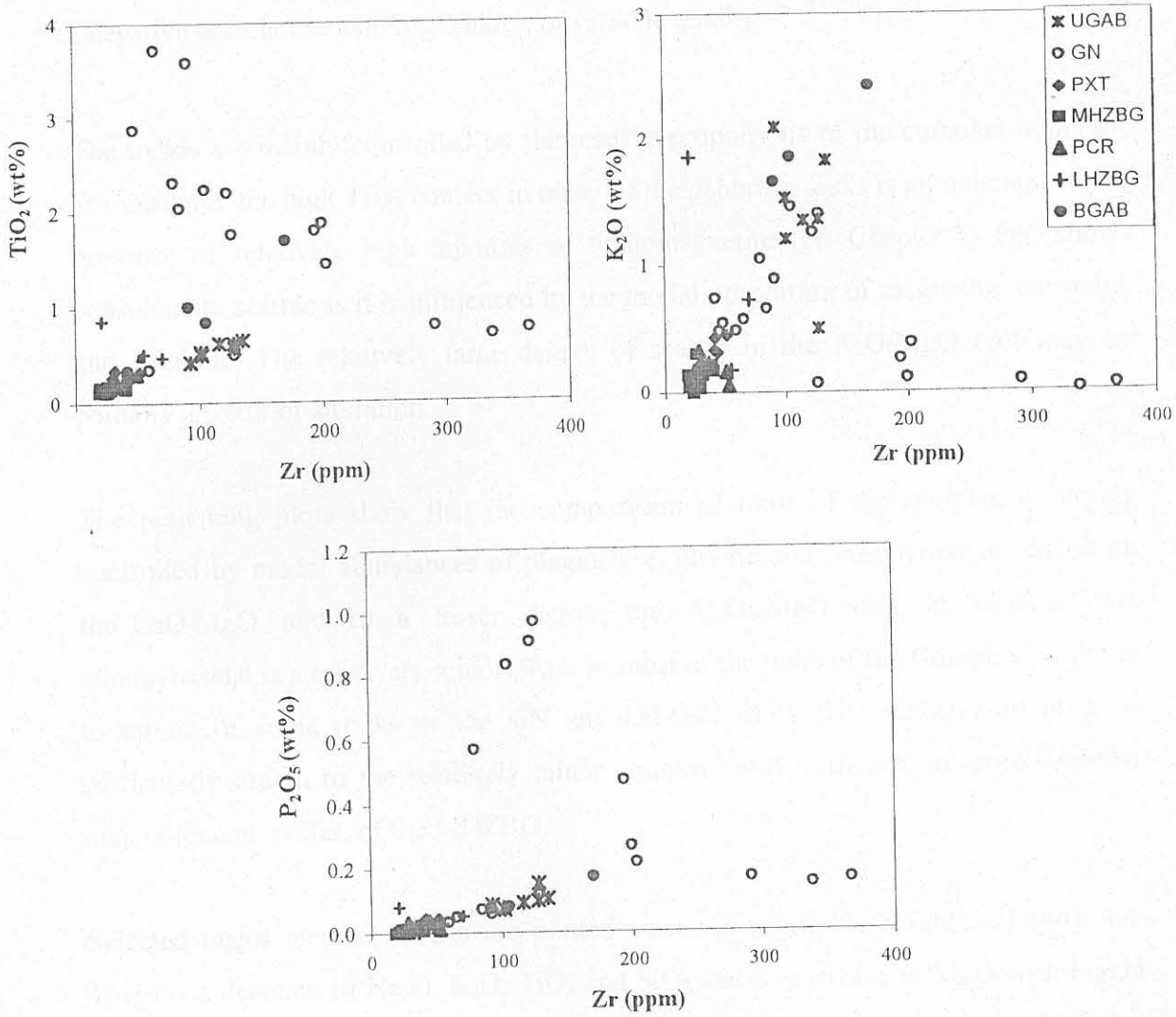

Fig.4.2. Variation diagrams for selected element oxides plotted against Zr

4.3. Major Element Chemistry

In general, more primitive igneous rocks are richer in MgO and poorer in FeO, Na_2O, K_2O, CaO and SiO_2 than more evolved rocks. Thus these oxides alone or in some combination, may be used as indices of differentiation. Selected major element oxides are plotted against MgO in Figure 4.3. Apart from FeO, all major element oxides show a negative correlation with MgO albeit of variable quality.

The trends are mainly controlled by the relative proportions of the cumulus minerals. For example, the high TiO_2 content in many of the gabbroic rocks is an indicator of the presence of relatively high amounts of titanomagnetite (cf. Chapter 3). FeO shows considerable scatter as it is influenced by the modal proportion of magnetite, chromite, and sulphide. The relatively large degree of scatter in the K_2O/MgO plot may be partially a result of alteration.

The remaining plots show that the composition of most of the samples is largely controlled by modal abundances of plagioclase, olivine and orthopyroxene. Based on the CaO/MgO and, to a lesser degree, the Al_2O_3/MgO plot, it is clear that clinopyroxene is a relatively minor phase in most of the units of the Complex, with the exception of some rocks of the GN and LHZBG units. The reader's attention is particularly drawn to the relatively minor compositional variation, in terms of most major element oxides, of the MHZBG.

Selected major element oxides are plotted versus stratigraphic height in Figure 4.4. There is a decrease in Na_2O, K_2O, TiO_2 and SiO_2 and an increase in MgO with height from the base of the Complex to the base of the MHZBG which is opposite of what is expected in a progressively differentiating magma chamber. The most noticeable feature of the diagrams is the primitive nature of the MHZBG indicated by the relatively low Na_2O, K_2O, TiO_2 and SiO_2 and high MgO values and the lack of variation of these oxides with height. The latter feature is again contrary to the trend expected during differentiation upon cooling. From the top of the MHZBG to the top of the GN, normal differentiation trends are observed, but a marked reversal is seen at the base of the UGAB.

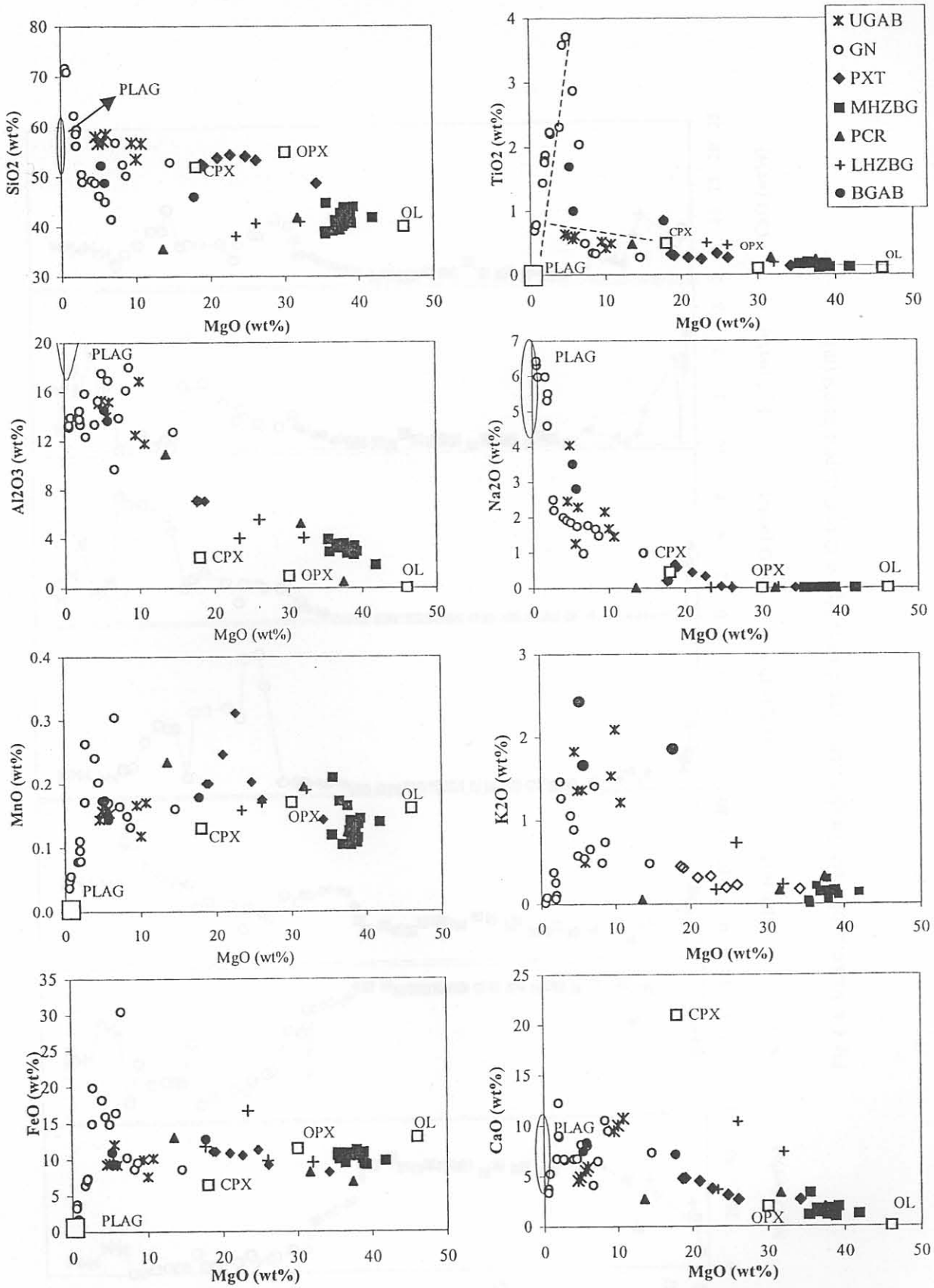

Fig. 4.3. Variation diagrams for major elements, plotted against MgO.
(Compositions of mineral phases are from Gauert (1998))

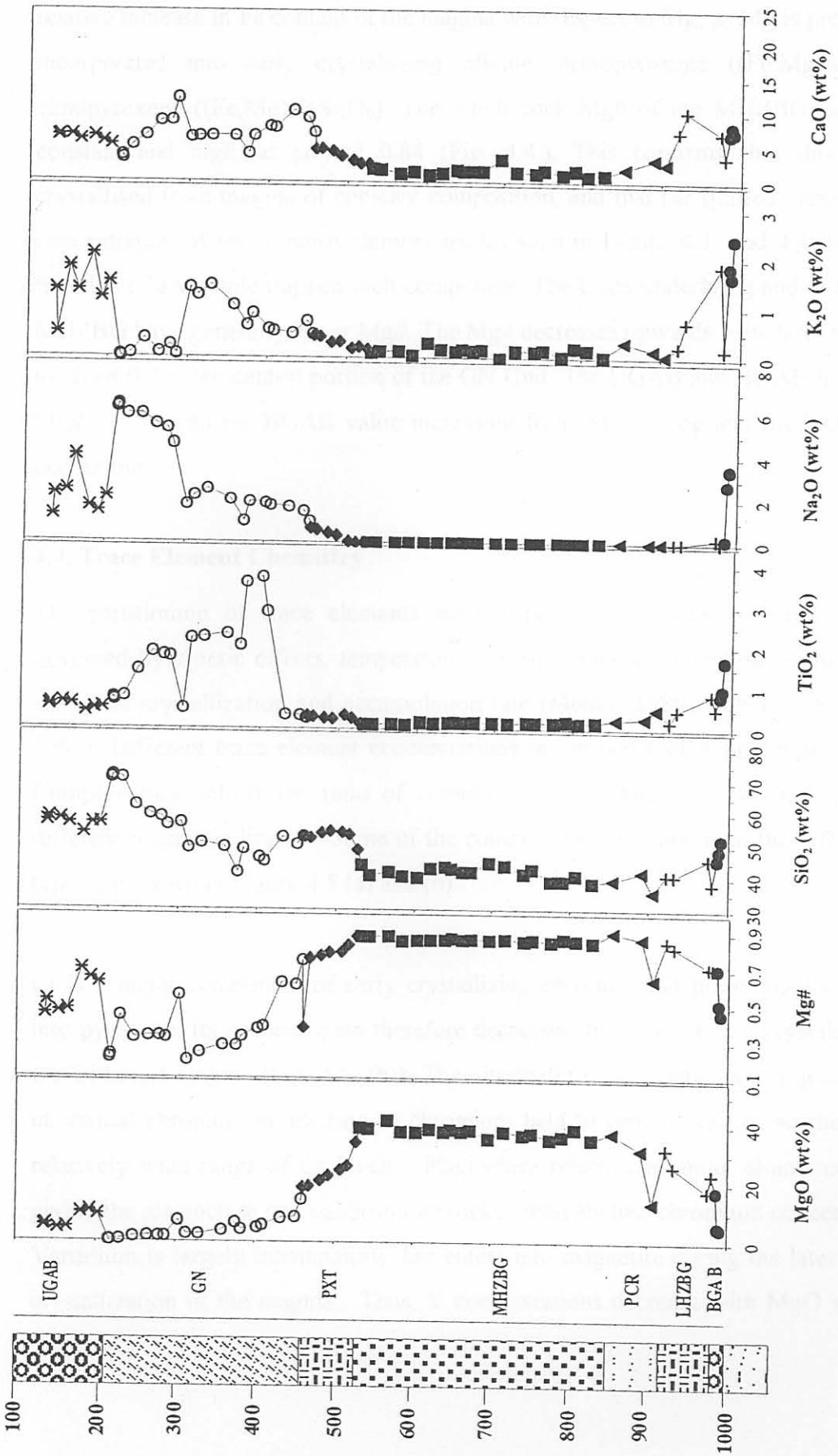

Fig.4.4. Variation of selected major element oxides and Mg# with stratigraphic height (m).

The variation of the Mg number (calculated as the ratio MgO/(MgO + FeO) and hereafter abbreviated to Mg#) reflects the fractionation trend of magma, namely the relative increase in Fe content of the magma with respect to Mg, as Mg is preferentially incorporated into early crystallizing olivine, orthopyroxene ($(Fe,Mg)Si_2O_6$) and clinopyroxene ($(Fe,Mg)CaSi_2O_6$). The whole-rock Mg# of the MHZBG is relatively constant and high, at around 0.84 (Fig. 4.4.). This confirms that this Unit has crystallised from magma of constant composition, and that the limited variation in the concentration of some major element oxides seen in Figure 4.3. and 4.4. is largely a function of a variable trapped melt component. The Units underlying and overlying the MHZBG have generally lower Mg#. The Mg# decreases upwards from 0.84 in the PXT to about 0.2 in the central portion of the GN Unit. The UGAB and BGAB have similar Mg# (~0.5) with the BGAB value increasing from base to top and the UGAB value decreasing.

4.4. Trace Element Chemistry

The partitioning of trace elements with respect to the rock-forming minerals is governed by kinetic effects, temperature, pressure, melt composition, ionic radii, site sizes and crystallization and accumulation rate (Möller, 1988; Ulmer, 1989; Hanson, 1989). Different trace element concentrations in various rock types of the Uitkomst Complex may reflect the ratio of cumulus to intercumulus phases and possibly a different magmatic lineage. Some of the compositional variations in the different rock types are shown in Figure 4.5.(a) and (b).

Cr is a major component of early crystallizing chromite and preferentially partitions into pyroxene. Its concentration therefore decreases during fractional crystallization of the Uitkomst magma (Fig. 4.5. (b)). The ultramafic rocks contain varying amounts of interstitial chromite, in addition to chromium held in orthopyroxene, so they show a relatively wide range of Cr levels. Plagioclase rejects chromium almost completely giving the plagioclase rich gabbronorite rocks relatively low chromium concentrations. Vanadium is largely incompatible, but enters into magnetite during the later stages of crystallization of the magma. Thus, V concentrations decrease with MgO within the

GN (Fig. 4.5. (a)). The exceptionally high V value in one sample from the GN is attributed to the abundance of titanomagnetite, which can be identified in thin section.

Strontium has an ionic radius of 1.18Å allowing it to substitute for Ca (1.01Å) (D = 1.83, Rollinson, 1993) and K (1.33Å). The partitioning of Sr into plagioclase is more pronounced than into other cumulus phases and ultramafic rocks show depletion in Sr relative to norites and gabbronorites of the BGAB and GN units (Fig. 4.5.(a)). There is a variation factor of about 5 in the gabbroic Units amongst samples with the same MgO content (about 5%) indicating the presence of Mg-free phases other than plagioclase, including quartz, magnetite, and K-feldspar, which all accommodate little or no Sr.

P_2O_5 is present only in trace to minor amounts and behaves as an incompatible element throughout much of the Complex. However, in some of the GN samples P_2O_5 contents increase significantly, due to the crystallization of apatite (Chapter 3).

Rb, Y, Nb, Th, Ta, P and Zr and the REE (D values less than unity) do not enter significantly into other cation sites in the major cumulus minerals of the Uitkomst Complex apart from Rb into K-feldspar (D = 3.06, Rollinson, 1993) in the GN. These elements become concentrated in the magma during differentiation until minerals such as zircon and apatite crystallize at a late stage. Low concentrations of Zr, Y and Rb in the ultramafic rocks therefore indicate the primitive nature of the magma and low proportions of trapped melt. Assuming that the Uitkomst Complex crystallized from magma similar to the B1-type magma of the Bushveld Complex (De Waal *et al.*, 2001), the ultramafic rocks contain about 20-30% trapped melt. This is in accord with the petrographic determinations, indicating roughly 20% intercumulus material. The gabbroic rocks show the largest variation in highly incompatible trace elements (Fig. 4.5. (a) and (b)) indicative of their enrichment in the differentiating magma. The gabbroic rocks should show the appearance of K-feldspar, apatite, zircon, and possibly trace amounts of other phases such as monazite, sphene etc. however these could not be petrographically identified, due to the pervasive alteration of the differentiated rocks of the Complex.

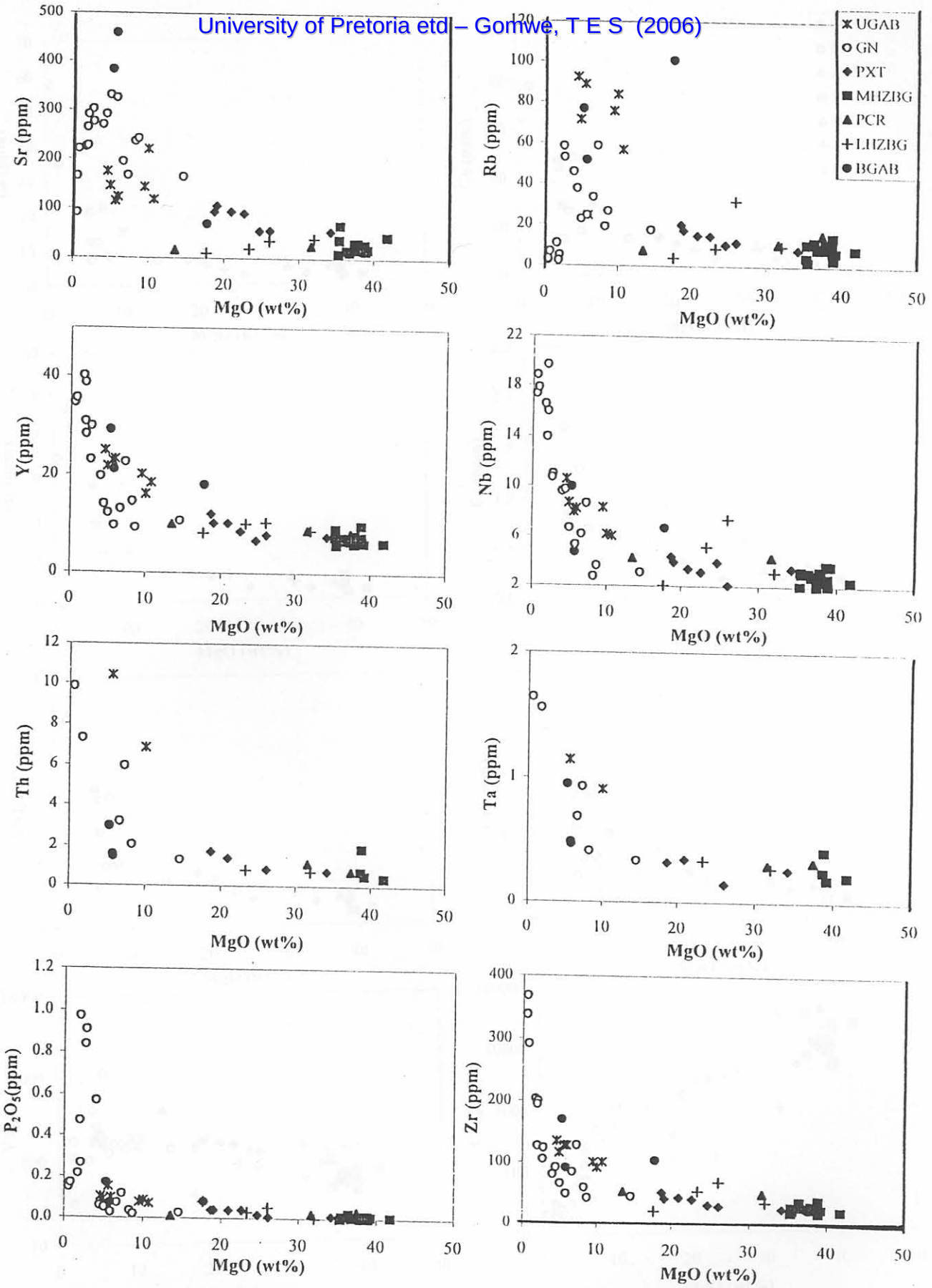

Fig.4.5.(a) Variation diagrams for selected trace elements versus MgO.

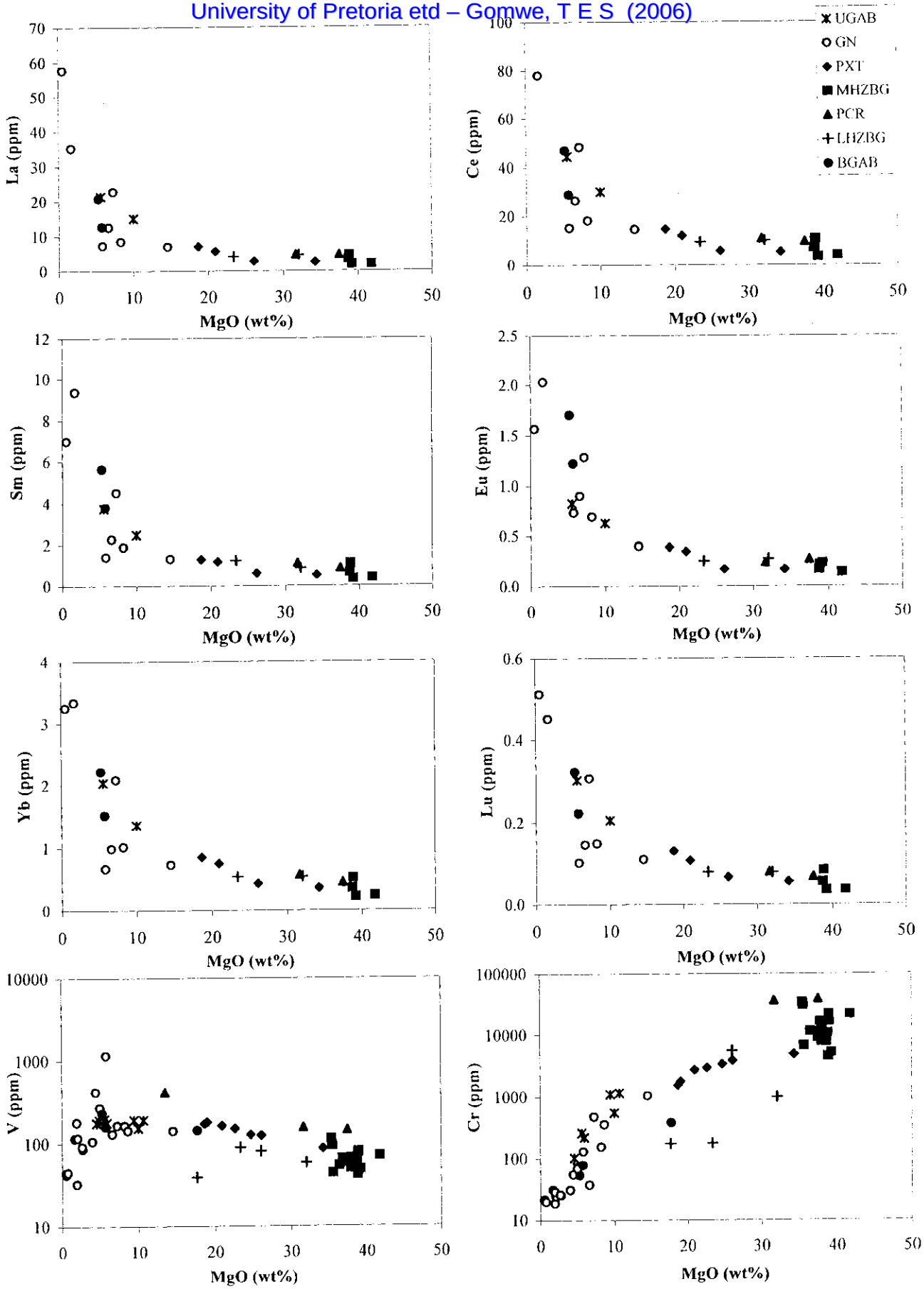

Fig.4.5.(b) Variation diagrams for selected trace elements and REE versus MgO.

Copper partitions preferentially into sulphides (Barnes and Maier, 1999) and Cu contents above 10-20 ppm indicate the presence of excess sulphide relative to the trapped melt. Fig. 4.6. shows that most of the samples have Cu values greater than this and that there is no direct correlation between Cu and MgO concentration, indicating the presence of cumulus sulphide. This point is also stressed by the plot of C/Zr versus MgO (Fig. 4.6.). The Cu/Zr ratio in the parental magma of the Bushveld Complex (B1) and of the chilled margins of the Uitkomst Complex is about 1. Therefore, if the Complex were a closed system, the bulk value of the Uitkomst Complex should equally be one. However, most of the Units show values exceeding unity (Fig. 4.6.), showing that most rocks of the Uitkomst Complex contain cumulus sulphides. In the UGAB and GN, Cu/Zr is <1, indicating that these rocks crystallized from metal depleted magma that had experienced a previous sulphide segregation event.

Nickel shows a relatively good positive correlation with MgO, particularly in the GN and UGAB Units. This is due to the compatible behaviour of Ni with respect to olivine (D=5.9-2.9), pyroxenes and chromite (D=29). In the BGAB and the ultramafic units the presence of sulphides overprints the signature of the silicates and chromite.

Cobalt also partitions into sulphides (D = 70, Barnes and Maier, 1999) as well as spinel (D=7.4 for magnetite, Rollinson, 1993) and olivine (D=6.6, Rollinson, 1993). Thus, in the sulphide-poor lithologies cobalt concentrations depend largely on modal proportions of olivine and chromite. This is reflected by the relatively high Co content of the sulphide-poor MHZBG Unit (Fig. 4.6.). In contrast, many samples from the sulphide-poor gabbroic rocks have low Co concentrations.

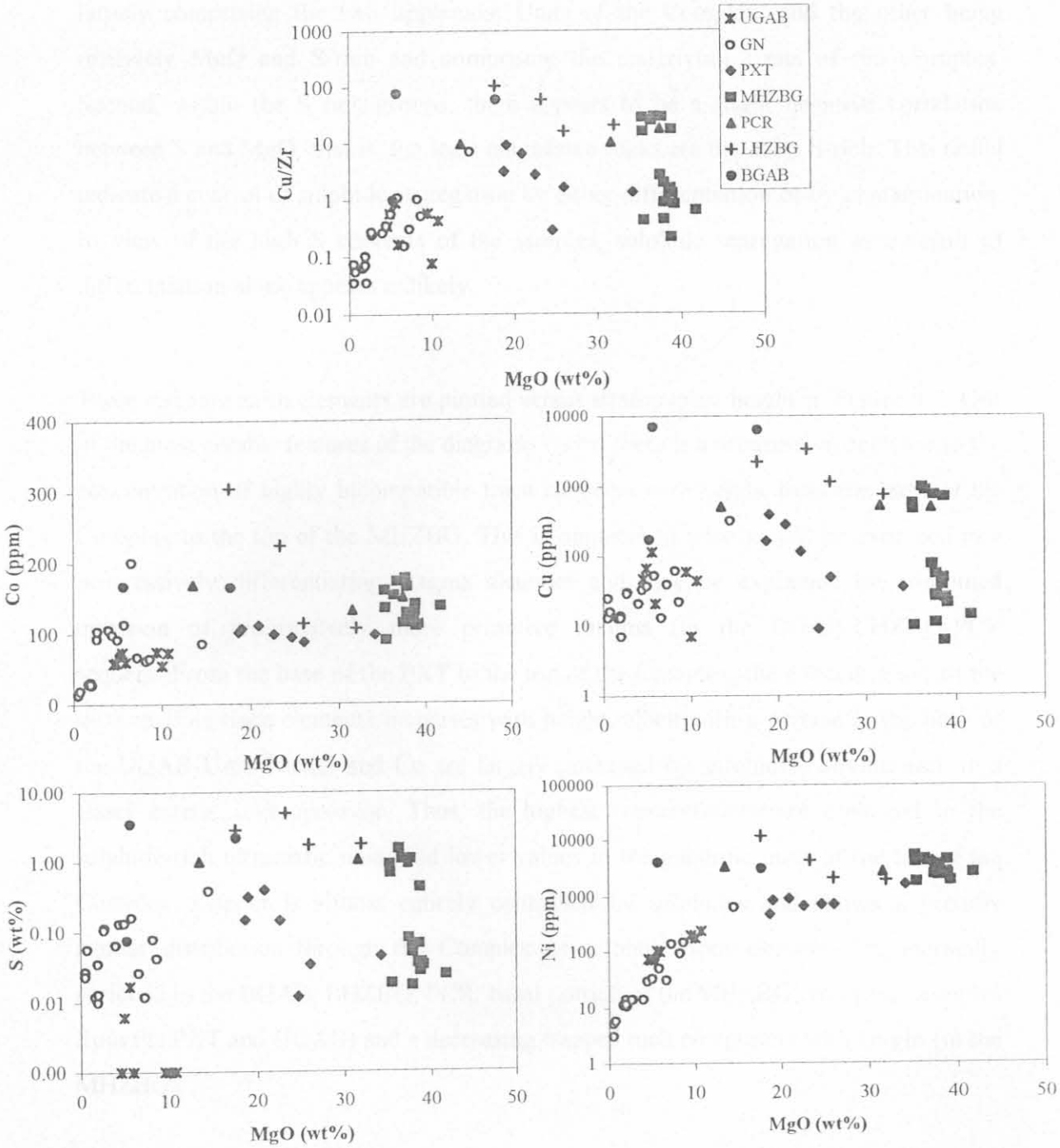

Fig.4.6. Variation diagrams for Cu/Zr and selected chalcophile trace elements plotted against MgO.

Several features are noteworthy in the S/MgO plot (Fig. 4.6.). First, the samples appear to fall into two distinct compositional fields, one being relatively MgO and S-poor and largely comprising the two uppermost Units of the Complex, and the other being relatively MgO and S-rich and comprising the underlying Units of the Complex. Second, within the S rich groups, there appears to be a slight negative correlation between S and MgO, that is, the least magnesian rocks are the most S-rich. This could indicate a control of sulphide segregation by either differentiation or by contamination. In view of the high S contents of the samples, sulphide segregation as a result of differentiation alone appears unlikely.

Trace and rare earth elements are plotted versus stratigraphic height in Figure 4.7. One of the most notable features of the diagrams is that there is a progressive decrease in the concentration of highly incompatible trace elements with height from the base of the Complex to the top of the MHZBG. This is opposite to what would be expected in a progressively differentiating magma chamber and may be explained by combined intrusion of progressively more primitive magma (in the BGAB-LHZBG-PCR sequenceFrom the base of the PXT to the top of the Complex, the concentration of the incompatible trace elements increases with height, albeit with a reverse at the base of the UGAB Unit. Nickel and Co are largely governed by sulphides, olivine and, to a lesser extent, orthopyroxene. Thus, the highest concentrations are observed in the sulphide-rich ultramafic units and lower values in the gabbroic units at the top of the Complex. Copper is almost entirely controlled by sulphides and shows a broadly similar distribution through the Complex as sulphur. Both elements are markedly enriched in the BGAB, LHZBG, PCR, basal portion of the MHZBG, and some samples from the PXT and UGAB) and a decreasing trapped melt component with height (in the MHZBG).

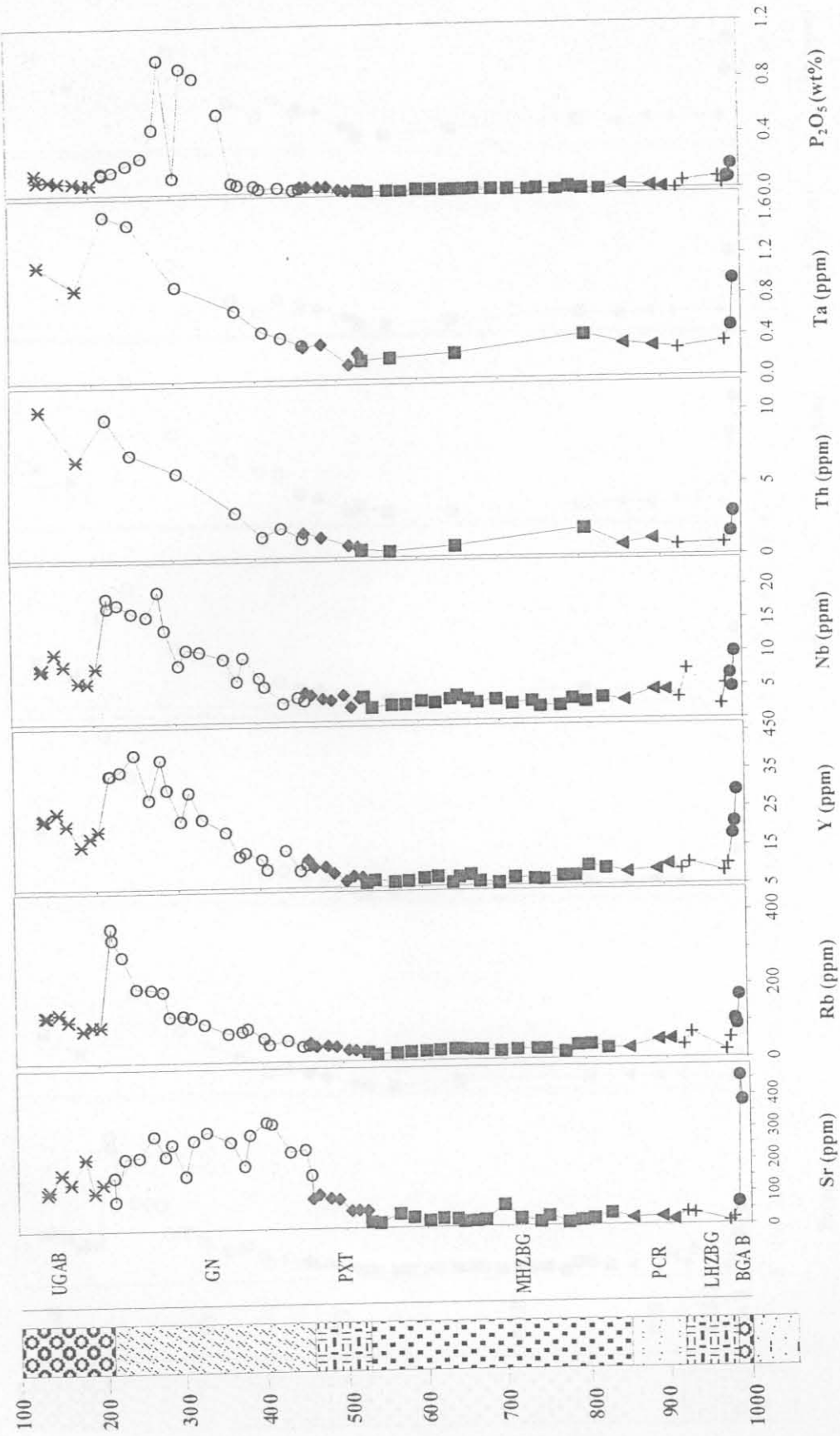

Fig.4.7. (a) Variation diagrams for selected trace elements versus stratigraphic height (m).

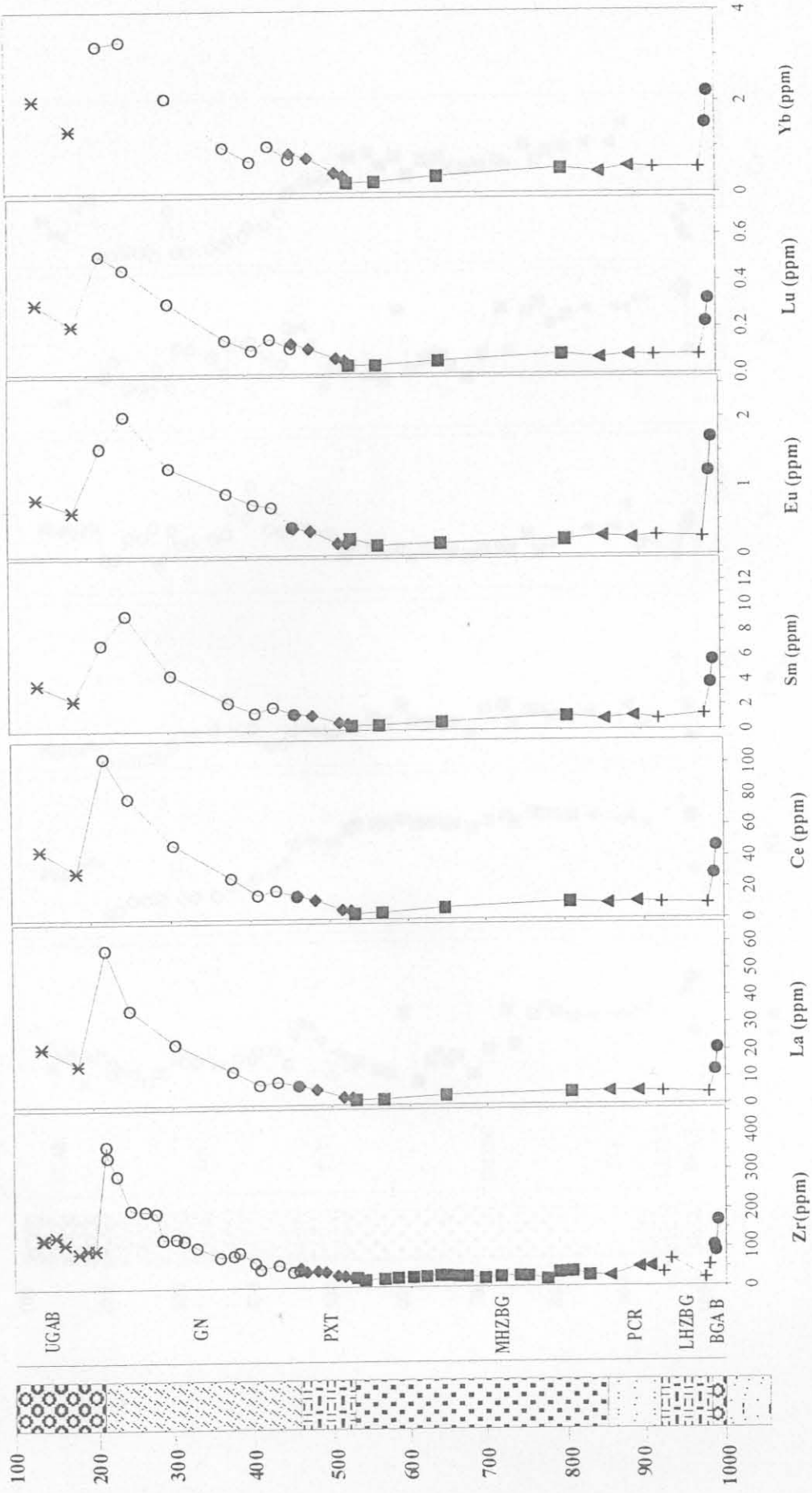

Fig.4.7. (b) Variation diagrams for selected trace elements versus stratigraphic height (m).

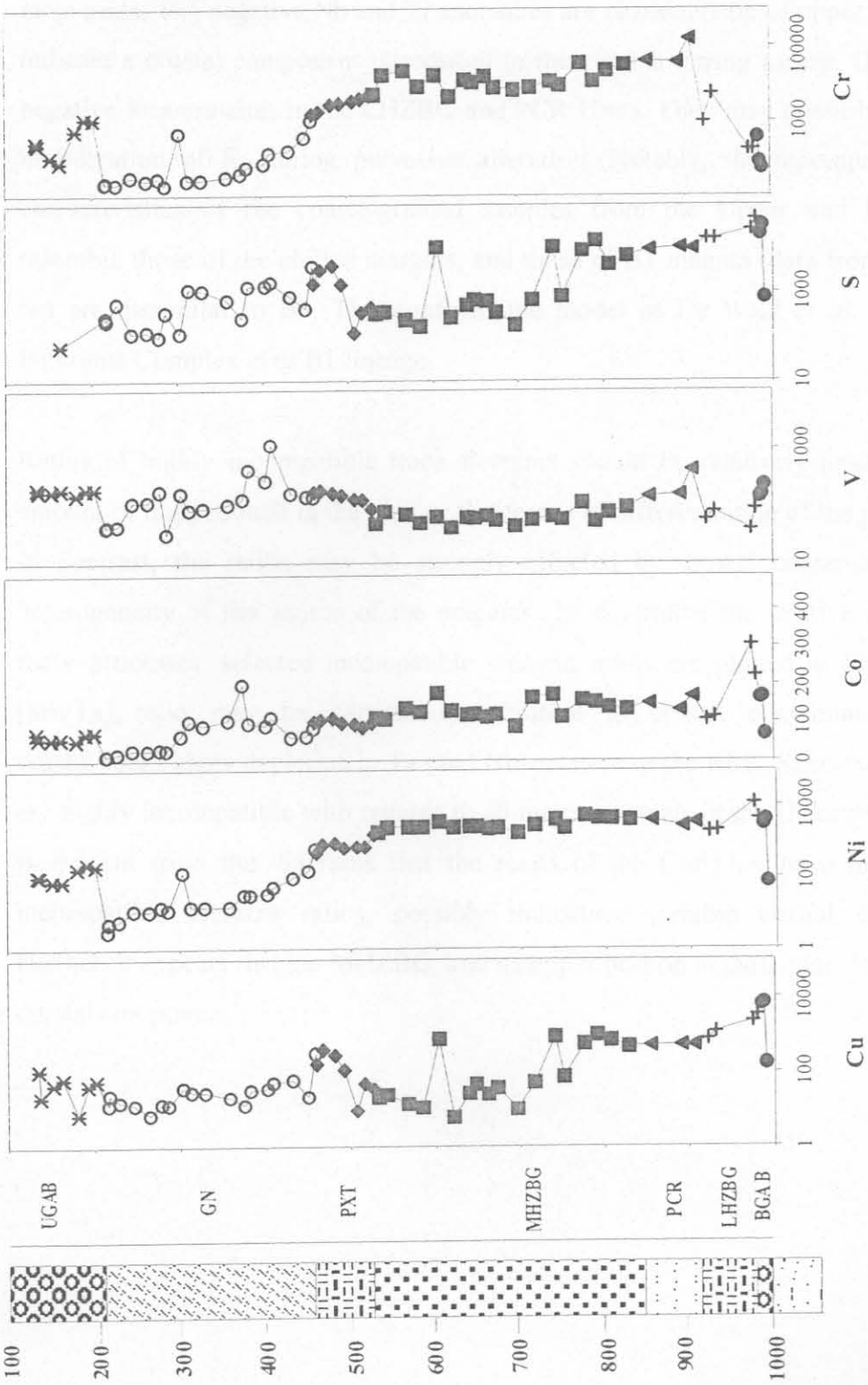

Fig.4.7(c) Variation diagrams for selected trace elements (ppm) versus stratigraphic height (m).

Spider diagrams of incompatible trace elements show that there is a similarity in shape between the units of the Complex (Fig. 4.8.). There is a negative Ti and Nb anomaly in most units. The negative Nb and Ti anomalies are characteristic of upper crust and may indicate a crustal component introduced to the magma during ascent. Of note are the negative Sr anomalies in the LHZBG and PCR Units. They may possibly be related to mobilization of Sr during pervasive alteration. Notably, the incompatible element characteristics of the coarse-grained samples from the Upper and Basal Gabbro resemble those of the chilled margins, and those of B1 magma (data from Curl, 2001), but are dissimilar to B3. This confirms the model of De Waal *et al.* 2001 that the Uitkomst Complex is of B1 lineage.

Ratios of highly incompatible trace elements should be relatively unaffected by the amount of trapped melt in the rock or the degree of differentiation of the parent magma. In contrast, the ratios may be strongly affected by crustal contamination, or by heterogeneity of the source of the magmas. To determine the relative importance of these processes, selected incompatible element ratios are plotted in Figure 4.9. The $[Sm/Ta]_n$ ratio may be particularly sensitive to crustal contamination, as many crustal rocks show depletion in Ta (and Nb) relative to the REE. Samarium, Th and Ta are highly incompatible with regards to all major minerals in the Uitkomst Complex. It is evident from the diagrams that the rocks of the Complex have highly variable incompatible element ratios, possibly indicating variable crustal contamination. Further, it appears that the MHZBG, and its upper portion in particular, have the lowest crustal component.

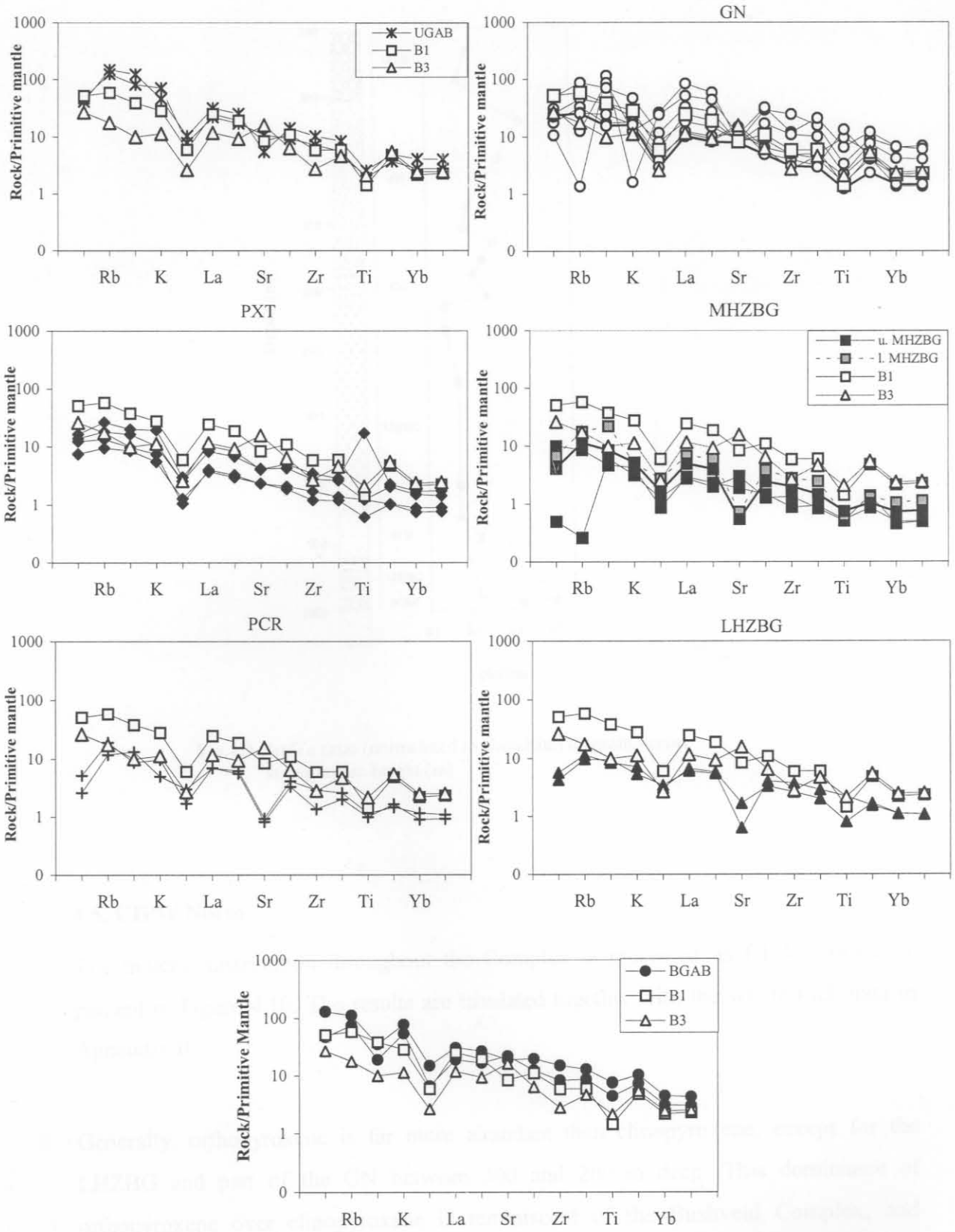

Fig. 4.8. Comparison between the average composition of B1-and B3-magmas and the different Units of the Utkomst Complex (B1 and B3 data from Curl, 2001. Mantle normalization factors are from Sun and McDonough, 1989).

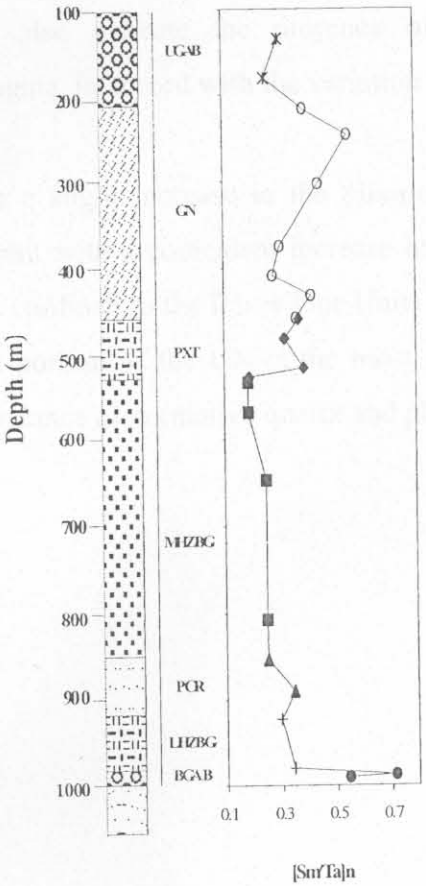

Fig.4.9. Sm/Ta ratio (normalized to chondrite) diagram versus stratigraphic height (m)

4.5. CIPW Norm

The mineral distribution throughout the Complex is presented as CIPW normative percent in Figure 4.10. The results are tabulated together with the whole rock data in Appendix II.

Generally, orthopyroxene is far more abundant than clinopyroxene, except for the LHZBG and part of the GN between 300 and 200 m deep. This dominance of orthopyroxene over clinopyroxene is reminiscent of the Bushveld Complex, and expected in view of the results of De Waal et al. (2001) who established a common age and magmatic lineage for the two complexes. The appearance of orthopyroxene before

clinopyroxene may also indicate the presence of a crustally derived siliceous component in the magma, in accord with the variation seen in Figure 4.9.

There appears to be a slight increase in the olivine content towards the top of the MHZBG, in agreement with a coincident increase in whole-rock Mg# (Fig. 4.6. (a)). Normative olivine is confined to the lower four Units and a few isolated samples in the GN. The uppermost portion of the GN is the most differentiated of the Complex as indicated by the abundance of normative quartz and plagioclase.

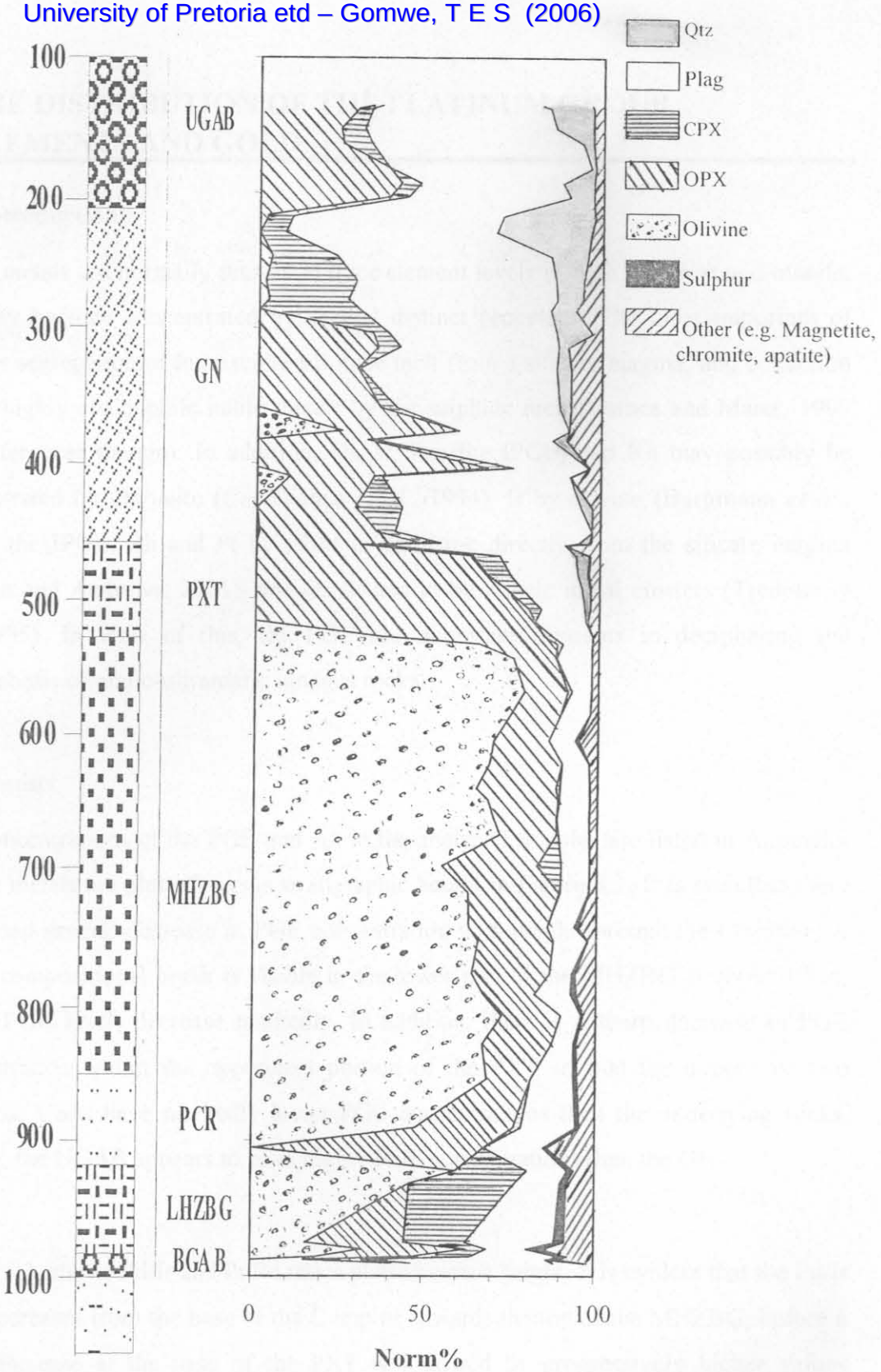

Fig. 4.10. Normalized data including sulphur concentrations Versus stratigraphic height (m)

5. THE DISTRIBUTION OF THE PLATINUM GROUP ELEMENTS AND GOLD

5.1. Introduction

Noble metals are normally present at trace element levels in both the crust and mantle, but may become concentrated by several distinct processes. The most important of these is segregation of immiscible sulphide melt from a silicate magma, and collection of the highly chalcophile noble metals by the sulphide melt (Barnes and Maier, 1999 and references therein). In addition, Os, Ir, Ru (the IPGE) and Rh may possibly be concentrated by chromite (Capobianco *et al.*, 1994), Ir by olivine (Bürgmann *et al.*, 1987), the IPGE, Rh and Pt by PGM crystallising directly from the silicate magma (Brenan and Andrews, 2001), and Os, Ir and Pt by atomic metal clusters (Tredoux *et al.*, 1995). In view of this, the PGE are important elements in deciphering the petrogenesis of mafic-ultramafic igneous rocks.

5.2. Results

The concentrations of the PGE and Au in the analysed samples are listed in Appendix II. The metals are plotted versus stratigraphic height in Figure 5.1. It is seen that there is a broad general decrease in PGE concentration with height through the Complex. A minor compositional break is visible in the lower part of the MHZBG at about 790m, where PGE levels decrease markedly. In addition, there is a sharp decrease in PGE concentration within the uppermost portion of the PXT so that the uppermost two Gabbroic Units have markedly lower PGE concentrations than the underlying rocks. Finally, the UGAB appears to have higher PGE concentrations than the GN.

Figure 5.2. shows Pd/Ir and Pt/Pd ratios plotted versus height. It is evident that the Pd/Ir ratio decreases from the base of the Complex towards the top of the MHZBG, before a sharp increase at the base of the PXT is followed by progressively higher values towards the top of the Complex. This is the opposite of what is observed in other layered intrusions such as the Bushveld Complex (Maier and Barnes, 1999), where Pd/Ir increases with height. The reason for this pattern is that Pd/Ir is a crude

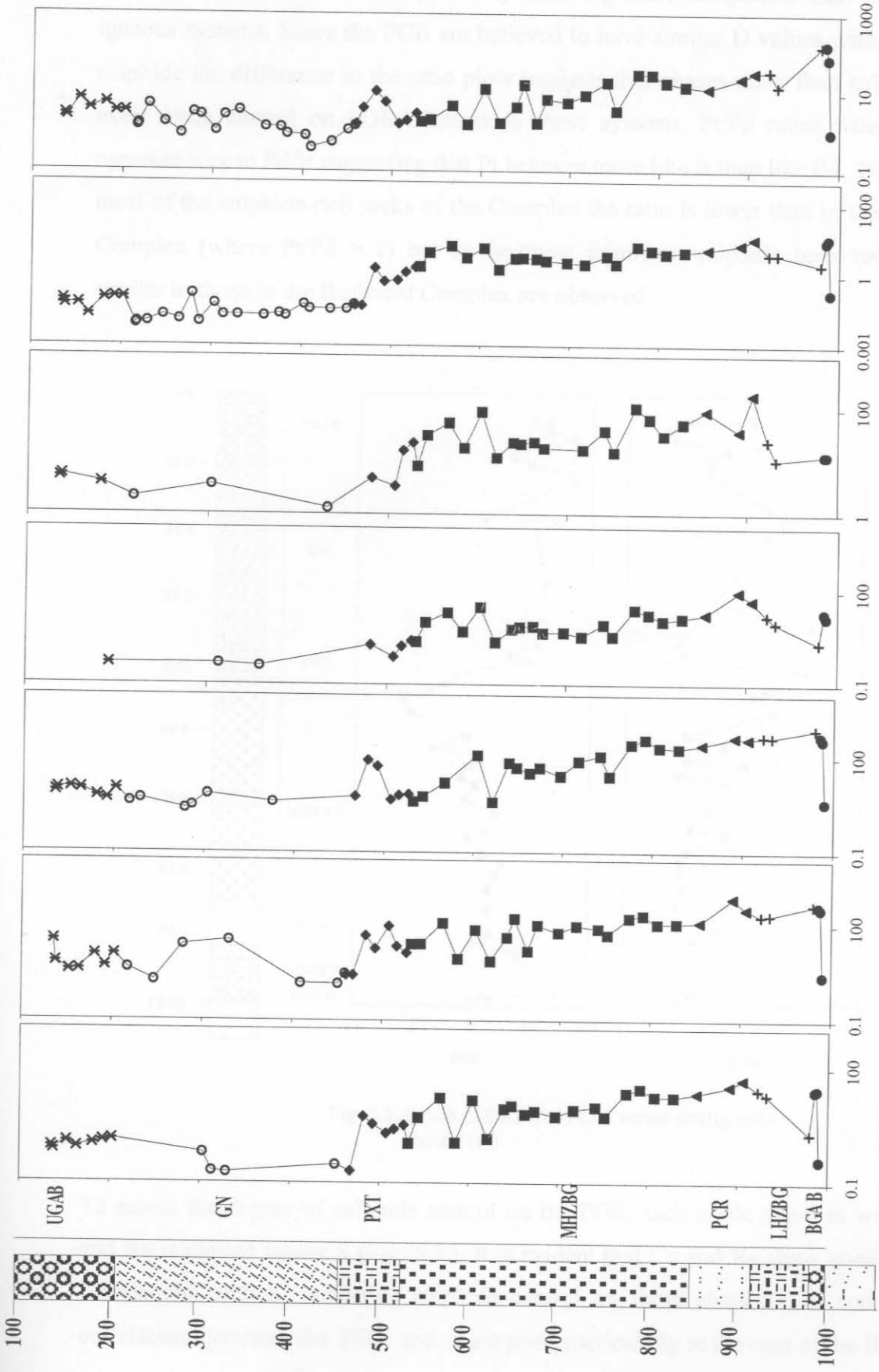

Fig. 5.1. Concentration of PGE and Au plotted versus stratigraphic height (m).

differentiation index, with Ir apparently behaving more compatible than Pd in many igneous systems. Since the PGE are believed to have similar D values with respect to sulphide the difference in the ratio plots suggests that phases other than sulphide also exert some control on PGE contents in these systems. Pt/Pd ratios behave in the opposite way to Pd/Ir suggesting that Pt behaves more like Ir than like Pd. Notably, for most of the sulphide-rich rocks of the Complex the ratio is lower than in the Bushveld Complex (where Pt/Pd > 1) but in the most primitive, sulphide poor rocks, ratios similar to those in the Bushveld Complex are observed.

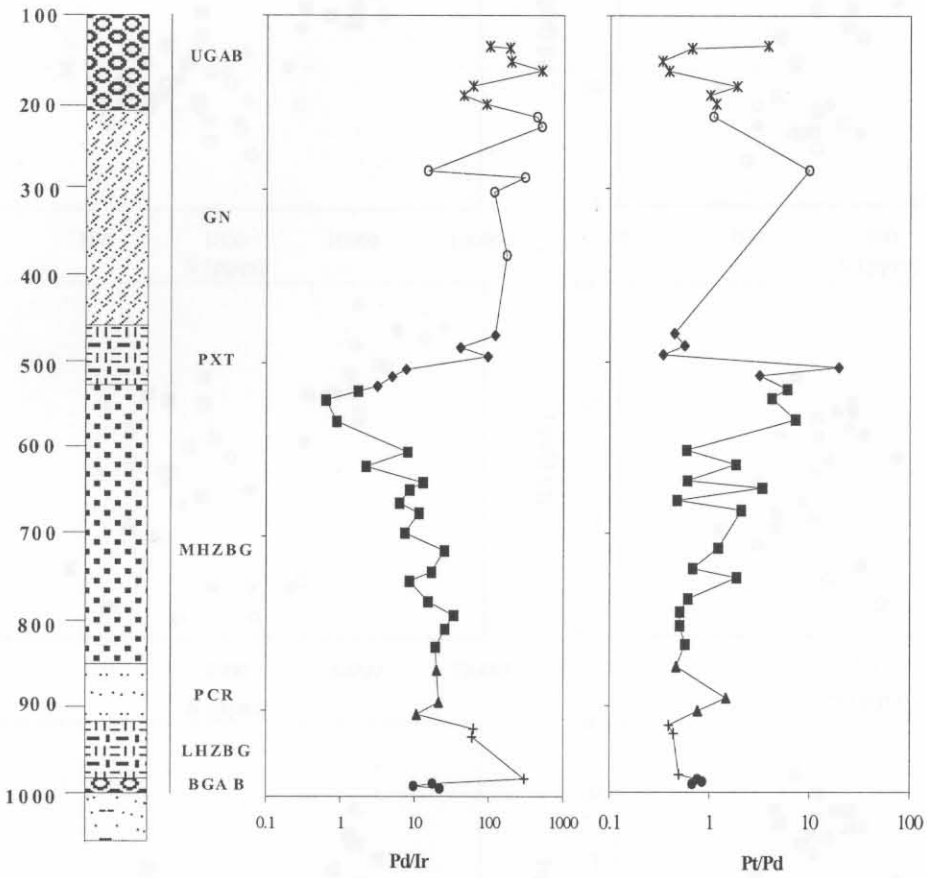

Fig. 5.2. Ratios of Pd/Ir and Pt/Pd versus stratigraphic height (m)

To assess the degree of sulphide control on the PGE, each noble metal as well as Cu and Re is plotted versus S (Fig. 5.3.). It is evident that Cu and Re show good positive correlations with S, indicating sulphide control on these elements. In contrast, the correlation between the PGE and S are poor, particularly in the case of the IPGE, Rh

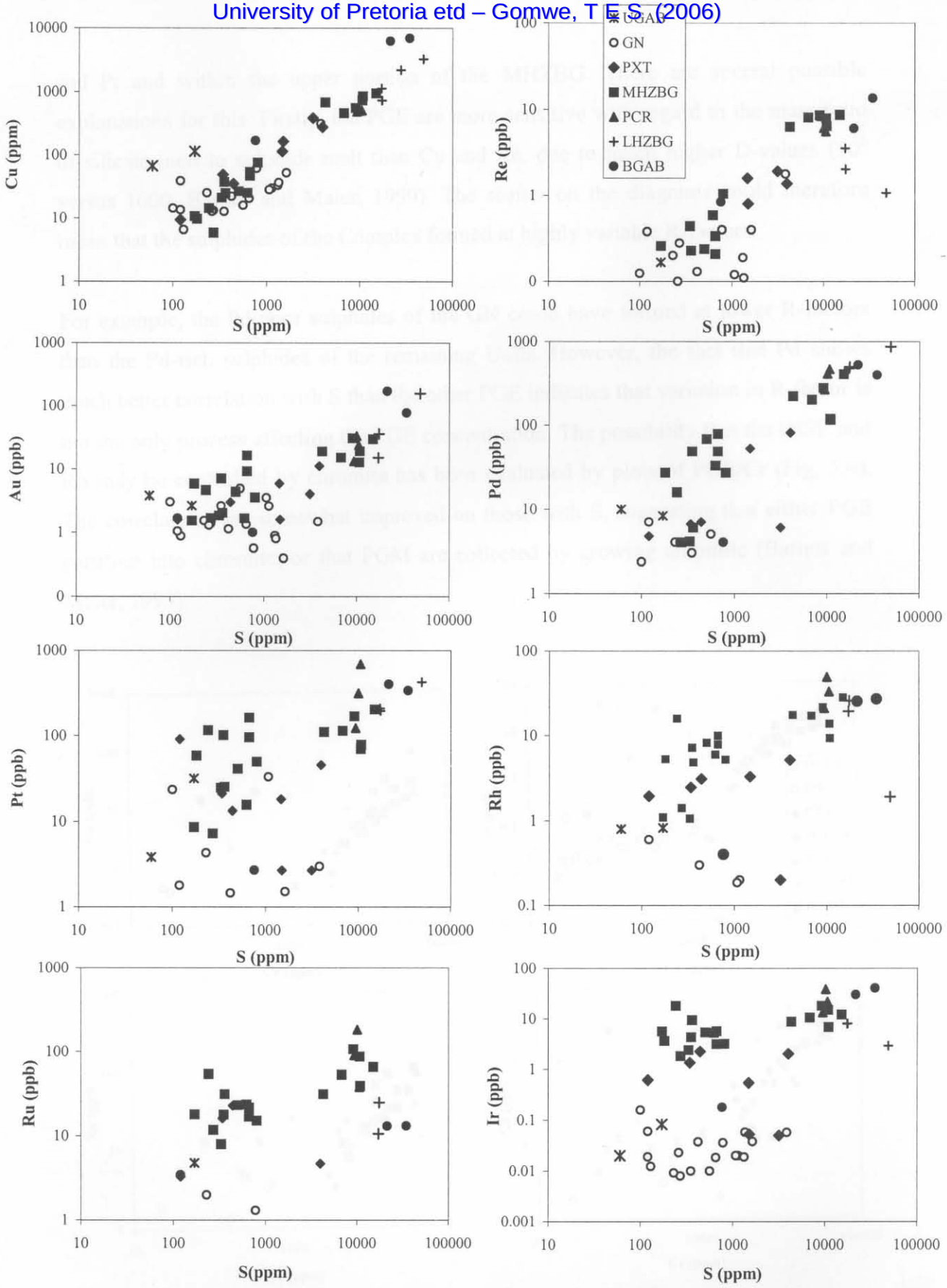

Fig 5.3. Variation diagrams of PGE, Cu and Re versus S.

and Pt and within the upper portion of the MHZBG. There are several possible explanations for this. Firstly, the PGE are more sensitive with regard to the mass ratio of silicate melt to sulphide melt than Cu and Re, due to much higher D-values (10^6 versus 1000, Barnes and Maier, 1999). The scatter on the diagrams could therefore mean that the sulphides of the Complex formed at highly variable R-factors.

For example, the Pd-poor sulphides of the GN could have formed at lower R-factors than the Pd-rich sulphides of the remaining Units. However, the fact that Pd shows much better correlation with S than the other PGE indicates that variation in R-factor is not the only process affecting the PGE concentration. The possibility that the IPGE and Rh may be controlled by chromite has been evaluated by plots of PGE/Cr (Fig. 5.4). The correlations are somewhat improved on those with S, suggesting that either PGE partition into chromite, or that PGM are collected by growing chromite (Barnes and Maier, 1999).

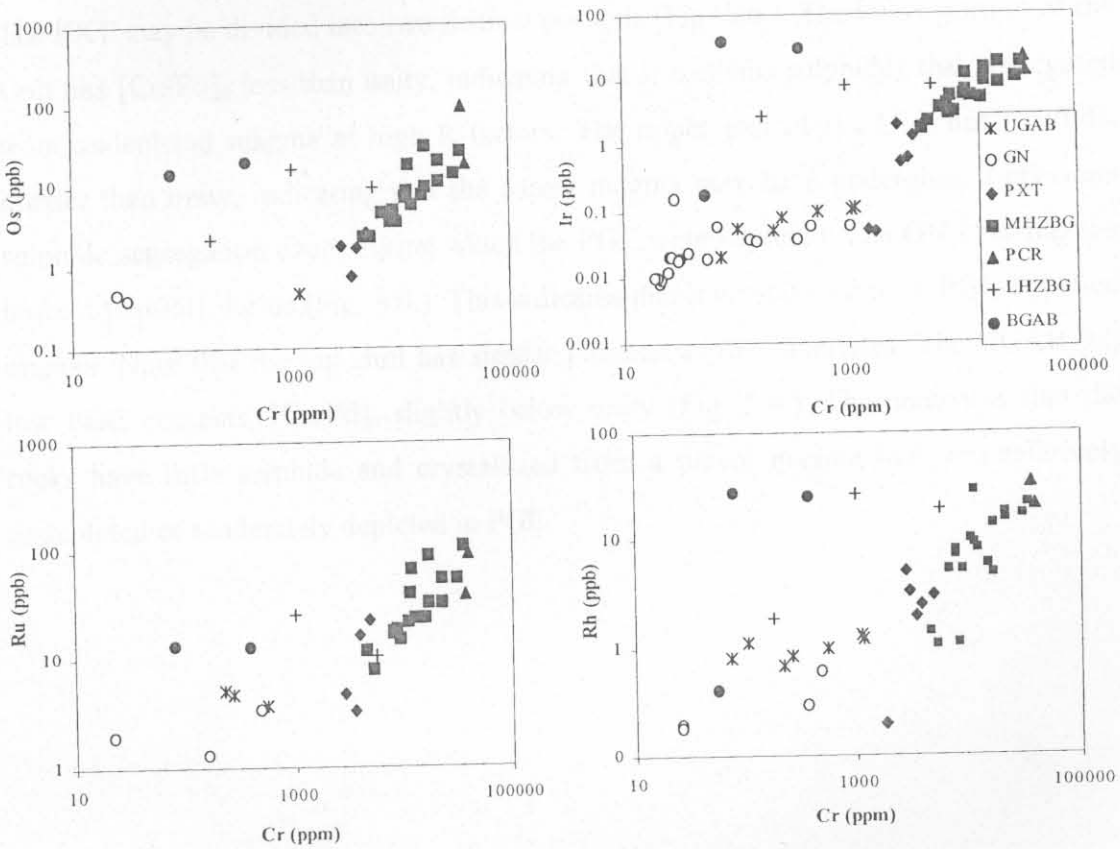

Fig. 5.4. Variation diagrams of IPGE versus Cr.

5.3. Spider plots

The noble metal concentrations are normalized to model mantle and plotted in order of increasing melting temperature in Figure 5.5. Nickel, Cu and Au are added to the graph due to their broadly similar behaviour to PGM's during fractionation. Several features are highlighted. The BGAB has relatively fractionated PGE patterns, with a progressive increase from Ni to Cu. $[Cu/Pd]_n$ is >1. Such a pattern may be expected to represent sulphides that segregated from undepleted magma at relatively low R factors, at which the difference in partitioning between the PGE and Cu or Ni is swamped by the large amount of sulphides. The LHZBG, PCR and Lower MHZBG have different patterns, in that $[Cu/Pd]_n$ is largely less than unity, indicating that the sulphides of these Units segregated at high R-factors. The remainder of the MHZBG has relatively flat patterns with $[Cu/Pd]_n$ at less than unity indicating the presence of cumulus PGE, but the relatively high IPGE/PPGE ratio suggests partial control of the PGE by either monosulphide solid solution (mss) or PGM.

The PXT may be divided into two distinct portions (Fig. 5.6.). The lower portion of the Unit has $[Cu/Pd]_n$ less than unity, indicating that it contains sulphides that segregated from undepleted magma at high R-factors. The upper part of the Unit has $[Cu/Pd]_n$ greater than unity, indicating that the parent magma may have undergone a previous sulphide segregation event during which the PGE were depleted. The GN Unit has the highest $[Cu/Pd]_n$ ratios (Fig. 5.6.). This indicates that it crystallized from PGE-depleted magma. Note that the top-chill has similar patterns as the cumulates. The UGAB has low PGE contents, $[Cu/Pd]_n$ slightly below unity (Fig. 5.6.). This indicates that the rocks have little sulphide and crystallized from a parent magma that was relatively undepleted or moderately depleted in PGE.

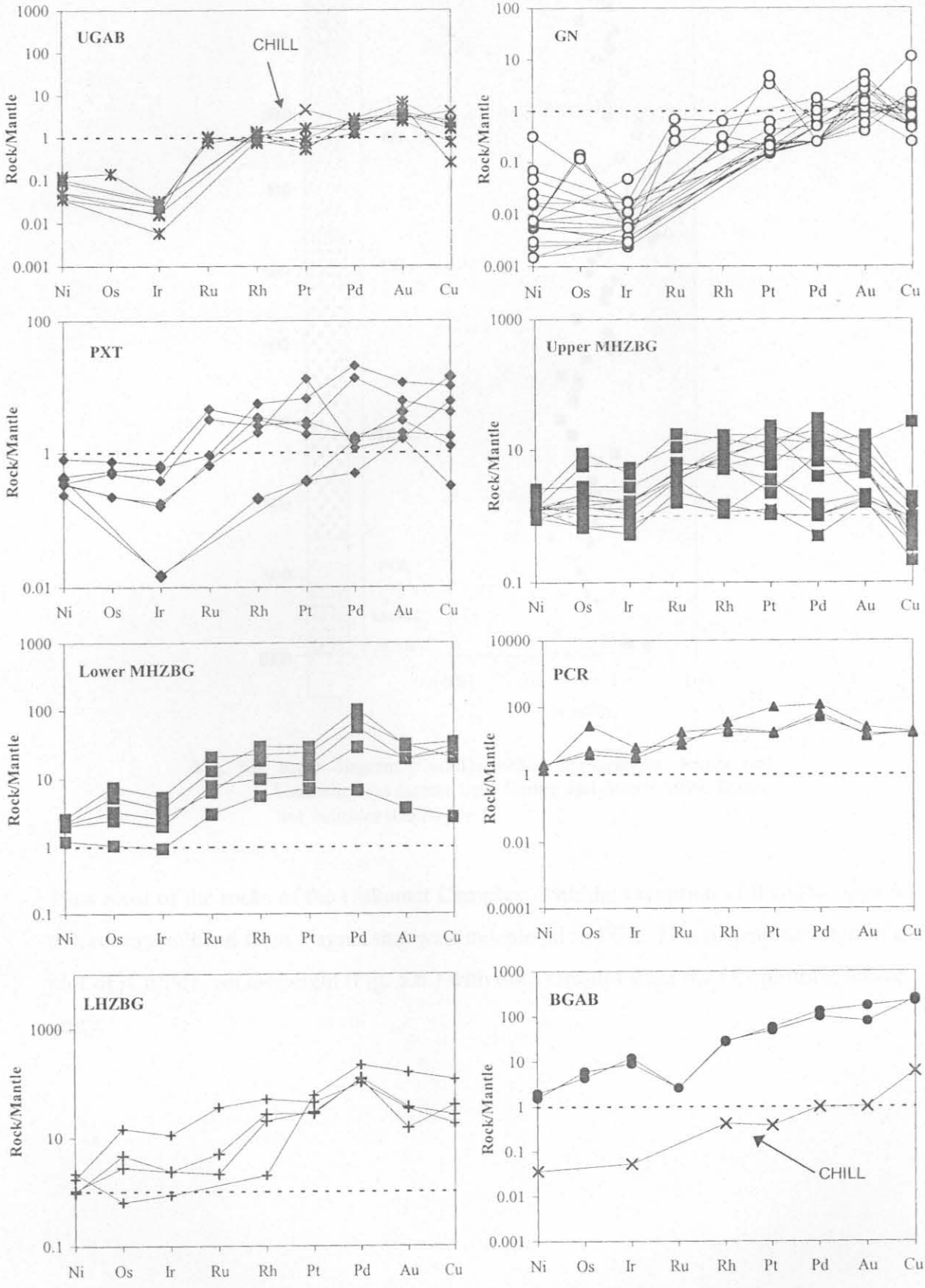

Fig. 5.5. PGE variation through the Complex. Normalization factors from Barnes and Maier (1999).

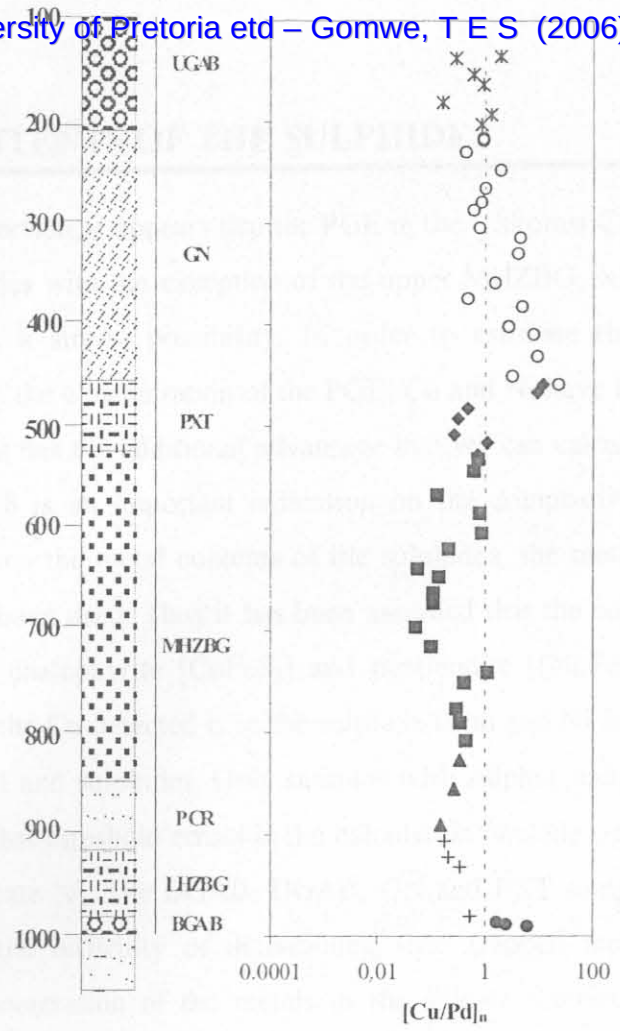

Fig. 5.6. Ratio diagram [Cu/Pd]n versus stratigraphic height (m) Normalization factors from Barnes and Maier, 1999. Dotted line indicates [Cu/Pd]n = 1.

Thus most of the rocks of the Uitkomst Complex, with the exception of the GN, appear to have crystallized from magma that was undepleted in PGE. This is demonstrated in a plot of $[Cu/Pd]_n$ versus height (Fig. 5.6.) with only samples from the GN plotting above unity.

6. METAL CONTENTS OF THE SULPHIDES

From the previous section, it appears that the PGE in the Uitkomst Complex are largely governed by sulphides with the exception of the upper MHZBG, where PGM, mss or chromite control is a strong possibility. In order to estimate the R-factor during sulphide segregation the concentration of the PGE, Cu and Ni have been normalised to 100% sulphide. This has the additional advantage that we can calculate Cu/Ni ratio of the sulphides, which is an important indication on the composition of the parental magma. In calculating the metal contents of the sulphides, the method of Barnes and Francis (1995) has been used. Thus it has been assumed that the sulphides are mainly pyrrhotite [$Fe_{1-x}S$], chalcopyrite [$CuFeS_2$] and pentlandite [$(Ni,Fe)_8S_9$]. It is further assumed that all of the Cu detected is in the sulphide form and Ni is hosted by olivine, trapped silicate melt and sulphides. Only samples with sulphur values above 0.1 were selected, as below that threshold errors in the calculation become significant due to the contribution of silicate Ni. The BGAB, UGAB, GN and PXT samples have not been calculated due to the difficulty of determining their trapped melt component. In calculating the concentration of the metals in the silicate fraction of the remaining samples, Bushveld B1 magma has been assumed as parental magma to the Uitkomst Complex.

All Fe in the rocks was initially reported as Fe_2O_3. This is recalculated to allow for Fe in sulphides (Fe_S):

$$Fe_S = 1.527 \times S - 0.6592 \times (Cu - Cu_{sil}) - 0.5285 \times (Ni - Ni_{sil}) \quad (1)$$

Cu contents of the silicates are largely represented by trapped melt. B1 magma has about 60 ppm Cu, and the proportion of trapped melt has been estimated as $(Zr_{(wr)} / Zr_{(B1)}) \times 100$. Nickel contents of the Uitkomst silicates are largely governed by trapped melt and by olivines. Olivine compositions have been determined by C. Li and are given in Appendix IV. The recalculation factor for 100% sulphide (F) is:

$$F = 100 / \{Fe_{(s)} + S + (Ni - Ni_{sil}) + (Cu - Cu_{sil})\} \quad (2)$$

The sulphide normalized metal contents are listed in Appendix IV. All chalcophile elements are then multiplied by the factor (F), less the silicate component as in equations 3, 4 and 5.

$$Ni_{sul} = \{Ni_{anal} - Ni_{sil}\} \times F \quad (3)$$

$$Cu_{sul} = \{Cu_{anal} - Cu_{sil}\} \times F \quad (4)$$

$$PGE_{sul} = \{PGE_{anal} - PGE_{sil}\} \times F \quad (5)$$

Based on the normalized metal data we can estimate the R-factors that applied during sulphide segregation based on the following equation (Maier *et al.*, 1998).

$$C_c = \frac{C_o \times D \times (R+1)}{(R+D)} \quad (6)$$

Which can be rearranged to:

$$R = \frac{C_0D - C_CD}{C_C - C_0D} \quad (7)$$

C_0 and C_C are the concentration of the metal in the initial silicate melt and the sulphide melts, respectively. For the sulphide-rich BGAB, LHZBG and PCR R-factors of between 600 and 1 000 can be calculated. Sulphide-normalised Cu/Ni ratios are plotted in Figure 6.1. For most samples, Cu/Ni varies between about 0.2 and 3, broadly in agreement with crystallization from Bushveld B1 magma (Table 3).

There are two peaks in the Cu/Ni ratio, just below 700 m and at about 580 m, coinciding with two sulphide poor samples of the MHZBG and suggesting that the high values are due to uncertainty in the estimation of silicate Ni.

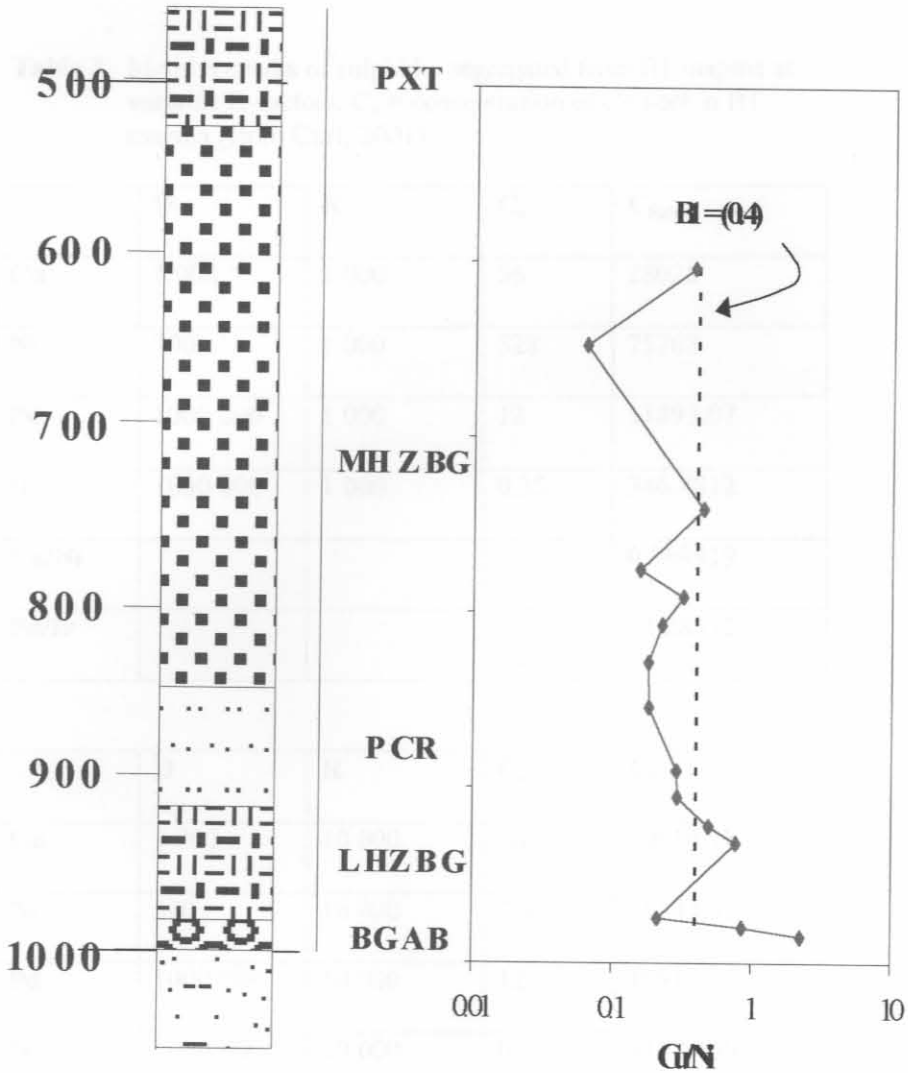

Fig. 6.1 Ratio of Sulphide normalized Cu/Ni versus stratigraphic height (m)

Based on the available data it appears that the PGE in the BGAB, PCR, LHZBG and lower MHZBG appear to be largely controlled by sulphides that segregated at R-factors of around 1000 from undepleted magmas.

The PGE in the upper MHZBG appear to be additionally controlled by PGM possibly associated with disseminated chromite. The PGE in the PXT and GN Units are largely

controlled by metal-poor sulphides that segregated from PGE depleted magma, or by trapped silicate melt undepleted in noble metals in the case of the GN Unit.

Table 3. Metal contents of sulphides segregated from B1 magma at variable R-factors. C_o = concentration of element in B1 magma (from Curl, 2001)

	D	R	C_o	C_{Sulf}
Cu	1 000	1 000	56	28028
Ni	300	1 000	328	75768
Pd	1000 000	1 000	12	11893.07
Ir	1000 000	1 000	0.35	346.8812
Cu/Ni				0.369919
Pd/Ir				34.28572

	D	R	C_o	C_{Sulf}
Cu	1 000	10 000	56	50914.18
Ni	300	10 000	328	95543.53
Pd	1000 000	10 000	12	109101.8
Ir	1000 000	10 000	0.35	3182.136
Cu/Ni				0.532890
Pd/Ir				34.28571

7. Sm-Nd ISOTOPIC GEOCHEMISTRY

7.1. Introduction

Neodymium occurs as several stable isotopes in nature, i.e. ^{142}Nd to ^{148}Nd and ^{150}Nd. ^{143}Nd is the decay product of ^{143}Sm ($\lambda = 6.54 \times 10^{-11} a^{-1}$) (DePaolo, 1988). As a result, the amount of ^{143}Nd, and the proportion of ^{143}Nd relative to other isotopes of Nd increases with time, within any rock or mineral that contains the mother element, Sm. For bulk earth these relationships can be illustrated by means of a schematic isotope growth curve (Fig. 7.1.). Clearly, primary partial melts of the upper mantle will have progressively increasing initial $^{143}Nd/^{144}Nd$ ratios with decreasing age.

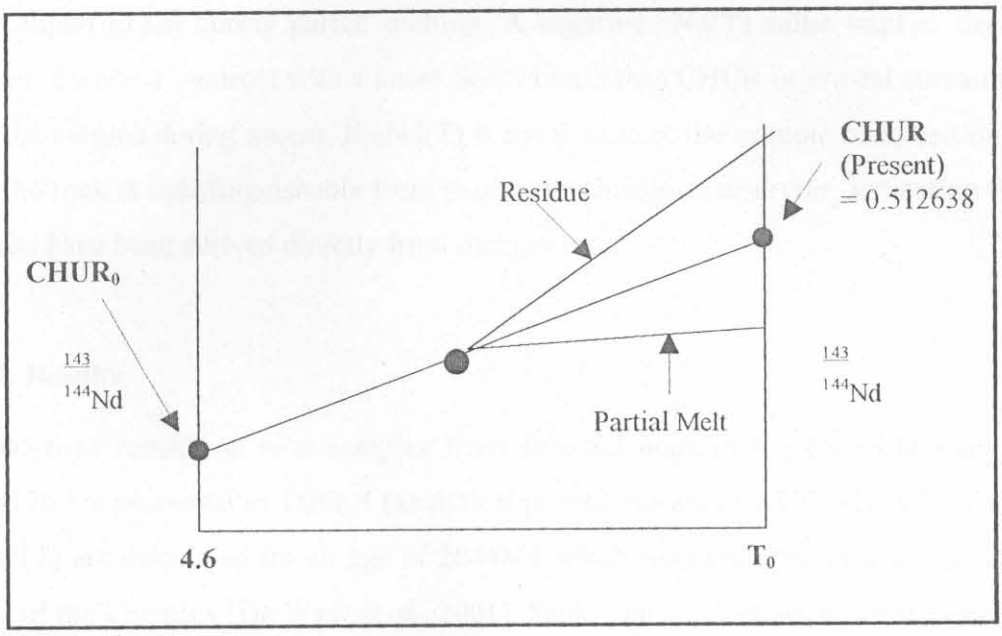

Fig.7.1. The change of $^{143}Nd/^{144}Nd$ ratio with time from 4.6 Ga to the present (T_0) in a chondritic uniform reservoir (CHUR) that undergoes partial melting.

During partial melting of the mantle LREE behave more incompatibly than HREE. As a result, the mother isotope ^{147}Sm tends to be concentrated relative to ^{143}Nd in the residue, whereas ^{143}Nd is relatively concentrated in the partial melts (Fig. 7.1.). Partial melts of previously depleted mantle will have high initial $^{143}Nd/^{144}Nd$ ratios relative to $CHUR_T$, while mantle melts that interact with older crust, or partial melts from enriched lithospheric mantle sources, will have low $^{143}Nd/^{144}Nd$ ratios relative to

$CHUR_T$. The parameter that defines the comparison between the sample and the chondritic mantle is referred to as εNd(T):

$$\varepsilon Nd(T) = \left[\frac{(^{143}Nd/^{144}Nd)}{(^{143}Nd/^{144}Nd)_{CHUR}} - 1 \right] \times 10^4 \qquad (8)$$

Thus, εNd(T) values may provide information about the magma source. Positive εNd(T) values imply that the magma came from "depleted" sources having higher Sm/Nd ratios than CHUR, that is, the rocks were derived from residual solids in the reservoir after magma had been extracted at an earlier time. These reservoirs are depleted in large ion lithophile (LIL) elements that are preferentially partitioned into the liquid phase during partial melting. A negative εNd(T) value implies derivation from "enriched" sources with a lower Sm/Nd ratio than CHUR or crustal contamination of the magma during ascent. If εNd(T) is equal to zero, the isotopic composition of Nd in the rock is indistinguishable from that in the chondritic reservoir, indicating that the rocks have been derived directly from that reservoir.

7.1. Results

Analytical results on nine samples from selected units in the borehole intersection SH176 are presented in Table 4 (analytical procedures are in APPENDIX I). Values of εNd(T) are calculated for an age of 2044Ma which represents the best estimate of the age of the Complex (De Waal *et al.*, 2001). Samarium concentrations vary from 0.66 to about 7ppm and Nd concentrations between 4.4 and 39.7ppm. There is a positive correlation between Sm and Nd (Fig. 7.2.(a)) with sample SH176 UP8 of the GN having the highest Sm and Nd values and SH176 UP32 of the PXT having the lowest values (Table 4).

Figure 7.2.(b) shows $^{143}Nd/^{144}Nd$ plotted versus $^{147}Sm/^{144}Nd$. It is evident that the data do not define an isochron, which is best explained by selective crustal contamination of some or all of the Uitkomst rocks. Thus, age estimates by this method would have no geological significance. This model is supported by the εNd(T) values of the samples which range between -3.4 and -7.6 indicative of a significant crustal component.

Table 4. Neodymium and strontium isotope data. Epsilon Nd values calculated for an age of 2044Ma

Sample No	Unit	Depth (m)	Nd (ppm)	Sm (ppm)	$^{147}Sm/^{144}Nd$	$^{143}Nd/^{144}Nd$ (measured)	Error	Nd (T=2044Ma)
SH176UP1	UGAB	135.41	19.1	3.75	0.12449	0.511401	80	-5.4
SH176UP5	UGAB	181.09	12.6	2.48	0.12548	0.511301	9	-7.6
SH176UP8	GN	216.22	39.7	6.99	0.11302	0.511213	13	-5.9
SH176UP19	GN	375.42	12.1	2.26	0.12230	0.511356	8	-5.8
SH176UP23	GN	432.11	8.92	1.89	0.13349	0.511472	11	-6.6
SH176UP26	PXT	459.75	6.88	1.3	0.12873	0.511416	8	-6.7
SH176UP32	PXT	527.04	2.443	0.531	0.13139	0.511336	8	-8.3
SH176UP40	MHZBG	647.6	3.38	0.66	0.14118	0.511648	7	-6.03
SH176UP49	MHZBG	807.04	5.3	1.12	0.12714	0.511486	14	-4.68
SH176UP51	PCR	854.06	4.43	0.88	0.12126	0.511493	37	-3.38
SH176UP60	BGAB	990.29	23.179	5.524	0.14405	0.511438	58	-8.8

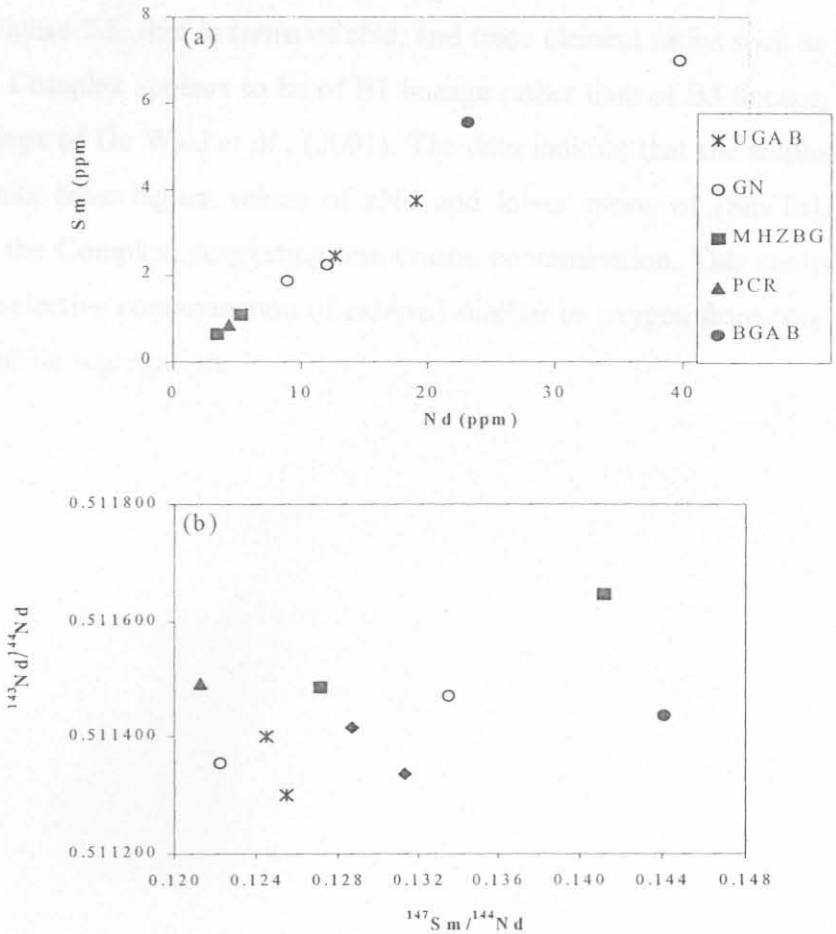

Fig. 7.2. Sm-Nd variation diagrams (a) Sm vs. Nd. (b) $^{143}Nd/^{144}Nd$ versus $^{147}Sm/^{144}Nd$ isochron diagram.

7.3. Stratigraphic variation in εNd

The εNd(T) as well as the $[Sm/Ta]_n$ ratios are plotted against stratigraphic height (Fig. 7.3.) to enable comparison with data obtained by Maier *et al.*, (2000) on Bushveld cumulates and parental magmas. These authors showed that the Bushveld Complex was contaminated with progressively more depleted crust. The parental magmas to the Lower Zone (LZ) and Lower Critical Zone (LCZ), i.e. B1 magma, assimilated relatively small amounts of partial melts of undepleted crust that were highly enriched in incompatible trace elements. The Main Zone (MZ) magmas (B3 magma) assimilated larger amounts of residual crust that was less enriched in incompatible trace elements. As a result, B1 magmas and associated cumulates show a higher εNd (-5 to -6), but are enriched in highly incompatible trace elements relative to B3 magmas and cumulates (εNd -6.5 to -7.5).

It is seen in Figure 7.3. that in terms of εNd, and trace element ratios such as $[Sm/Ta]_n$, the Uitkomst Complex appears to be of B1 lineage rather than of B3 lineage, in accord with the findings of De Waal *et al.*, (2001). The data indicate that the sulphide-bearing rocks and units have higher values of εNd and lower ratios of $[Sm/Ta]_n$ than the remainder of the Complex, suggesting less crustal contamination. This can possibly be explained by selective contamination of external sulphur or oxygen from country rocks, triggering sulphide segregation.

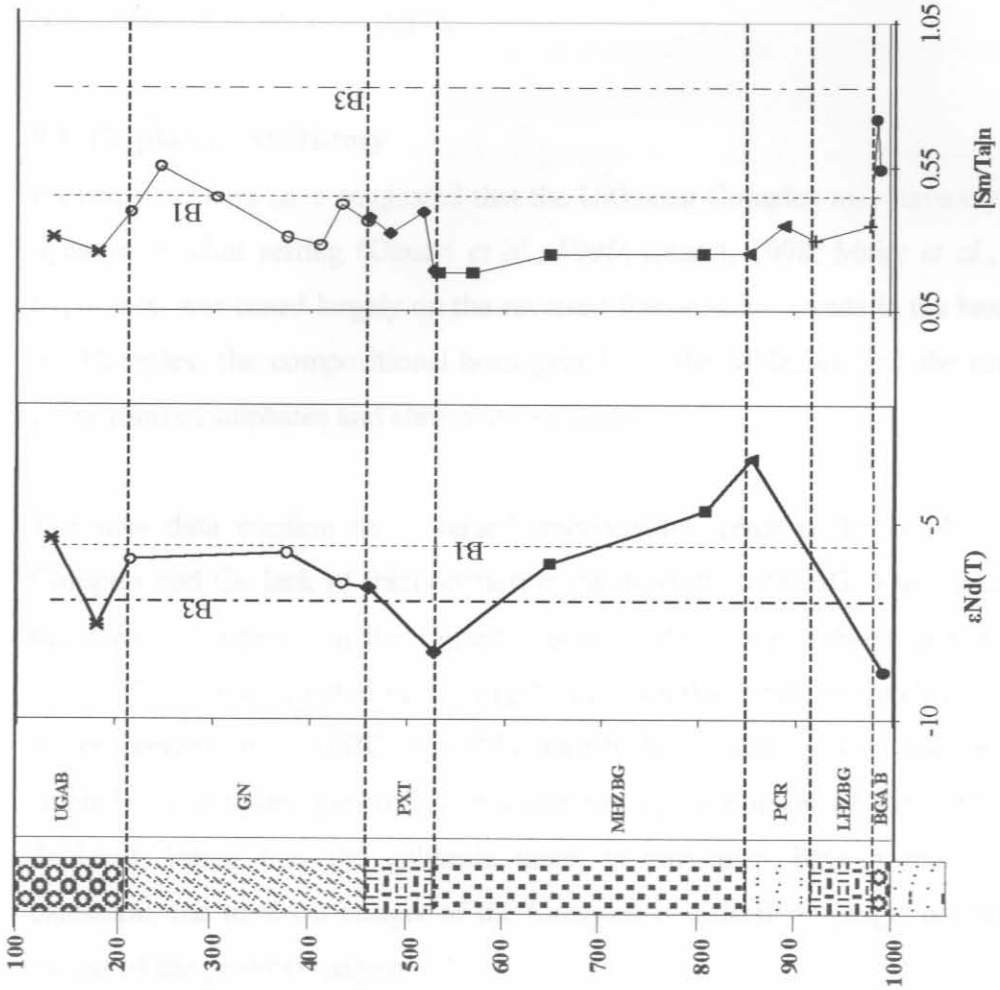

Fig. 7.3. Stratigraphic variation of [Sm/Ta]n. Depth is in meters. Average B1 and B3 values are from Curl (2001).

8. DISCUSSION AND CONCLUSIONS

The objectives of this project were three-fold. Firstly I aimed to constrain whether the Uitkomst Complex crystallized as a closed system or in a dynamic magma conduit setting. Secondly, I planned to determine whether the lithological units of the Complex crystallized from magma of different lineage, and whether any of the parental magmas can be compositionally related to the parental magmas of the Bushveld Complex. Thirdly I tried to clarify whether the sulphides segregated in response to crustal contamination *in situ* or at depth.

8.1. Emplacement History

Previous workers have suggested that the Uitkomst Complex may have crystallized in a dynamic conduit setting (Gauert *et al.*, 1995; Gauert, 1998; Maier *et al.*, 1998). This hypothesis was based largely on the reversed fractionation trends in the basal portion of the Complex, the compositional homogeneity of the MHZBG, and the relatively large proportion of sulphides and chromite to silicates.

The new data confirm the reversed fractionation trend in the basal portion of the Complex and the lack of fractionation in much of the MHZBG. The argument of there being excess sulphide in the Complex is more difficult to substantiate. Figure 4.6.(a) shows Cu/Zr ratios plotted versus MgO. It is seen that while the BGAB, LHZBG, PCR, lower portion of MHZBG and PXT clearly have cumulus Cu (and by implication, sulphide), the upper gabbroic Units and the upper portion of the MHZBG are Cu-depleted. Being that the gabbroic units, in particular, have a much wider lateral extension, the total Cu budget of the Complex is difficult to judge, but need not be in excess of the parental magma.

Distribution patterns of the PGE provide more insight. Pd/Ir ratios have been shown to behave in an opposite way to what would be expected in a closed system (Fig. 5.2.). They decrease with height up to the top of the MHZBG, whereas in the Bushveld Complex, Pd/Ir increases with height indicating that Ir is more compatible than Pd during crystallization of igneous rocks. This suggests that in the Uitkomst Complex, the upper portions of the MHZBG are not related to the underlying Units by means of *in*

situ fractionation. $[Cu/Pd]_n$ ratios (Fig. 5.6.) support this argument. Successive Units of the Complex up to the top of the MHZBG are undepleted in Pd relative to Cu. Were these mostly sulphide-rich Units related to each other by *in situ* fractionation; one would expect progressive Pd depletion of the rocks with height.

The olivine data of Li *et al.* (2002) also indicate that the individual Units are not related by *in situ* fractionation. They showed that there are two types of olivine present in the intrusion (Fig. 8.1.) (i) a primitive olivine that occurs in all the harzburgite units and the PXT and (ii) a highly evolved olivine that occurs in the GN. The primitive olivine is divided into 3 sub-types depending on the amount of Ni-depletion. These are (a) Ni-undepleted olivine (Ni >3000ppm), occurring in the sulphide-poor upper MHZBG (b) A moderately Ni-depleted (1300-2300ppm Ni) olivine occurring in the sulphide-rich LHZBG, PCR, and the lower portion of the MHZBG (c) A highly depleted olivine (<500ppm Ni) found in the upper portion of the PXT.

A final argument for the conduit model is the bimodality in the S and MgO contents of the rocks (Fig. 4.6.). This would be unexpected if the rocks represented a closed system and instead suggest the involvement of distinct magma pulses that were possibly contaminated by distinct country rocks, triggering sulphide segregation.

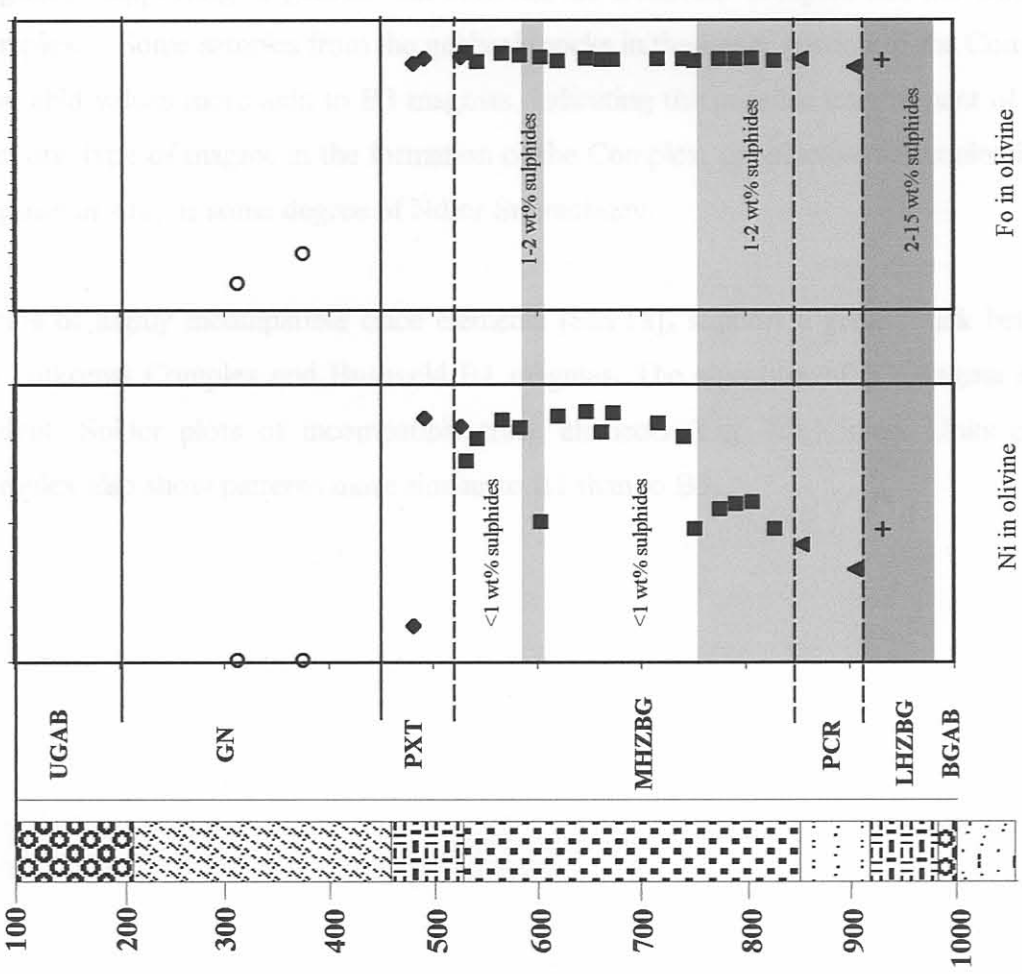

Fig.8.1. Olivine Ni (ppm) and Fo content (mol%) against stratigraphic height (m).

8.2. The Nature of the Parental Magmas

Previous authors suggested that the Uitkomst Complex crystallized from several distinct parental magmas (De Waal and Gauert, 1997) and that these magmas are related to Bushveld B1 and B2 magmas. (Gauert *et al.*, 1995; De Waal *et al.*, 2000). This proposal may be assessed by comparing Nd isotopes and ratios of highly incompatible trace elements from the Uitkomst Complex and the Bushveld Complex. Figure 7.3. shows the εNd(T), values of the Uitkomst Complex are similar to B1 magmas, supporting a genetic link between the Bushveld Complex and the Uitkomst Complex. Some samples from the gabbroic rocks in the upper portion of the Complex have εNd values more akin to B3 magmas, indicating the possible involvement of more than one type of magma in the formation of the Complex, or selective contamination of magmas *in situ*, or some degree of Nd or Sm mobility.

Ratios of highly incompatible trace elements $[Sm/Ta]_n$ support a genetic link between the Uitkomst Complex and Bushveld B1 magmas. The signature of B3 magma is less evident. Spider plots of incompatible trace elements (Fig. 4.8.) in all Units of the Complex also show patterns more similar to B1 than to B3.

8.3. The origin of the sulphide mineralization

The metal concentrations of the rocks of the Uitkomst Complex may be used to clarify two questions (a) did the sulphides segregate *in situ* due to contamination or mixing of contrasting magmas (b) did the magmas segregate at depth and then become entrained by successive surges of ascending magma.

Gauert *et al.* (1995) suggest that degassing of dolomite in the LHZBG caused an increase in oxygen fugacity of the magma and acted as a "trigger mechanism" for the precipitation of sulphide and chromite. The sulphur isotopic data of Li *et al.* (2002) and some of my trace element data support this model. The sulphides of the mineralized Units have $\delta^{34}S$ between -8 and 2, in accord with the S isotopic signature of pyrite-bearing shaly intervals in Malmani dolomites in the Fochville area. In contrast, the sulphides of the S-poor Units have a mantle signature. Li *et al.*, discard the possibility of the S of the sulphide-rich Units being derived from the Timeball Hill Shale, as the latter have S-isotopic signatures (-12 to -18) that are too divergent from the Uitkomst sulphides. At the same time, the fact that the sulphide-bearing and the sulphide-poor ultramafic rocks have similar incompatible trace element values (Fig. 4.10. and Fig. 7.3.) suggests that assimilation of external S was not accompanied by significant silicate assimilation. This may indicate that the S was added to the magma by means of devolatization analogous to the situation in parts of the Duluth Complex (Ripley and Alawi, 1988). If the sulphides segregated in response to contamination of the magma with dolomite, then a model of entrainment of the sulphides from depth is precluded. However, some relatively localised entrainment of sulphides remains a possibility.

The relatively low Cu/Ni ratios of the sulphides in the LHZBG, PCR and MHZBG can be modelled by sulphide segregation from B1 magma.

9. ACKNOWLEDGEMENTS

I am indebted to CERMOD, at the University of Pretoria, for their funding of this project. I would also like to thank Nkomati Mine of Anglovaal for the material support, and their provision of the core material.

My sincerest appreciation to Professor Wolfgang Maier for his supervision and guidance during the duration of this project, I learned a great deal. I would also like to thank Dr. Chusi Li for assisting with the difficult job of crushing, and explaining the olivine geochemistry. Thank you to Professor S-J Barnes (University of Quebec), Professor Reid (University of Cape Town), Dr. S. Prevec (University of the Witswatersrand), and Maggi Loubser (University of Pretoria) for their analysis on my samples and Marko and Peter in the rock lab at the University of Pretoria for making the thin sections. I am grateful to Professor Roland Merkle for the use of his digital camera and microscope, Sabine Verryn for use of her computer hardware, and scanner and to Dr. Ian Graham for his help with the metamorphic petrography. Gratitude in great measure goes to Lori Tuovila for her proof reading and constructive comments.

Special thanks to my friends for having the confidence in me and who gave me the moral support needed to finish this project. I am forever grateful of my parent's love, faith and confidence in me.

10. REFERENCES

Agranier, A. (1999). *Etude pétrologique et géochimique de bordures figées de l'intrusion d'Uitkmost, Afrique du Sud.* Maîtrise de Sciences de la Terre. Univ. Joseph Fourrier, Grenoble 32pp.

Allen, I. (1990). *The Geology and Geochemistry of the Uitkomst Layered Complex, Eastern Transvaal.* B.Sc. Hons. thesis (unpubl.) Univ. Witwatersrand, Johannesburg, 47pp.

Anhaeusser, C.R., Robb, L.J. & Botha, J.M.(jr) (1981). Provisional Geological map of the Barberton Greenstone Belt and surrounding granitic terrane, Eastern Transvaal and Swaziland. *In*: Contributions to the Geology of the Barberton Mountain Land, Sec. Publ. *Geol. Soc. S. Afr.*, **9.**

Barnes, S.-J. and Francis, D. (1995). The distribution of platinum-group elements, Nickel, Copper and Gold in the Muskox layered intrusion, Northwest territories, Canada. *Econ. Geol.* **90,** 133-154.

Barnes, S.-J., Makovicky, E., Karup-Møller, S., Makovicky, M. & Rose-Hansen, J., (1997). Partition coefficients for Ni, Cu, Pd, Pt, Rh and Ir between Monosulphide Solid solution and sulphide liquid and the implications for the formation of compositionally zoned Ni-Cu sulphide bodies by fractional crystallization of sulphide liquid. *Can. J. Earth Sci.* **34**, 366-374.

Barnes, S.-J. & Maier, W.D., (1999). The fractionation of Ni, Cu and the noble metals in silicate and sulphide liquids. *In*: Keays, R.R., Lesher, C.M., Lightfoot, P.C. & Farrow, C.E.G. (eds), *Dynamic Processes in Magmatic Ore Deposits and their application in mineral exploration.* Geological Association of Canada, Short Course Volume **13**, 69-106.

Bennett, H. & Oliver, G. (1992). *XRF Analysis of Ceramics, Minerals and Applied Materials.* John Wiley & Son. p 67-93.

Brenan, J.M. & Andrews, D. (2001). High temperature stability of Laurite and Ru-Os-Ir alloy and their role in PGE fractionation in mafic magmas. *Can. Mineral.* **39**, 341-360.

Burger, A.J. & Coertze, F.J. (1976). Age determinations – April 1972 to March 1994. *Ann. Geol. Surv. S. Afri.* **10,** 135-141.

Bürgmann, G.E., Arndt, N.T., Hofmann, A.W. & Tobschall, H.J. (1987). Noble metal abundances in komatiite suites from Alexo, Ontario and Gorgona Island, Columbia. *Geochim. Chosmochim. Acta*, **51**, 2159-2169.

Button, A. (1973). *A regional study of the stratigraphy and development of the Transvaal Basin in the eastern and northeastern Transvaal.* PhD thesis (unpubl.), Univ. Witwatersrand, Johannesburg, S. A.

Button, A. (1986) The Transvaal Sub-basin of the Transvaal Sequence. *In*: Anhaeusser, C.R. & Maske, S. (ed) *Mineral Deposits of S. Afr* 811-817. Geol. Soc. S. A. Johannesburg.

Capobianco, C.J., Hervig, R.L. & Drake, M.J. (1994). Experiments on crystal/liquid partitioning of Ru, Rh and Pd for magnetite and hematite solid solutions crystallized from silicate melt. *Chem. Geol.* **113,** 23-43.

Curl, E.A. (2001). *Parental magmas of the Bushveld Complex, South Africa.* Ph.D. thesis (unpubl.), Monash Univ. Australia. 140pp.

Davies, G. & Tredoux, M. (1985). The Platinum-Group Element and Gold Contents of the Marginal Rocks and Sills of the Bushveld Complex. *Econ. Geol.* **80,** 838-848.

Deer, W.A., Howie, R.A. & Zussman, J. (1992). *An introduction to the rock forming minerals*. Longman Scientific and Technical England. 696pp.

DePaolo, D.J. (1988) *Neodymium Isotope geochemistry: An introduction.* Springer-Verlag Berlin Heidelberg. 187pp.

De Waal, S.A. & Gauert, C.D.K. (1997). The Basal Gabbro Unit and the identity of the parental magma of the Uitkomst Complex, Badplaas, South Africa. *S. Afri J. Geol.*. **100(4),** 349-361.

De Waal, S.A. & Armstrong, R.A. (2000). The age of the Marble Hall diorite, its relationship to the Uitkomst Complex, and evidence for a new magma type associated with the Bushveld event. *S. Afr. J. Geol.* **103(2),** 128-140.

De Waal, S.A., Maier, W.D., Armstrong, R.A. & Gauert, C.D.K. (2001) Parental Magma and emplacement of the stratiform Uitkomst Complex, South Africa. *Can. Mineral.* **39,** 557-572.

Eales, H.V., Maier, W.D. & Teigler, B. (1991). The significance of corroded feldspar inclusions in pyroxenites and norites of the Lower and Critical Zones, Western Bushveld Complex. *Mineralogical Magazine.* **55,** 479-486.

Eriksson, K.A. (1973). The Timeball Hill Formation - a fossil delta. *J. Sedim. Petrol.* **43,** 1046 - 1053.

Eriksson, P.G. (1988) The sedimentology of the Rooihoogte Formation Transvaal Sequence. *S. Afr. J. Geol.* **91,** 477 - 489.

Eriksson, P.G., Schweitzer, J.K, Bosch, P.J.A., Schereiber, U.M., Van Deventer, J.L., & Hatton, C.J. (1993). The Transvaal Sequence: and overview. *J. Afr. Earth Sci.* **16 1/2,** 25-51.

Figueiredo de Heredia, M.C. (1980). *Geochemistry of High-Grade metamorphic Rocks North East Bahia Brazil.* PhD thesis (unpubl.), Univ. W. Ontario, Canada. 220pp.

Gauert, C.D.K., de Waal, S.A. & Wallmach, T. (1995) Geology of the ultrabasic to basic Uitkomst complex, eastern Transvaal, South Africa: an overview. *J. Afr. Earth Sci.* **21:4,** 553-570.

Gauert, C.D.K. (1998) *The petrogenesis of the Uitkomst Complex, Mpumalanga Province, South Africa.* PhD thesis (unpubl.), Univ. Pretoria, South Africa. 315pp.

Hanson, G.N. (1989). An approach to trace element modelling using a simple igneous system as an example. *In*: Ribbe, P.H., (ed) *Geochemistry and mineralogy or rare earth elements*: Reviews in mineralogy, Mineral. Soc. Am. **21**, 79-97.

Harmer, R.E. & Armstrong, R.A. (2000) Duration of Bushveld Complex (*sensu lato*) magmatism: Constraints from new SHRIMP zircon chronology. *In: Workshop on the Bushveld Complex – Abstracts and Programs,* Gethlane Lodge, Burgersfort, 18-21 November 2000.

Henry, G., Clendenin, C.W. & Charlesworth, E.G. (1990). *Depositional facies of the Black Reef Quartzite Formation in the eastern Transvaal*. Geocongress 1990 (Cape Town, South Africa): Abstracts 230 – 233.

Hornsey, A.R. (1999). *The genesis and evolution of the Nkomati Mine Ni-sulphide deposit, Mpumalanga Province, South Africa*. MSc thesis (unpubl.) Univ. Natal (Durban), 224pp.

Kenyon, A.K., Attridge, R.L. & Coetzee, G.L. (1986). The Uitkomst nickel-copper deposits eastern Transvaal In Mineral Deposits of South Africa (C.R. Anhauesser, S. Maske, (eds)) *Geol. Soc. S. Afr.* 1009-1019.

Kullerud, G., Yund, R.A. & Moh, G.H. (1969). Phase relations in the Cu-Fe-S, Cu-Ni-S and Fe-Ni-S systems. *Econ. Geol., Monograph* **4**, 323-349.

Li, C., Barnes, S.-J., Makovicky, E., Rose-Hansen, J & Makovicky, M. (1996). Partitioning of Nickel, Copper, Iridium, Rhodium, Platinum and Palladium between monosulphide solid solution and sulphide liquids: effects of composition and temperature. *Geochim. Cosmochim. Acta*, **60**, 1231-1238.

Li, C., Ripley, M., Maier, W.D., & Gomwe, T.E.S. (2002). Olivine and sulfur isotopic compositions of the Uitkomst sulfide-bearing intrusion, South Africa: records for multiple flows of magmas and their roles in ore formation in a magma conduit. *Chem. Geol.* in press.

Le Maitre, R.W. (Ed.) (1989). *A Classification of Igneous Rocks and Glossary of Terms. Recommendations of the International Union of Geological Sciences Subcomminssion on the Systematics of Igneous Rocks.* Blackwell Scientific Publications, Oxford, UK., 193pp.

Maier, W.D., Barnes. S.-J., & de Waal S.A (1998). Exploration for magmatic Ni-Cu-PGE sulphide deposits: a review of recent advances in the use of geochemical tools and their application to some South African ores. *S. Afr. J. Geol.* **101 (3)**, 237-253.

Maier, W.D. & Barnes. S.-J. (1999). Platinum-Group Elements in Silicate Rocks of the Lower, Critical and Main Zones at Union Section, Western Bushveld Complex. *J. Petro.* **40,** 1647-1671.

Maier, W.D., Arndt, N.T. & Curl, E.A. (2000) Progressive crustal contamination of the Bushveld Complex: evidence from isotopic analyses of the cumulate rocks. *Contrib. Mineral Petrol.* **140**, 316-327.

McDonough W.F. & Sun S.-s. (1995). The composition of the Earth. *Chem. Geol.* **120**, 223-253.

Möller, P. (1988). The dependence of partition coefficients on differences of ionic volumes in crustal-melt systems. *Contr. Mineral. Petrol.* **99,** 62-69.

Naldrett, A.J. (1997). Key factors in the genesis of Noril'sk, Sudbury, Jinchuan, Voisey's Bay and other world class Ni-Cu-PGE deposits: Implications for exploration. *Austr. J. Earth Sci.* **44**, 283-315.

Nixon, N., Eriksson, P.G., Jacobs, R. & Snyman, C.P. (1988). Early Proterozoic micro-algal structures in carbonaceous shales of the Pretoria Group, southwest of Potchefstroom. *S. Afr. J. Geology.* **84**, 592-595.

Reczko, B.F.F., (1994). *The geochemistry of the Transvaal Supergroup.* Ph.D. thesis (unpubl.) Univ. Pretoria, 700pp.

Richard, L.R. (1988-1997). *Mineralogical and Petrological data processing System (ver. 2.02).*

Ripley, E.M. & Alawi, J.A. (1988). Petrogenesis of pelitic xenoliths at Babbitt Cu-Ni deposit, Duluth Complex Minnesota, USA. *Lithos* **21**, 143-159.

Rollinson, D. (1993). *Using geochemical: evaluation, presentation, interpretation.* London: Longman Scintific & Technical. 352pp

Ramdohr, P., (1980). *The ore minerals and their intergrowths* – 2nd edition. Pergamon Press ltd., Oxford, England. 1205p.

Sharpe, M.R., Bahat, D., & Von Gruenewaldt, G. (1981). The concentric elliptical structure of the feeder sites to the Bushveld Complex and possible economic implications. *Trans. Geol. Soc. S. Afr.*, **84**, 239-244.

Strauss, T.A.L. (1995). Petrography and geochemistry of the Basal Gabbro, Unit Uitkomst Complex. M.Sc. thesis (unpubl.), Rhodes Univ. 103pp

Sun, S-s. & McDonough, W.F. (1989). Chemical and isotopic systematics of oceanic basalts: implications or mantle composition and processes. *In*: Saunders, A.D. & Norry

M.J. (eds) *Magmatisim in the ocean basins.* Spec. Publ. **42**, Geol. Soc., Oxford, 313-345.

Theart, H.F.L. & De Nooy, C.D. (2001). The platinum-group minerals in two parts of the massive sulphide body of the Uitkomst Complex, Mpumalanga, South Africa. *S. Afr. J. Geol.*, in press.

Tischler, S.E., Cawthorn, R.G., Kingston, G.A. & Maske, S. (1981). Magmatic Cu-Ni-PGE mineralization at Waterfall Gorge Insizwa, Pondoland, Transkei. *Can. Mineral.* **19,** 607-618.

Tredoux, M., Lindsay, N.M., Davies, G. & McDonald, I. (1995). The fractionation of platinum-group elements in magmatic systems, with the suggestion of a novel casual mechanism. *S. Afr. J. Geol.*, **98**, 157-167.

Ulmer, P. (1989). The dependence of the Fe^{2+}-Mg cation-partitioning between olivine and basaltic lquid on pressure, temperature composition. An experimental study to 30 kbars. *Contr. Mineral. Petrol.* **101**, 261-273.

Van Zyl, A.M. (1996). *The sulphides of the Uitkomst Complex, Badplaas, South Africa.* MSc thesis (unpubl.), Univ. Pretoria 122pp.

Von Scheibler, W.H.T.M., Cawthorn, R.G., Kenyon, A.K. & Allen, I.V.M. (1995). Ni-Cu sulphide mineralization in the Uitkomst intrusion. *Geol. Soc. S. Afr. Centennial Geocongress '95 Ext. Abstr,* **1,** 133-136.

Wagner, P.A. (1929). *The platinum deposits and mines of South Africa.* Oliver and Boyd, Edinburgh and London. 326pp.

Walraven, F. & Martini, J. (1995). Zircon Pb-evaporation age determination of the Oak Tree Formation, Chuniespoort Group, Transvaal Sequence: Implications for Transvaal-Griqualand West basin correlations. *S. Afr. J. Geol.* **98(1)**, 58-67.

APPENDIX I

ANALYTICAL METHODS

XRF SAMPLE PREPARATION

TABLE OF STANDARDS AND LIMITS OF DETECTION

ISOTOPE ANALYSIS, THERMAL IONIZATION MASS SPECTROMETRY

TABLE OF Sm/Nd ANALYSIS

ICP-MS SAMPLE PREPARATION

LECO SAMPLE PREPARATION

XRF Analysis.

APPARATUS:	ARL 8420 wavelength dispersive XRF Spectrometer.
SAMPLE PREPARATION:	Samples were dried and roasted at 1000°C to determine % Loss on Ignition.
	Major element analyses were executed on fused beads, following the standard method used in the XRF laboratory of the University of Pretoria, as adapted from Bennet and Oliver's (1992) proposed method. 1g pre-roasted sample + 6g Lithium Tetra borate flux mixed in a 5% Au/Pt crucible and fused at 1050°C in a muffle furnace with occasional swirling. A glass disk is poured into a preheated Pt/Au mould and bottom surface analyzed.
	Trace elements were analyzed on pressed powder pellets, using a saturated Movial solution as a binder.
CALIBRATION:	XRF Spectrometer was calibrated with Certified reference materials. NBSGSC fundamental parameter program was used for matrix correction of major elements as well as Cl, Co, Cr, V, Ba, Sc and S. Rh Compton peak ratio method was used for the other trace elements.

Standard deviation and limit of detection are listed in the Table

STANDARD DEVIATION AND LIMITS OF DETECTION ON XRF

	std dev. (%)	LOD	LIT		GSNcert	JG1cert
SiO_2	0.4	0.02	<0.02	SiO_2	65.8	72.3
TiO_2	0.03	0.0032	<0.01	TiO_2	0.68	0.26
AL_2O_3	0.3	0.01	<0.01	AL_2O_3	14.67	14.2
Fe_2O_3	0.3	0.0097	<0.01	Fe_2O_3	3.75	2.14
MnO	0.0065	0.0013	<0.01	MnO	0.056	0.063
MgO	0.1	0.0118	<0.01	MgO	2.3	0.74
CaO	0.07	0.01	<0.01	CaO	2.5	2.18
Na_2O	0.11	0.0265	<0.03	Na_2O	3.77	3.39
K_2O	0.06	0.005	<0.01	K_2O	4.63	3.97
P_2O_5	0.08	0.01	<0.01	P_2O_5	0.28	0.097
Cr_2O_3	0.0053	0.0006	<0.01	Cr_2O_3	0.008	0.0094
NiO	0.01	0.0013	<0.01	NiO	0.0043	0.0008
V_2O_5	0.0018	0.0008	<0.01	V_2O_5	0.0116	0.0045
ZrO_2	0.005	0.0009	<0.01	ZrO_2	0.0317	0.0146
CuO	0.0037	0.0003	<0.01	CuO	0.0025	0.0002
LOI				LOI	1.32	0.46
TOTAL				TOTAL	0	0

	std dev. (ppm)	LOD	LIT	PPM	GSNcert	JG1cert
Cu	3	2	<2	Cu	20	1.5
Ga	2	2	<2	Ga	22	17
Mo	1	1	<1	Mo	1.2	1.46
Nb	3	2	<2	Nb	21	12.6
NI	6	3	<3	NI	34	6
Pb	3	3	<3	Pb	53	26.2
Rb	5	3	<3	Rb	185	181
Sr	4	3	<3	Sr	570	184
Th	6	5	<5	Th	42	13.5
U	6	3	<3	U	8	3.3
Y	3	3	<3	Y	19	30
Zn	5	4	<4	Zn	48	41.5
Zr	6	10	<10	Zr	235	108
Ba	50	50	<50	Ba		
Cl	100	11	<11	Cl	1400	462
Cr	40	15	<15	Cr	450	60
%S	0.02	0.01	<0.01	%S	65	4
Sc	5	1	<1	Sc	55	64.6
V	10	1	<1	V	0.01	0.001
				Sc	7.3	6.5
				V	65	25

GSNcert and JGI cert are Certified standards used in the XRF Laboratories in Pretoria
LOD = Limit of detection LIT = limit noted in results table

Sm/Nd Analysis

APPARATUS: Automated VG 354 Thermal Ionization Mass Spectrometer with 5 collectors

SAMPLE PREPARATION: Approximately 0.2. grams of sample powder and about 2 drops (approximately 10-15 mg) of spike (contains known concentration of Sm and Nd) are added into clean teflon containers. Half a milliliter of 16N nitric acid (HNO_3) and 5 ml 42% HF acid are added, enough to cover the bottom of the bomb. Seal the bomb-vessels and heat sample at 100°C overnight to dissolve.

Open vessels and allow the liquid to evaporate off. To the dried residue add 1 ml of Boric acid and 5 ml of 2.5N HCl to dissolve any insoluble fluoride salts that might have been produced by reaction of the rock powder with HF. Dry off the sample at about 50°C overnight.

Dissolve the dry residue in 1 ml of 2.5.norm. HCl. The sample solution is then centrifuged to separate out the undissolved substance from the dissolved.

Different chemical elements (such as lead, uranium, strontium, rare earth elements, and others) are separated from the rest of the components of the rock using "ion exchange chromatography" using dilute acids (hydrochloric acid) and special columns and resins.

The purified elemental salt is evaporated down onto a wire filament about a millimeter wide, and a group of these "beads" are loaded into the source of a mass spectrometer, which can hold about five beads at once.

The sample is heated until it vaporizes and ionizes, and the electrically charged ions are accelerated down a tube and deflected by a magnetic field (magnet shown at right), which separates particles of the element with different masses (isotopes). The ratio of different isotopes is measured.

A table of the analysis is shown in the table.

SAMPLE DISSOLUTIONS **T. GOMWE**

							Measured data						Calculated data					
BOMB LAB ID	SAMPLE ID	WEIGHT	Sm-Nd SPIKE	DROPS	DATE	143/144	±	150/144	149/147	147/152	149/152	Nd	Sm	147/144	143/144	E 2044	
1	SH176UP40	0.20132	0.01992	2	01/02/08	0.511648	7	0.539179			1.006952	3.332	0.778	0.14118	0.511583	-6.03	Note; error on
2	SH176UP49	0.21583	0.01140	2	01/02/08	0.511486	14	0.342515			0.707568	5.085	1.07	0.12714	0.511463	-4.68	E 2044 will be about
3	SH176UP51	0.21196	0.01720	2	01/02/08	0.511493	37	0.435049			0.891112	4.17	0.837	0.12126	0.51145	-3.38	± 0.6 E units
4	SH176UP60	0.24309	0.01787	3	01/02/08	0.51144	58	0.266478				23.18	5.524	0.1441	0.51144	-8.8	
6	SH176UP8	0.23871	0.01143	2	01/02/08	0.511213	13	0.249930	*0.970278*	*0.560853*	0.544183	36.22	6.77	0.11302	0.51121	-5.9	
8	BLANK	0.00000	0.00540	1	01/02/08												
9	WR	0.25995	0.02155	4	01/02/08												
10	PLAG	0.30268	0.02137	4	01/02/08	0.510628	8	0.361045	*1.586185*	*0.561387*	0.890464	5.78	0.73	0.07167	0.51060	-8.0	
11	SH176UP1	0.21071	0.01728	3	01/02/05	0.511401	80	0.282304	*1.071683*	*0.560940*	0.601150	18.27	3.76	0.12449	0.51139	-5.4	
12	SH176UP5	0.25127	0.01270	2	01/02/05	0.511301	9	0.280300	*1.063916*	*0.560933*	0.596786	11.77	2.44	0.12548	0.51129	-7.6	
14	SH176UP19	0.20917	0.01372	2	01/02/05	0.511356	8	0.296411	*1.121185*	*0.560983*	0.628966	11.17	2.26	0.12230	0.51134	-5.8	
15	SH176UP23	0.20545	0.01625	2	01/02/05	0.511472	11	0.326124	*1.194979*	*0.561047*	0.670439	9.08	1.99	0.13349	0.51145	-6.6	
16	SH176UP26	0.20450	0.01913	3	01/02/05	0.511416	8	0.388156	*1.400881*	*0.561226*	0.786211	6.29	1.34	0.12873	0.51138	-6.7	
standard	Goodfellow Nd					0.511098	9										
standard	Goodfellow Nd																
	Goodfellow Nd					0.511244	19										

ICP-MS Analysis (from UCT http://www.uct.ac.za/depts/geolsci/icpms/home/home.html)

APPARATUS:

Perkin Elmer / Sciex Elan 6000 inductively coupled plasma mass spectrometer equipped with a acid-resistant cross flow nebuliser, a *Ryton*^{TM} Scott-type spraychamber and a Perkin Elmer AS 90 autosampler.

SAMPLE PREPARATION:

In the case of solid samples analyzed by laser ablation ICP-MS and liquid samples analyzed by solution ICP-MS, sample preparation may be minimal. Rock samples to be analyzed by solution ICP-MS have to be dissolved by ***acid digestion***. Various digestion methods involving a range of different ultra clean acids (e.g. HF, HNO_3, HCl, $HClO_4$, aqua regia) may be used to dissolve various types of materials. Digestion in a microwave oven may speed-up the procedure and help to ensure that all of the sample material is dissolved. Fusion procedures using one of a number of fluxing agents may be required to dissolve refractory minerals such as zircon in some instances. For quantitative analysis, it is crucial that all of the sample material is entirely dissolved.

One of the simplest acid digestion procedures involves the digestion of 50-100 mg of fine, homogenous sample powder in a mixture of HNO_3 and HF in heated, closed teflon beakers, followed by evaporation to complete dryness and two further stages of digestion in HNO_3 and evaporation. The final stage of sample preparation involves dissolution in ~ 2 % HNO_3 internal standard stock solution containing 10 ppb of all the internal standards required for analysis. Most rock samples have to be diluted by a factor of at least 1000-2000 times in order to lower the total dissolved solid content of the final solution to a level at which clogging of interface cone orifices is not a problem

CALIBRATION:

For quantitative ICP-MS analysis, calibration is most commonly achieved by *external standardization*. The signal intensities of all analyte isotopes are measured in a blank as well as in one or more artificial or natural standards with different, known analyte concentrations that cover the concentration range of interest. The (hopefully) linear relationship between the blank-corrected standards on a diagram of signal intensity vs concentration is used to establish a calibration curve that may be used to calculate the

concentration of the analytes in samples of unknown composition. Isotopes commonly used as internal standards in solution ICP-MS include ^{9}Be, ^{45}Sc, ^{89}Y, ^{103}Rh, ^{115}In and ^{209}Bi.

ANALYTICAL RANGE AND DETECTION LIMITS:

The analytical range of solution ICP-MS extends from the ppt (parts per trillion) to the ppm (parts per million) regions. Solution ICP-MS combines perfectly with a good major and minor element technique such as X-ray fluorescence spectrometry (XRFS). For most elements that can be determined by solution ICP-MS, best-scenario theoretical detection limits are in the ppt range (some in the ppb range).

ACCURACY AND PRECISION:

In most cases, accuracies and precisions of ~ 1 - 3 % may be expected for solution ICP-MS for all elements. Accuracies and precisions of ~ 1 - 10 % are typical for most elements analyzed by laser ablation ICP-MS.

LECO Analysis.

APPARATUS: Perkin Elmer Elan 6000, Autosampler, FIAS
LECO CHN 1000

SAMPLE PREP:

- Preferably finely ground, oven- dried material stored in desiccators, or air-dried and corrected for moisture content.
- 200-400 mg soil
- The reference solutions (or standards) are prepared using pure solutions bought for the atomic absorption or using rocks known (reference samples) amalgamated and put in solution in the same way as the unknown ones. The technique of calibration compared to natural rocks is used as it is less practical and not easy to make sure that the setting in solution is perfect. Moreover, it is necessary to make several dilutions to be within the detection limits of the apparatus (typically between 1 and 5 g/mL. The solutions must have concentrations of 1000 g/mL and they should be diluted to be in the linear part of the spectrum.

FINAL DILUTIONS:

- Samples are generally acidified solutions (1%HNO_3) with <2% TDS (total dissolved solids)
- An internal standard of Rh or Ir is usually added to the samples, blanks and standards
- Should be made up with MilliQ 18MW water into acid washed vials
- Note that for extract solutions, a final dilution to <0.2% TDS may make the heavy metals of interest undetectable
- The sample volume required depends on number of elements measured; minimum 10 mL
- Final dilutions should not be prepared until you're ready to measure them as ppb range must be used within 1 week and stored in the fridge.
- Measurement Range: > 0.05% C or S

APPENDIX II

ANALYTICAL DATA

MAJOR AND TRACE ELEMENT DATA FROM XRF

PGE, Au AND Cu DATA FROM INAA

SULPHUR CONTENT FROM LECO TITRATION

TRACE ELEMENT DATA FROM ICP-MS

Ni AND Fo VALUES FOR OLIVINE

LIST OF SAMPLES ANALYSED

Sample	Depth (m)	Rock Type	Rock Unit
SH176 UP 1	135.41 - 135.65	Gabbro	top chill
SH176 UP 2	137.45 - 137.83	Gabbro	GN Unit
SH176 UP 3	152.25 - 152.58	Gabbro	GN Unit
SH176 UP 4	163.33 - 163.69	Gabbro	GN Unit
SH176 UP 5	181.09 - 181.40	Gabbro	GN Unit
SH176 UP 6	192.25 - 192.59	Gabbronorite	GN Unit
SH176 UP 7	202.29 - 202.64	Gabbronorite	GN Unit
SH176 UP 8	216.22 - 216.53	Norite	GN Unit
SH176 UP 9	217.28 - 217.72	Norite	GN Unit
SH176 UP 10	229.21 - 229.52	Norite	GN Unit
SH176 UP 11	246.52 - 246.93	Norite	GN Unit
SH176 UP 12	264.52 - 264.79	Norite	GN Unit
SH176 UP 13	278.54 - 278.79	Norite	GN Unit
SH176 UP 14	286.40 - 268.67	Norite	GN Unit
SH176 UP 15	303.17 - 303.48	Pyroxenite	GN Unit
SH176 UP 16	313.12 - 313.47	Norite	GN Unit
SH176 UP 17	329.19 - 329.71	Norite	GN Unit
SH176 UP 18	358.33 - 358.65	Norite	GN Unit
SH176 UP 19	375.42 - 375.77	Pyroxenite	GN Unit
SH176 UP 20	382.48 - 382.80	Norite	GN Unit
SH176 UP 21	402.64 - 402.97	Norite	GN Unit
SH176 UP 22	409.04 - 409.28	Norite	GN Unit
SH176 UP 23	432.11 - 432.49	Norite	GN Unit
SH176 UP 24	450.44 - 450.74	Norite	GN Unit
SH176 UP 25	458.36 - 458.71	Norite	GN Unit
SH176 UP 26	459.75 - 459.99	Pyroxenite	PXT Unit
SH176 UP 27	467.30 - 467.55	Pyroxenite	PXT Unit
SH176 UP 28	481.48 - 481.87	Pyroxenite	PXT Unit
SH176 UP 29	492.04 - 492.42	Pyroxenite	PXT Unit
SH176 UP 30	507.15 - 507.49	Pyroxenite	PXT Unit
SH176 UP 31	516.08 - 516.37	Pyroxenite	PXT Unit
SH176 UP 32	527.04 - 527.38	Pyroxenite	PXT Unit
SH176 UP 33	532.17 - 532.43	Peridotite	MHZBG Unit
SH176 UP 34	547.66 - 547.94	Peridotite	MHZBG Unit
SH176 UP 35	567.14 - 567.45	Peridotite	MHZBG Unit
SH176 UP 36	584.22 - 584.55	Pyroxenite	MHZBG Unit
SH176 UP 37	603.60 - 603.90	Peridotite	MHZBG Unit
SH176 UP 38	620.50 - 620.83	Peridotite	MHZBG Unit
SH176 UP 39	639.10 - 639.46	Peridotite	MHZBG Unit
SH176 UP 40	647.60 - 647.79	Peridotite	MHZBG Unit
SH176 UP 41	662.34 - 662.67	Peridotite	MHZBG Unit
SH176 UP 42	673.34 - 673.63	Peridotite	MHZBG Unit
SH176 UP 43	696.61 - 696.94	Pyroxenite	MHZBG Unit
SH176 UP 44	716.60 - 716.95	Peridotite	MHZBG Unit
SH176 UP 45	741.04 - 741.29	Peridotite	MHZBG Unit
SH176 UP 46	751.42 - 751.67	Peridotite	MHZBG Unit
SH176 UP 47	775.52 - 775.88	Peridotite	MHZBG Unit
SH176 UP 48	791.06 - 791.44	Peridotite	MHZBG Unit
SH176 UP 49	807.04 - 807.44	Peridotite	MHZBG Unit
SH176 UP 50	828.32 - 828.76	Peridotite	MHZBG Unit
SH176 UP 51	854.06 - 854.37	Pyroxenite	PCR
SH176 UP 52	890.56 - 890.84	Chromititic Pyroxenite	PCR
SH176 UP 53	905.16 - 905.61	Chromititic Pyroxenite	PCR
SH176 UP 54	922.05 - 922.41	Pyroxenite	LHZBG
SH176 UP 55	931.50 - 931.82	Pyroxenite	LHZBG
SH176 UP 56	974.61 - 974.95	Wherlite	LHZBG
SH176 UP 57	974.67 - 974.93	Peridotite	LHZBG
SH176 UP 58	985.33 - 985.84	Peridotite	LHZBG
SH176 UP 59	987.55 - 987.89	Gabbro	BGAB
SH176 UP 60	990.29 - 990.49	Gabbro	BGAB

MAJOR, TRACE AND PGE DATA

Rock Unit		UGAB	UGAB	UGAB	UGAB	UGAB	UGAB	UGAB	GN	GN	GN	GN	GN	GN	GN	GN	GN
Sample	GSN	SH176UP1	SH176UP2	SH176UP3	SH176UP4	SH176UP5	SH176UP6	SH176UP7	SH176UP8	SH176UP9	SH176UP10	SH176UP11	SH176UP12	SH176UP13	SH176UP14	SH176UP15	SH176UP16
Depth (m)		135.41	137.45	152.25	163.33	181.09	192.25	202.29	216.22	217.28	229.21	246.52	264.52	278.54	286.40	303.17	313.12
SiO2	66.90	57.05	57.03	57.84	56.36	54.10	55.74	56.39	69.45	70.39	70.25	61.91	57.81	57.19	54.80	56.94	48.17
TiO2	0.65	0.56	0.61	0.64	0.61	0.42	0.48	0.52	0.74	0.68	0.78	1.43	1.82	1.75	1.72	0.49	2.17
Al2O3	15.04	13.96	14.84	14.97	15.22	17.00	11.57	12.40	12.86	13.04	13.79	13.82	12.95	14.07	13.40	13.89	12.17
Fe2O3	3.63	13.42	10.41	10.31	10.56	8.54	11.10	11.01	4.20	3.65	2.05	7.13	8.06	7.68	8.01	11.44	22.03
MnO	0.05	0.16	0.15	0.14	0.16	0.12	0.17	0.16	0.05	0.04	0.05	0.08	0.08	0.11	0.09	0.16	0.26
MgO	2.27	5.58	5.83	4.56	4.89	10.10	10.53	9.40	0.55	0.53	0.77	1.70	2.01	1.92	1.92	7.27	2.73
CaO	2.51	6.58	6.73	6.71	6.01	6.65	5.79	5.36	3.67	3.29	5.21	6.70	8.65	8.81	11.93	6.50	6.52
Na2O	4.01	1.24	2.42	2.46	4.02	1.68	1.42	2.14	6.18	6.30	5.93	5.94	5.34	5.17	4.48	1.77	2.17
K2O	4.72	1.36	0.50	1.82	1.34	2.11	1.19	1.52	0.05	0.02	0.08	0.38	0.10	0.25	0.06	1.41	1.24
P2O5	0.31	0.15	0.10	0.10	0.09	0.09	0.07	0.08	0.16	0.15	0.17	0.21	0.26	0.46	0.95	0.12	0.90
Cr2O3	0.01	0.05	0.03	0.02	0.01	0.01	0.15	0.14	<0.01	<0.01	<0.01	<0.01	<0.01	<0.01	0.00	0.08	<0.01
NiO	0.01	0.01	0.01	0.01	0.01	0.00	0.03	0.03	<0.01	<0.01	<0.01	<0.01	<0.01	<0.01	0.00	0.02	<0.01
V2O5	0.01	0.03	0.03	0.03	0.03	0.01	0.03	0.03	0.01	0.01	0.01	0.02	0.03	0.02	0.00	0.03	0.02
ZrO2	0.03	0.02	0.02	0.02	0.02	0.00	0.02	0.02	0.05	0.04	0.03	0.03	0.04	0.03	0.01	0.02	0.01
LOI	1.29	1.22	1.85	1.06	1.30	1.05	1.14	1.22	2.50	2.67	2.26	1.82	1.49	1.16	2.01	1.34	1.44
TOTAL	101.43	101.40	100.57	100.70	100.62	101.88	99.43	100.41	100.47	100.81	101.39	101.17	98.64	98.62	99.39	101.47	99.82
ppm																	
As	3	3	3	5	3	3	3	3	3	4	3	3	3	3	3	5	4
Cu	-	114	21	47	67	7	44	59	13	25	16	13	7	14	13	39	30
Ga	20	10	17	17	18	17	14	16	19	17	20	19	19	18	19	18	21
Mo	1	4	3	2	2	1	2	2	1	1	1	1	1	1	1	1	3
Nb	24	8	8	11	9	6	6	8	19	17	18	17	16	20	14	9	11
Ni	35	105	101	75	73	175	239	204	3	5	6	11	11	14	12	138	14
Pb	54	23	13	17	15	7	17	16	3	5	6	6	5	3	6	13	11
Rb	186	89	25	93	71	84	57	76	3	3	7	11	5	3	2	59	53
Sr	563	115	123	175	146	221	119	144	165	91	221	225	291	228	264	168	276
Th	41	9	12	14	11	7	8	8	8	13	7	9	3	7	11	8	4
U	7	3	6	3	3	3	3	4	3	3	3	3	3	3	3	3	3
W	481	6	6	6	6	6	6	6	6	6	6	6	6	6	6	6	6
Y	21	23	23	25	22	16	18	20	35	35	36	40	28	39	31	23	30
Zn	43	86	40	67	78	40	73	81	18	14	17	18	22	19	20	90	138
Zr	216	128	128	135	116	92	102	101	368	338	291	203	200	194	127	128	123
Cl	580	1310	382	702	278	273	301	450	263	242	485	528	519	588	621	599	1956
Co	47	73	59	57	59	54	72	73	13	13	19	28	27	31	28	66	104
Cr	60	262	222	104	74	550	1166	1108	21	22	20	32	25	29	19	473	26
F	2678	100	100	100	100	100	100	100	257	332	238	145	189	284	316	100	100
S	-	170	<50	<50	60	<50	<50	<50	270	230	560	120	130	100	350	120	1140
Sc	9	24	27	26	32	23	33	33	10	9	15	21	20	34	14	32	35
V	65	195	178	176	189	154	190	190	42	44	45	116	117	179	33	165	86
Ni	-	105	101	75	73	175	239	204	3	5	6	11	11	14	12	138	14
ppb																	
Os		<0.6	<0.4	<0.4	<0.3	<0.5	0.5	<0.6	<0.4	<0.5	<0.7	<0.3	<0.4	<0.6	<0.3	<0.3	0.5
Ir		0.083	0.053	0.057	0.020	0.100	0.113	0.110	0.008	0.009	0.010	0.019	0.012	0.160	0.010	0.060	0.020
Ru		5	5	<2	<4	4	<1	<2	<2	<2	<3	<2	<1	<4	<2	3	<4
Rh		0.8	0.7	1.1	0.8	1.0	1.2	1.3	<0.3	<0.3	<0.5	<0.4	<0.4	<0.7	<0.7	0.6	0.2
Pt		32	7	4	4	11	5	12	<3	4	<2	2	1	23	<2	<8	<2
Pd		8	10	11	10	6	5	10	<3	<5	<6	1	<2	2	<4	7	<2
Au		2.67	2.39	6.76	3.83	5.34	3.24	3.28	1.37	1.53	4.94	1.69	0.87	3.06	2.66	1.04	2.63
Re		0.17	0.21	<0.24	<0.25	<0.21	<0.21	<0.22	0.28	0.20	<0.23	0.38	<0.22	0.12	<0.14	<0.19	<0.14
Se		109	21	61	74	6	50	57	11	24	17	17	10	16	13	47	43

<1 = below detection limit of 1

MAJOR, TRACE AND PGE DATA

Rock Unit	GN	GN	GN	GN	GN	GN	GN	GN	GN	PXT	PXT	PXT	PXT	PXT	PXT	PXT
Sample	SH176UP17	SH176UP18	SH176UP19	SH176UP20	SH176UP21	SH176UP22	SH176UP23	SH176UP24	SH176UP25	SH176UP26	SH176UP27	SH176UP28	SH176UP29	SH176UP30	SH176UP31	SH176UP32
Depth (m)	329.19	358.33	375.42	382.48	402.64	409.04	432.11	450.44	458.36	459.75	467.30	481.48	492.04	507.15	516.08	527.04
SiO2	50.40	49.56	42.44	49.05	54.71	45.02	52.40	49.27	53.14	52.60	52.29	54.02	54.34	54.17	53.79	47.80
TiO2	2.23	2.33	2.09	3.61	0.32	2.87	0.34	0.32	0.27	0.32	0.30	0.27	0.24	0.34	0.27	0.13
Al2O3	15.80	13.43	9.91	15.34	7.05	16.92	16.07	17.65	12.78	7.09	7.13	6.14	5.49	4.29	6.35	3.84
Fe2O3	16.80	20.52	34.67	18.15	12.71	18.63	9.78	10.54	10.38	12.17	12.14	12.86	11.97	12.56	10.40	9.04
MnO	0.17	0.24	0.31	0.20	0.20	0.17	0.15	0.13	0.16	0.20	0.20	0.25	0.31	0.20	0.18	0.14
MgO	2.67	4.03	6.77	4.48	19.65	5.81	8.22	8.48	14.62	18.69	19.04	21.00	22.61	24.73	26.31	33.66
CaO	6.70	6.74	4.19	6.78	5.06	8.00	10.50	9.29	7.35	4.76	4.81	4.49	3.72	3.11	2.68	2.58
Na2O	2.50	2.01	0.99	1.92	0.59	1.74	1.66	1.43	0.98	0.66	0.58	0.44	0.33	0.04	0.01	0.01
K2O	1.46	1.06	0.67	0.90	0.44	0.55	0.49	0.73	0.49	0.45	0.43	0.31	0.33	0.19	0.22	0.17
P2O5	0.84	0.58	0.08	0.06	0.02	0.03	0.04	0.02	0.03	0.04	0.04	0.04	0.04	0.02	0.01	0.01
Cr2O3	<0.01	<0.01	0.01	<0.01	0.20	0.03	0.02	0.06	0.14	0.2	0.23	0.36	0.38	0.44	0.50	0.71
NiO	<0.01	<0.01	<0.01	<0.01	0.06	<0.01	0.01	0.02	0.08	0.06	0.11	0.12	0.08	0.08	0.10	0.21
V2O5	0.02	0.02	0.03	0.08	0.03	0.22	0.03	0.02	0.03	0.03	0.03	0.03	0.03	0.02	0.02	0.02
ZrO2	0.01	0.01	<0.01	0.01	0.01	0.01	0.01	0.01	0.01	0.01	0.01	0.01	0.01	0.01	0.01	0.01
LOI	1.89	0.40	-1.16	0.25	0.12	0.50	0.91	2.25	0.78	0.73	1.39	0.68	0.14	-0.05	0.08	2.76
TOTAL	101.49	100.93	101.01	100.85	101.18	100.49	100.63	100.23	101.24	98.01	98.73	101.01	100.02	100.16	100.91	101.10
ppm																
As	4	3	5	3	3	5	3	3	3	3	3	3	4	3	3	3
Cu	29	21	13	33	37	53	62	22	315	164	387	278	115	9	49	35
Ga	21	20	16	22	23	24	16	15	12	10	10	7	7	7	7	6
Mo	1	2	2	1	2	1	2	2	1	1	1	2	1	1	1	1
Nb	11	10	6	10	7	5	3	4	3	4	4	3	3	4	2	3
Ni	15	14	31	30	33	51	94	150	637	481	846	906	677	718	720	1615
Pb	9	7	8	15	7	10	3	3	6	3	13	9	9	6	3	3
Rb	58	46	34	38	23	25	19	27	18	20	17	15	14	10	11	8
Sr	302	270	196	292	331	325	237	244	166	93	106	94	90	54	55	54
Th	6	4	4	3	3	3	3	3	4	3	3	4	3	3	3	3
U	3	3	6	3	3	3	3	3	3	3	3	3	3	3	3	3
W	6	6	6	6	6	6	6	6	6	6	6	6	6	6	6	6
Y	23	20	13	14	12	10	15	9	11	12	10	10	9	7	8	8
Zn	110	117	139	144	87	84	61	49	63	74	88	77	77	62	62	52
Zr	105	80	85	92	65	48	59	42	45	51	42	43	41	32	30	26
Cl	1287	1313	1623	1153	593	496	346	252	196	234	676	202	411	190	226	306
Co	92	106	201	98	92	113	60	64	84	101	106	111	98	94	87	97
Cr	26	31	38	56	70	131	156	357	1051	1558	1813	2768	2990	3429	3909	4861
F	100	100	100	100	100	100	100	100	100	100	100	100	100	100	100	100
S	1070	650	260	1320	1350	1630	780	420	3820	1500	3140	3970	1470	120	340	440
Sc	31	27	11	35	24	22	21	18	26	36	36	31	31	27	23	19
V	91	106	130	417	268	1147	164	143	141	172	180	163	150	127	125	87
Ni	15	14	31	30	33	51	94	150	637	481	846	906	677	718	720	1615
ppb																
Os	<0.6	0.4	<0.5	<0.5	<0.5	<0.5	<0.3	<0.3	<0.4	<0.6	<0.7	1.8	<0.2	0.8	1.7	2.6
Ir	0.020	0.018	0.023	0.019	0.058	0.038	0.036	0.037	0.057	0.053	0.050	2.012	0.550	0.619	1.348	2.238
Ru	<4	<4	<3	<2	<2	<2	1	<2	<2	<3	<4	5	<8	3	16	23
Rh	0.2	<0.4	<0.2	<0.2	<0.2	<0.1	<0.2	0.3	<0.3	<0.4	0.2	5.2	3.3	1.9	2.4	3.1
Pt	33	<1	<1	1	1	2	1	1	3	3	3	46	18	91	21	13
Pd	<2	<3	<5	<2	<3	1	1	<2	<3	<3	6	82	53	5	7	<8
Au	3.55	1.34	1.29	0.88	0.80	0.40	0.56	1.13	1.48	1.60	4.09	11.12	5.90	1.58	1.97	3.03
Re	0.12	21	13	33	37	53	62	22	315	164	387	278	115	9	49	35
Se	37	29	21	43	48	70	69	27	307	170	340	266	133	56	55	40

<1 = below detection limit of 1

MAJOR, TRACE AND PGE DATA

Rock Unit	MHZBG	MHZBG	MHZBG	MHZBG	MHZBG	MHZBG	MHZBG	MHZBG	MHZBG	MHZBG	MHZBG	MHZBG	MHZBG	MHZBG	MHZBG	MHZBG
Sample	SH176UP33	SH176UP34	SH176UP35	SH176UP36	SH176UP37	SH176UP38	SH176UP39	SH176UP40	SH176UP41	SH176UP42	SH176UP43	SH176UP44	SH176UP45	SH176UP46	SH176UP47	SH176UP48
Depth (m)	532.17	547.66	567.14	584.22	603.60	620.50	639.10	647.60	662.34	673.34	696.61	716.60	741.04	751.42	775.52	791.06
SiO2	40.87	37.47	39.53	37.41	36.40	39.25	39.32	39.77	38.36	38.30	36.22	39.46	37.24	38.46	35.94	35.62
TiO2	0.11	0.11	0.11	0.10	0.16	0.13	0.15	0.16	0.15	0.16	0.13	0.13	0.15	0.15	0.15	0.18
Al2O3	2.73	3.12	1.76	2.76	2.92	2.69	2.65	2.71	2.86	2.70	2.36	2.51	2.89	3.22	3.60	3.23
Fe2O3	9.61	9.66	10.34	11.63	12.91	11.18	10.71	10.51	10.94	10.84	9.07	10.55	12.99	10.54	12.40	12.54
MnO	0.13	0.13	0.13	0.13	0.11	0.12	0.09	0.10	0.10	0.11	0.17	0.10	0.09	0.15	0.11	0.16
MgO	36.47	35.82	39.53	35.07	34.25	35.52	34.35	36.01	34.83	35.29	28.81	34.18	33.18	33.73	32.54	33.14
CaO	1.81	1.67	1.15	1.42	1.01	1.20	1.63	1.47	1.50	1.51	2.71	1.36	1.21	1.56	1.06	1.60
Na2O	0.01	0.01	0.01	0.01	0.01	0.01	0.01	0.01	0.01	0.01	0.00	0.01	0.01	0.01	0.00	0.01
K2O	0.10	0.12	0.13	0.05	0.27	0.16	0.13	0.16	0.14	0.16	0.00	0.14	0.12	0.15	0.04	0.19
P2O5	0.01	<0.01	0.01	<0.01	0.01	0.01	0.01	0.01	0.01	0.01	0.01	0.01	0.00	0.01	<0.01	0.02
Cr2O3	0.93	3.62	1.54	3.64	2.18	0.88	1.22	1.74	2.51	2.09	1.31	1.27	1.80	1.69	5.57	3.74
NiO	0.24	0.30	0.33	0.29	0.61	0.32	0.32	0.34	0.30	0.34	0.28	0.36	0.51	0.32	0.65	0.61
V2O5	0.01	0.02	0.01	0.02	0.01	0.01	0.01	0.01	0.02	0.01	0.01	0.01	0.02	0.01	0.03	0.02
ZrO2	0.01	0.01	0.01	0.01	0.01	0.01	0.01	0.01	0.01	0.01	0.01	0.01	0.01	0.01	<0.01	0.01
LOI	8.88	8.65	6.99	8.38	9.07	9.35	8.12	7.72	7.82	7.49	18.14	8.89	9.07	9.15	9.07	10.03
TOTAL	101.92	100.69	101.58	100.91	99.93	100.83	98.73	100.72	99.55	99.04	99.23	99.00	99.29	99.14	101.16	101.07
ppm																
As	3	4	3	3	3	3	3	3	3	3	101	3	3	3	3	4
Cu	21	25	14	11	740	6	27	48	26	38	10	54	858	76	560	955
Ga	5	4	5	4	6	6	6	6	5	5	5	5	5	5	7	5
Mo	2	1	1	2	1	1	2	1	1	1	1	1	1	1	1	1
Nb	4	2	2	2	3	3	3	4	3	3	3	2	3	2	2	3
Ni	1857	2512	2583	2551	3593	2515	2647	2668	2322	2484	1799	2889	4091	2431	5206	4490
Pb	3	3	8	3	40	3	6	3	6	3	3	4	3	6	3	3
Rb	7	3	8	8	9	7	11	11	8	9	2	9	8	10	4	12
Sr	19	16	43	32	21	28	25	16	18	20	66	24	13	30	10	17
Th	3	3	3	3	4	3	3	3	3	3	3	3	3	3	3	3
U	3	3	3	3	3	3	3	3	3	3	3	3	3	3	3	3
W	6	6	6	6	6	6	6	6	6	6	6	6	6	6	6	6
Y	6	7	6	6	7	8	6	7	8	6	6	7	7	7	7	7
Zn	50	54	49	48	82	48	55	47	50	44	80	42	66	56	93	53
Zr	26	19	22	25	26	28	31	30	29	29	24	28	29	28	20	38
Cl	926	879	756	1592	225	615	391	293	401	209	8	331	182	667	115	334
Co	112	109	137	128	177	130	120	121	114	120	89	165	172	114	159	153
Cr	5241	16950	22027	8394	16767	4558	12573	10884	15415	7796	6751	7920	11341	9030	34937	11581
F	100	100	100	100	100	100	100	100	100	100	100	100	100	100	100	100
S	330	360	240	170	10640	270	500	660	620	350	180	660	10770	800	9040	14980
Sc	11	11	11	10	10	10	12	12	12	11	8	13	10	11	12	9
V	49	80	71	50	65	42	63	62	67	56	44	57	66	59	114	54
Ni	1857	2512	2583	2551	3593	2515	2647	2668	2322	2484	1799	2889	4091	2431	5206	4490
ppb																
Os	2.4	9.7	19.9	5.0	30.0	2.3	6.0	7.1	7.5	4.6	4.8	3.6	8.5	3.6	25.6	18.1
Ir	2.410	9.441	18.286	5.658	15.072	1.824	5.410	5.740	5.280	4.360	3.680	3.160	6.940	3.210	18.310	12.179
Ru	8	32	55	18	87	12	23	22	24	18	<12	17	40	15	107	66
Rh	1.1	4.9	15.9	1.1	13.9	1.4	8.3	10.0	6.1	7.3	5.3	7.9	9.4	5.3	21.9	28.4
Pt	25	25	116	9	71	7	41	164	16	102	59	97	79	50	170	205
Pd	4	6	16	<3	120	4	69	49	33	49	<28	79	117	27	278	409
Au	1.86	2.06	4.69	1.55	12.79	1.69	4.43	16.48	1.69	7.12	5.90	9.19	19.35	3.62	31.44	30.16
Re	21	25	<0.30	0.26	7.91	<0.2	0.24	0.21	0.59	0.44	<0.93	0.34	6.45	1.05	8.58	955
Se	23	26	117	44	835	72	33	47	25	41	7	83	852	71	590	1012

<1 = below detection limit of 1

MAJOR, TRACE AND PGE DATA

Rock Unit	MHZBG	PCR	PCR	PCR	LHZBG	LHZBG	LHZBG	LHZBG	LHZBG	LHZBG	BGAB	BGAB
Sample	SH176UP49	SH176UP50	SH176UP51	SH176UP52	SH176UP53	SH176UP54	SH176UP55	SH176UP56	SH176UP57	SH176UP58	SH176UP59	SH176UP60
Depth (m)	807.04	828.32	854.06	890.56	905.16	922.05	931.50	974.61	974.67	985.33	987.55	990.29
SiO2	36.80	36.39	35.12	38.70	35.40	38.27	38.51	43.80	35.41	44.05	47.39	50.65
TiO2	0.13	0.16	0.21	0.25	0.48	0.18	0.44	0.82	0.47	0.81	0.97	1.64
Al2O3	2.42	3.72	4.62	4.85	10.84	3.77	5.27	6.79	3.73	6.82	13.27	14.04
Fe2O3	11.58	12.60	8.58	10.59	16.30	13.57	13.88	17.47	27.20	17.49	16.74	11.93
MnO	0.10	0.11	0.11	0.18	0.23	0.18	0.16	0.17	0.15	0.17	0.14	0.17
MgO	35.07	33.43	33.42	29.29	13.45	29.94	24.65	16.85	21.69	17.01	5.59	5.12
CaO	0.86	1.06	1.75	3.10	2.70	6.89	9.83	6.84	3.39	6.84	8.09	7.25
Na2O	0.01	0.01	0.01	0.00	0.01	0.01	0.01	0.20	0.01	0.19	2.73	3.39
K2O	0.15	0.03	0.29	0.15	0.05	0.22	0.69	1.77	0.16	1.78	1.62	2.35
P2O5	0.01	<0.01	0.03	0.02	0.01	<0.01	0.05	0.08	0.03	0.08	0.07	0.17
Cr2O3	2.71	6.19	4.77	5.11	19.70	0.15	0.88	0.07	0.04	0.07	0.01	0.00
NiO	0.42	0.66	0.30	0.25	0.19	0.26	0.28	0.46	0.57	0.46	0.54	0.01
V2O5	0.02	0.03	0.04	0.05	0.08	0.01	0.02	0.03	0.02	0.03	0.03	0.04
ZrO2	0.01	<0.01	0.00	0.00	0.00	0.01	0.01	0.01	<0.01	0.03	0.01	0.02
LOI	9.52	7.03	8.23	8.15	1.24	7.50	5.80	3.83	7.16	3.83	2.51	1.60
TOTAL	99.81	101.43	97.48	100.69	100.68	100.93	100.47	99.18	100.02	99.66	99.71	98.36
ppm												
As	3	3	3	3	4	4	3	3	4	3	3	3
Cu	685	464	490	509	505	736	1133	2199	3271	6262	6961	171
Ga	8	7	9	9	24	7	9	5	7	11	16	19
Mo	1	2	1	1	3	1	1	3	2	1	3	1
Nb	3	3	3	4	4	3	7	2	5	7	5	10
Ni	4388	4027	3848	2701	3407	1920	2073	11815	4331	3126	3997	73
Pb	3	3	3	5	9	10	6	14	7	4	20	9
Rb	14	11	15	11	7	10	32	4	9	101	52	77
Sr	21	38	22	25	16	39	35	10	20	68	458	383
Th	3	3	3	3	5	5	4	3	3	5	3	6
U	3	3	3	3	3	3	3	3	3	3	3	3
W	6	6	6	6	6	6	6	6	6	6	6	6
Y	10	9	8	9	10	9	10	8	10	18	21	29
Zn	74	83	106	126	343	43	63	120	113	108	104	86
Zr	40	29	28	51	53	36	70	21	55	105	91	170
Cl	348	221	247	195	187	528	386	56	160	508	369	540
Co	140	135	150	132	168	106	114	305	224	165	167	68
Cr	22038	31290	39489	37099	156467	993	5577	175	179	377	79	54
F	100	100	100	100	100	100	100	100	100	100	100	100
S	4250	6760	9340	10560	10030	17440	17180	27860	48640	21390	34650	760
Sc	9	7	8	12	18	8	3	9	14	14	17	21
V	77	94	146	156	416	59	81	39	90	143	158	229
Ni	4388	4027	3848	2701	3407	1920	2073	11815	4331	3126	3997	73
ppb												
Os	11.2	13.5	17.9	94.4	49.7	15.9	9.5	N/D	2.2	20.4	14.9	<0.5
Ir	8.766	10.600	13.300	22.011	38.487	8.130	7.996	N/D	2.920	30.250	40.653	0.180
Ru	32	54	90	38	183	25	11	N/D	<4.8	13	13	<2
Rh	17.7	17.4	21.3	33.3	49.4	26.1	19.6	N/D	1.9	25.7	27.3	0.4
Pt	112	114	123	691	316	197	210	N/D	428	404	341	3
Pd	222	201	265	466	410	501	478	N/D	868	526	399	4
Au	19.16	15.36	13.29	24.19	33.93	36.38	15.12	N/D	156.68	170.74	77.96	1.00
Re	685	464	490	509	505	736	1133	2199	3271	6262	6961	171
Se	673	553	546	542	782	746	1139	2497	3481	6007	6956	186

<1 = below detection limit of 1 N/D = NOT DETECTED

FeO, Mg# VALUES CALCUATED FOR BOREHOLE CORE SH176

Sample	GSN	SH176UP1	SH176UP2	SH176UP3	SH176UP4	SH176UP5	SH176UP6	SH176UP7	SH176UP8	SH176UP9	SH176UP10
FeO		12.20	9.46	9.37	9.60	7.76	10.09	10.01	3.76	3.27	1.75
Fe2O3+FeO	3.63	13.42	10.41	10.31	10.56	8.54	11.10	11.01	4.20	3.65	2.05
MgO	2.27	5.58	5.83	4.56	4.89	10.10	10.53	9.40	0.55	0.53	0.77
Mg#	1.000	0.449	0.523	0.465	0.476	0.699	0.650	0.626	0.207	0.225	0.439

Sample	SH176UP11	SH176UP12	SH176UP13	SH176UP14	SH176UP15	SH176UP16	SH176UP17	SH176UP18	SH176UP19	SH176UP20	SH176UP21
FeO	6.45	7.30	6.96	7.21	10.38	19.80	15.06	18.53	31.46	16.24	11.29
Fe2O3+FeO	7.13	8.06	7.68	8.01	11.44	22.03	16.80	20.52	34.67	18.15	12.71
MgO	1.70	2.01	1.92	1.92	7.27	2.73	2.67	4.03	6.77	4.48	19.65
Mg#	0.319	0.329	0.329	0.322	0.555	0.197	0.240	0.280	0.277	0.330	0.756

Sample	SH176UP22	SH176UP23	SH176UP24	SH176UP25	SH176UP26	SH176UP27	SH176UP28	SH176UP29	SH176UP30	SH176UP31	SH176UP32
FeO	16.62	8.75	9.50	8.71	14.82	13.17	10.93	10.64	11.35	9.44	8.17
Fe2O3+FeO	18.63	9.78	10.54	10.38	16.62	15.14	12.86	11.97	12.56	10.40	9.04
MgO	5.81	8.22	8.48	14.62	5.05	23.48	21.00	22.61	24.73	26.31	33.66
Mg#	0.384	0.626	0.614	0.750	0.378	0.761	0.774	0.791	0.795	0.833	0.880

Sample	SH176UP33	SH176UP34	SH176UP35	SH176UP36	SH176UP37	SH176UP38	SH176UP39	SH176UP40	SH176UP41	SH176UP42	SH176UP43
FeO	8.70	8.71	9.36	10.55	9.72	10.15	9.65	9.44	9.85	9.82	8.20
Fe2O3+FeO	9.61	9.66	10.34	11.63	12.91	11.18	10.71	10.51	10.94	10.84	9.07
MgO	36.47	35.82	39.53	35.07	34.25	35.52	34.35	36.01	34.83	35.29	28.81
Mg#	0.882	0.880	0.883	0.856	0.863	0.862	0.864	0.872	0.863	0.865	0.862

Sample	SH176UP44	SH176UP45	SH176UP46	SH176UP47	SH176UP48	SH176UP49	SH176UP50	SH176UP51	SH176UP52	SH176UP53	SH176UP54
FeO	9.49	9.75	9.42	9.55	8.55	9.76	10.16	5.98	8.47	12.92	8.94
Fe2O3+FeO	10.55	12.99	10.54	12.40	12.54	11.58	12.60	8.58	10.59	16.30	13.57
MgO	34.18	33.18	33.73	32.54	33.14	35.07	33.43	33.42	29.29	13.45	29.94
Mg#	0.865	0.859	0.865	0.859	0.874	0.865	0.854	0.909	0.860	0.650	0.857

Sample	SH176UP55	SH176UP56	SH176UP57	SH176UP58	SH176UP59	SH176UP60
FeO	9.31	15.88	24.72	15.90	15.22	10.84
Fe2O3+FeO	13.88	17.47	27.20	17.49	16.74	11.93
MgO	24.65	16.85	21.69	17.01	5.59	5.12
Mg#	0.825	0.654	0.610	0.656	0.396	0.457

ICP-MS DATA

Rock Unit	UGAB	UGAB	GN	GN	GN	GN	GN	GN	GN	PXT	PXT	PXT
Sample	SH176 UP1	SH176 UP5	SH176 UP8	SH176 UP11	SH176 UP15	SH176 UP19	SH176 UP22	SH176 UP23	SH176 UP25	SH176 UP26	SH176 UP28	SH176 UP31
Depth (m)	135.41	181.09	216.22	246.52	303.17	375.42	409.04	432.11	458.36	459.75	481.48	516.08
Sc	21.8	20.1	9.69	18.8	25.6	9.11	19.9	25.1	24.0	29.4	25.8	17.7
Se	0.23	*n.d.*	*n.d.*	*n.d.*	1.07	*n.d.*	0.15	*n.d.*	0.17	0.55	1.18	0.17
Rb	93.1	78.4	0.86	8.05	55.2	28.8	20.7	16.4	16.2	17.0	11.6	8.58
Sr	116	228	175	228	167	186	314	241	167	87.8	88.9	50.2
Y	17.5	12.7	30.2	36.0	19.1	8.97	6.18	9.42	6.51	7.24	6.15	3.32
Zr	115	80.8	274	134	123	55.3	45.1	56.9	34.8	39.6	31.7	19.4
Nb	7.41	5.62	18.6	17.2	8.38	5.82	3.31	2.79	2.14	2.19	1.86	0.75
Mo	2.73	0.31	0.26	0.53	1.02	0.92	0.46	0.58	0.37	0.40	0.70	0.32
Sb	1.76	1.49	1.45	1.22	0.44	0.21	0.085	0.15	0.088	0.10	0.15	0.061
Cs	14.9	1.66	0.072	0.21	4.31	2.88	3.08	2.63	2.66	1.53	1.39	0.93
Ba	280	323	73.2	211	331	175	122	154	160	114	96.8	85.3
La	21.4	15.0	57.7	35.2	22.8	12.6	7.37	8.54	7.06	7.08	5.66	2.80
Ce	44.6	30.2	104	78.0	48.2	26.4	15.3	18.3	14.7	14.8	12.1	5.91
Pr	4.89	3.27	10.6	9.87	5.57	2.98	1.72	2.14	1.69	1.64	1.42	0.69
Nd	19.1	12.6	39.7	43.5	22.9	12.1	7.07	8.92	6.79	6.88	5.87	2.87
Sm	3.75	2.48	6.99	9.36	4.53	2.26	1.41	1.89	1.33	1.30	1.19	0.61
Eu	0.83	0.63	1.57	2.03	1.28	0.90	0.73	0.69	0.40	0.39	0.35	0.17
Gd	3.60	2.41	6.20	8.46	4.25	2.11	1.31	1.84	1.27	1.31	1.21	0.55
Tb	0.55	0.37	0.90	1.23	0.62	0.30	0.19	0.28	0.20	0.21	0.19	0.087
Dy	3.54	2.37	5.51	7.40	3.80	1.80	1.19	1.81	1.21	1.30	1.21	0.58
Ho	0.71	0.48	1.10	1.36	0.76	0.35	0.23	0.37	0.25	0.28	0.24	0.13
Er	2.11	1.41	3.23	3.84	2.14	1.01	0.68	1.06	0.71	0.80	0.71	0.41
Tm	0.31	0.21	0.47	0.52	0.31	0.15	0.10	0.15	0.11	0.12	0.10	0.061
Yb	2.04	1.37	3.25	3.34	2.09	0.99	0.67	1.02	0.73	0.85	0.75	0.43
Lu	0.30	0.21	0.51	0.45	0.31	0.15	0.10	0.15	0.11	0.13	0.11	0.067
Hf	3.01	2.15	7.84	5.08	3.15	1.53	1.19	1.43	0.89	1.01	0.84	0.47
Ta	1.14	0.91	1.64	1.55	0.93	0.68	0.47	0.41	0.34	0.32	0.35	0.14
Pb	17.8	3.87	2.31	10.5	10.0	4.64	3.50	4.24	2.82	2.24	6.43	2.42
Th	10.4	6.87	9.85	7.30	5.98	3.20	1.47	2.08	1.32	1.73	1.40	0.83
U	5.63	2.48	3.66	2.44	2.40	1.11	0.60	0.91	0.43	0.50	0.81	0.37

Rock Unit	PXT	Upper MHZBG	Upper MHZBG	Upper MHZBG	Lower MHZBG	PCR	PCR	LHZBG	LHZBG	BGAB	BGAB
Sample	SH176 UP32	SH176 UP33	SH176 UP35	SH176 UP40	SH176 UP49	SH176 UP51	SH176 UP52	SH176 UP54	SH176 UP57	SH176 UP59	SH176 UP60
Depth (m)	527.04	532.17	567.14	647.6	807.04	854.06	890.56	922.05	979.67	987.55	990.29
Sc	12.7	5.09	7.07	7.48	7.26	6.90	10.2	11.1	12.1	19.2	20.2
Se	1.30	*n.d.*	0.98	0.86	1.67	3.13	1.39	3.50	16.1	7.38	*n.d.*
Rb	5.97	0.16	5.44	7.17	11.4	12.3	7.47	7.25	6.14	47.7	71.1
Sr	50.5	65.1	40.0	11.4	15.3	17.3	19.7	35.1	13.5	453	390
Y	2.90	1.92	2.09	3.23	4.84	3.84	5.50	4.59	5.41	15.8	22.9
Zr	13.5	15.1	9.77	22.8	31.5	15.1	31.8	28.7	41.4	91.9	164
Nb	0.92	0.91	0.61	1.23	1.99	1.20	2.11	2.17	2.43	4.72	10.5
Mo	0.39	0.19	0.24	0.57	0.59	0.51	0.44	0.28	0.53	1.01	0.80
Sb	0.077	10.6	0.031	0.051	0.28	0.27	4.31	1.02	2.21	0.56	0.96
Cs	0.67	0.14	0.67	0.99	1.11	2.09	1.62	1.19	1.20	1.54	1.78
Ba	51.5	3.39	69.0	28.8	46.6	35.4	17.8	38.8	29.0	321	899
La	2.61	1.94	2.04	3.45	4.63	4.78	4.74	4.60	4.14	12.7	20.8
Ce	5.44	3.57	4.19	7.22	10.9	9.84	11.0	10.2	9.62	29.0	47.0
Pr	0.63	0.42	0.48	0.84	1.30	1.13	1.31	1.15	1.22	3.74	5.89
Nd	2.55	1.73	2.01	3.38	5.30	4.43	5.52	4.40	5.41	16.5	26.1
Sm	0.53	0.37	0.41	0.66	1.12	0.88	1.13	0.87	1.25	3.80	5.63
Eu	0.17	0.24	0.14	0.17	0.22	0.27	0.24	0.28	0.25	1.22	1.70
Gd	0.53	0.34	0.41	0.64	1.03	0.82	1.07	0.84	1.19	3.61	5.53
Tb	0.085	0.054	0.062	0.10	0.16	0.12	0.16	0.13	0.18	0.54	0.80
Dy	0.55	0.34	0.40	0.60	0.94	0.75	1.07	0.83	1.10	3.27	4.71
Ho	0.11	0.074	0.080	0.12	0.18	0.15	0.21	0.18	0.21	0.62	0.89
Er	0.34	0.22	0.24	0.35	0.52	0.43	0.59	0.52	0.61	1.70	2.50
Tm	0.051	0.032	0.032	0.052	0.079	0.065	0.080	0.073	0.083	0.23	0.34
Yb	0.36	0.22	0.24	0.36	0.52	0.45	0.57	0.54	0.54	1.53	2.22
Lu	0.056	0.036	0.036	0.056	0.083	0.068	0.080	0.079	0.079	0.22	0.32
Hf	0.36	0.38	0.25	0.55	0.80	0.38	0.81	0.74	1.00	2.36	4.06
Th	0.26	0.18	0.20	0.25	0.41	0.32	0.30	0.27	0.33	0.49	0.95
Ta	1.54	1.96	5.10	1.52	2.40	1.15	1.35	4.07	1.88	15.7	4.72
Pb	0.73	0.52	0.40	0.72	1.89	0.73	1.13	0.72	0.80	1.59	2.97
U	0.47	0.15	0.10	0.26	0.49	0.17	0.24	0.30	0.22	0.44	0.84

Ni AND Fo VALUES FOR OLIVINE OF SELECTED SAMPLES FOR BOREHOLE CORE SH176

Sample	Depth (m)	Ni (ppm)	Fo (mol%)	Unit
SH176UP16	313.12	34	9.41	GN
SH176UP19	375.42	32	19.89	GN
SH176UP28	481.48	528	85.13	PXT
SH176UP29	492.04	3514	86.81	PXT
SH176UP32	527.04	3395	87.20	PXT
SH176UP33	532.17	2907	88.94	MHZBG
SH176UP34	542.66	3225	85.97	MHZBG
SH176UP35	567.14	3494	88.74	MHZBG
SH176UP36	584.22	3382	88.01	MHZBG
SH176UP37	603.60	2035	87.50	MHZBG
SH176UP38	620.50	3548	86.12	MHZBG
SH176UP40	647.60	3618	87.05	MHZBG
SH176UP41	662.34	3321	86.52	MHZBG
SH176UP42	673.34	3593	86.54	MHZBG
SH176UP44	716.60	3453	86.70	MHZBG
SH176UP45	741.04	3252	86.81	MHZBG
SH176UP46	751.42	1930	86.19	MHZBG
SH176UP47	775.52	2213	86.71	MHZBG
SH176UP48	791.06	2293	86.80	MHZBG
SH176UP49	807.04	2317	86.90	MHZBG
SH176UP50	828.32	1932	86.03	MHZBG
SH176UP51	854.06	1690	86.59	PCR
SH176UP53	905.16	1333	83.67	PCR
SH176UP55	931.50	1910	86.21	LHZBG

APPENDIX III

NORMALIZED DATA

CIPW NORM

ICPMS DATA NORMALIZED TO CHONDRITE AND PRIMITIVE MANTLE

PGE DATA NORMALIZED TO PRIMITIVE MANTLE

CIPW NORM DATA

Rock Unit	top chill	UGAB	UGAB	UGAB	UGAB	UGAB	UGAB	GN	GN	GN	GN	GN	GN
Sample	SH176UP1	SH176UP2	SH176UP3	SH176UP4	SH176UP5	SH176UP6	SH176UP7	SH176UP8	SH176UP9	SH176UP10	SH176UP11	SH176UP12	SH176UP13
Depth (m)	135.41	137.45	152.25	163.33	181.09	192.25	202.29	216.22	217.28	229.21	246.52	264.52	278.54
SiO_2	57.05	57.03	57.84	56.36	54.10	55.74	56.39	69.45	70.39	70.25	61.91	57.81	57.19
TiO_2	0.56	0.61	0.64	0.61	0.42	0.48	0.52	0.74	0.68	0.78	1.43	1.82	1.75
Al_2O_3	13.96	14.84	14.97	15.22	17.00	11.57	12.40	12.86	13.04	13.79	13.82	12.95	14.07
Fe_2O_3	13.42	10.41	10.31	10.56	8.54	11.10	11.01	4.20	3.65	2.05	7.13	8.06	7.68
MnO	0.16	0.15	0.14	0.16	0.12	0.17	0.16	0.05	0.04	0.05	0.08	0.08	0.11
MgO	5.58	5.83	4.56	4.89	10.10	10.53	9.40	0.55	0.53	0.77	1.70	2.01	1.92
CaO	6.58	6.73	6.71	6.01	6.65	5.79	5.36	3.67	3.29	5.21	6.70	8.65	8.81
Na_2O	1.24	2.42	2.46	4.02	1.68	1.42	2.14	6.18	6.30	5.93	5.94	5.34	5.17
K_2O	1.36	0.50	1.82	1.34	2.11	1.19	1.52	0.05	0.02	0.08	0.38	0.10	0.25
P_2O_5	0.15	0.10	0.10	0.09	0.09	0.07	0.08	0.16	0.15	0.17	0.21	0.26	0.46
Cr_2O_3	0.05	0.03	0.02	0.01	0.01	0.15	0.14	<0.01	<0.01	<0.01	<0.01	<0.01	<0.01
NiO	0.01	0.01	0.01	0.01	0.00	0.03	0.03	<0.01	<0.01	<0.01	<0.01	<0.01	<0.01
V_2O_5	0.03	0.03	0.03	0.03	0.01	0.03	0.03	0.01	0.01	0.01	0.02	0.03	0.02
ZrO_2	0.02	0.02	0.02	0.02	0.00	0.02	0.02	0.05	0.04	0.03	0.03	0.04	0.03
LOI	1.22	1.85	1.06	1.30	1.05	1.14	1.22	2.50	2.67	2.26	1.82	1.49	1.16
TOTAL	101.40	100.57	100.70	100.62	101.88	99.43	100.41	100.47	100.81	101.39	101.17	98.64	98.62
Q (S)	14.02	12.26	10.49	2.86	1.22	8.83	6.63	25.4	26.49	27.26	10.41	7.92	7.34
or (KAS6)	8.04	3	10.81	7.99	12.38	7.18	9.08	0.3	0.12	0.48	2.26	0.61	1.52
ab (NAS6)	10.47	20.74	20.89	34.23	14.08	12.24	18.27	53.35	54.28	50.58	50.56	46.49	44.86
an (CAS2)	28.45	28.51	24.5	19.64	32.22	22.08	19.91	7.35	7.37	10.86	9.98	11.39	14.81
lc(KAS4)	0	0	0	0	0	0	0	0	0	0	0	0	0
ne(NAS2)	0	0	0	0	0	0	0	0	0	0	0	0	0
C(A)	0	0	0	0	0.03	0	0	0	0	0	0	0	0
ac(NFS4)	0	0	0	0	0	0	0	0	0	0	0	0	0
ns(NS)	0	0	0	0	0	0	0	0	0	0	0	0	0
Di wo(CS)	1.38	1.99	3.49	4.13	0	2.84	2.71	4.3	3.5	3.77	9.29	13.05	11.4
Di en(MS)	0.57	0.95	1.49	1.8	0	1.65	1.52	0.95	0.84	1.94	3.11	4.58	3.99
Di fs(FS)	0.83	1.01	2.01	2.32	0	1.06	1.08	3.64	2.87	1.72	6.48	8.81	7.7
Hy en(MS)	13.37	13.83	9.96	10.52	25.05	25.2	22.22	0.46	0.51	0	1.17	0.6	0.94
Hy fs(FS)	19.48	14.77	13.41	13.59	12.8	16.21	15.79	1.75	1.75	0	2.45	1.15	1.81
Ol fo(M2S)	0	0	0	0	0	0	0	0	0	0	0	0	0
Ol fa(F2S)	0	0	0	0	0	0	0	0	0	0	0	0	0
mt(FF)	2	1.54	1.51	1.57	1.23	1.64	1.61	0.72	0.62	0.48	1.1	1.26	1.19
he(F)	0	0	0	0	0	0	0	0	0	0	0	0	0
il(FT)	1.06	1.18	1.22	1.17	0.79	0.93	1	1.44	1.32	1.5	2.74	3.56	3.41
ap(CP)	0.33	0.22	0.22	0.2	0.19	0.16	0.18	0.36	0.33	0.37	0.46	0.58	1.03
Total	100	100	100	100	100	100	100	100	100	98.95	100	100	100
opx	32.85	28.6	23.37	24.11	37.85	41.41	38.01	2.21	2.26	0	3.62	1.75	2.75
cpx	2.78	3.95	6.99	8.25	0	5.55	5.31	8.89	7.21	7.43	18.88	26.44	23.09
plag	46.96	52.25	56.2	61.86	58.68	41.5	47.26	61	61.77	61.92	62.8	58.49	61.19
sulphur	0.017	0	0	0.006	0	0	0	0.027	0.023	0.056	0.012	0.013	0.01

CIPW NORM DATA

Rock Unit Sample Depth (m)	GN SH176UP14 286.40	GN SH176UP15 303.17	GN SH176 UP16 313.12	GN SH176UP17 329.19	GN SH176UP18 358.33	GN SH176UP19 375.42	GN SH176UP20 382.48	GN SH176UP21 402.64	PX in GN SH176UP22 409.04	GN SH176UP23 432.11	GN SH176UP24 450.44	GN Base SH176UP25 458.36
SiO_2	54.80	56.94	48.17	50.40	49.56	42.44	49.05	54.71	45.02	52.40	49.27	53.14
TiO_2	1.72	0.49	2.17	2.23	2.33	2.09	3.61	0.32	2.87	0.34	0.32	0.27
Al_2O_3	13.40	13.89	12.17	15.80	13.43	9.91	15.34	7.05	16.92	16.07	17.65	12.78
Fe_2O_3	8.01	11.44	22.03	16.80	20.52	34.67	18.15	12.71	18.63	9.78	10.54	10.38
MnO	0.09	0.16	0.26	0.17	0.24	0.31	0.20	0.20	0.17	0.15	0.13	0.16
MgO	1.92	7.27	2.73	2.67	4.03	6.77	4.48	19.65	5.81	8.22	8.48	14.62
CaO	11.93	6.50	6.52	6.70	6.74	4.19	6.78	5.06	8.00	10.50	9.29	7.35
Na_2O	4.48	1.77	2.17	2.50	2.01	0.99	1.92	0.59	1.74	1.66	1.43	0.98
K_2O	0.06	1.41	1.24	1.46	1.06	0.67	0.90	0.44	0.55	0.49	0.73	0.49
P_2O_5	0.95	0.12	0.90	0.84	0.58	0.08	0.06	0.02	0.03	0.04	0.02	0.03
Cr_2O_3	0.00	0.08	<0.01	<0.01	<0.01	0.01	<0.01	0.20	0.03	0.02	0.06	0.14
NiO	0.00	0.02	<0.01	<0.01	<0.01	<0.01	<0.01	0.06	<0.01	0.01	0.02	0.08
V_2O_5	0.00	0.03	0.02	0.02	0.02	0.03	0.08	0.03	0.22	0.03	0.02	0.03
ZrO_2	0.01	0.02	0.01	0.01	0.01	<0.01	0.01	0.01	0.01	0.01	0.01	0.01
LOI	2.01	1.34	1.44	1.89	0.40	-1.16	0.25	0.12	0.50	0.91	2.25	0.78
TOTAL	99.39	101.47	99.82	101.49	100.93	101.01	100.85	101.18	100.49	100.63	100.23	101.24
or (KAS6)	7.19	10.1	2.66	4.08	3.1	0	3.87	0.03	0	3.18	0	3.06
ab (NAS6)	0.36	8.34	7.46	8.67	6.24	3.88	5.3	2.49	3.26	2.91	4.41	2.89
an (CAS2)	38.89	14.96	18.65	21.22	16.9	8.19	16.15	4.77	14.74	14.08	12.35	8.27
lc(KAS4)	16.7	25.75	20.1	27.65	24.34	19.91	30.39	14.6	36.78	35.03	40.4	28.93
ne(NAS2)	0	0	0	0	0	0	0	0	0	0	0	0
C(A)	0	0	0	0	0	0	0	0	0	0	0	0
ac(NFS4)	0	0	0	0	0	0.09	0	0	0	0	0	0
ns(NS)	0	0	0	0	0	0	0	0	0	0	0	0
Di wo(CS)	0	0	0	0	0	0	0	0	0	0	0	0
Di en(MS)	14.44	2.43	3.1	0.33	2.32	0	1.15	3.88	1.19	7.11	2.76	3.05
Di fs(FS)	4.93	1.21	0.6	0.08	0.64	0	0.4	2.41	0.46	3.98	1.51	2.03
Hy en(MS)	9.92	1.16	2.73	0.27	1.8	0	0.78	1.23	0.75	2.84	1.14	0.79
Hy fs(FS)	0	16.96	6.33	6.62	9.39	8.53	10.75	44.55	9.31	16.64	19.53	34.45
Ol fo(M2S)	0	16.2	28.58	22.2	26.44	25.86	21.26	22.74	15.33	11.85	14.75	13.45
Ol fa(F2S)	0	0	0	0	0	5.63	0	0	3.36	0	0.43	0
mt(FF)	0	0	0	0	0	18.83	0	0	6.1	0	0.36	0
he(F)	1.32	1.7	3.6	2.77	3.17	5.02	3.01	2.68	3.19	1.65	1.69	2.51
il(FT)	0	0	0	0	0	0	0	0	0	0	0	0
ap(CP)	3.36	0.93	4.19	4.26	4.41	3.89	6.83	0.58	5.47	0.65	0.62	0.51
Total	2.13	0.26	2	1.84	1.26	0.17	0.13	0.04	0.07	0.09	0.04	0.07
	99.24	100	100	100	100	100	100	100	100	100	100	100
opx	0	33.16	34.91	28.82	35.83	34.39	32.01	67.29	24.64	28.49	34.28	47.9
cpx	29.29	4.8	6.43	0.68	4.76	0	2.33	7.52	2.4	13.93	5.41	5.87
plag	55.95	49.05	46.21	57.54	47.48	31.98	51.84	21.86	54.78	52.02	57.16	40.09
sulphur	0.035	0.012	0.114	0.107	0.065	0.026	0.132	0.135	0.163	0.078	0.042	0.382

CIPW NORM DATA

Rock Unit	PXT	PXT	PXT	PXT	PXT	PXT	PXT	U. MHZBG	U. MHZBG	U. MHZBG	U. MHZBG	U. MHZBG
Sample	SH176UP26	SH176UP27	SH176UP28	SH176UP29	SH176UP30	SH176UP31	SH176UP32	SH176UP33	SH176UP34	SH176UP35	SH176UP36	SH176UP37
Depth (m)	459.75	467.30	481.48	492.04	507.15	516.08	527.04	532.17	547.66	567.14	584.22	603.60
SiO_2	52.60	52.29	54.02	54.34	54.17	53.79	47.80	40.87	37.47	39.53	37.41	36.40
TiO_2	0.32	0.30	0.27	0.24	0.34	0.27	0.13	0.11	0.11	0.11	0.10	0.16
Al_2O_3	7.09	7.13	6.14	5.49	4.29	6.35	3.84	2.73	3.12	1.76	2.76	2.92
Fe_2O_3	12.17	12.14	12.86	11.97	12.56	10.40	9.04	9.61	9.66	10.34	11.63	12.91
MnO	0.20	0.20	0.25	0.31	0.20	0.18	0.14	0.13	0.13	0.13	0.13	0.11
MgO	18.69	19.04	21.00	22.61	24.73	26.31	33.66	36.47	35.82	39.53	35.07	34.25
CaO	4.76	4.81	4.49	3.72	3.11	2.68	2.58	1.81	1.67	1.15	1.42	1.01
Na_2O	0.66	0.58	0.44	0.33	0.04	0.01	0.01	0.01	0.01	0.01	0.01	0.01
K_2O	0.45	0.43	0.31	0.33	0.19	0.22	0.17	0.10	0.12	0.13	0.05	0.27
P_2O_5	0.04	0.04	0.04	0.04	0.02	0.01	0.01	0.01	<0.01	0.01	<0.01	0.01
Cr_2O_3	0.20	0.23	0.36	0.38	0.44	0.50	0.71	0.93	3.62	1.54	3.64	2.18
NiO	0.06	0.11	0.12	0.08	0.08	0.10	0.21	0.24	0.30	0.33	0.29	0.61
V_2O_5	0.03	0.03	0.03	0.03	0.02	0.02	0.02	0.01	0.02	0.01	0.02	0.01
ZrO_2	0.01	0.01	0.01	0.01	0.01	0.01	0.01	0.01	0.01	0.01	0.01	0.01
LOI	0.73	1.39	0.68	0.14	-0.05	0.08	2.76	8.88	8.65	6.99	8.38	9.07
TOTAL	98.01	98.73	101.01	100.02	100.16	100.91	101.10	101.92	100.69	101.58	100.91	99.93
or (KAS6)	0	3.69	2.73	2.32	1.61	0.42	0	0	0	0	0	0
ab (NAS6)	3.48	2.55	1.84	1.96	1.13	1.3	1.03	0.64	0.81	0.83	0.33	1.81
an (CAS2)	15.75	4.55	3.73	2.81	0.34	0.08	0.09	0.09	0.1	0.09	0.1	0.1
lc(KAS4)	37.56	15.01	13.87	12.59	10.99	13.22	10.18	7.73	9.2	4.71	7.96	5.63
ne(NAS2)	0	0	0	0	0	0	0	0	0	0	0	0
C(A)	0	0	0	0	0	0	0	0	0	0	0	0
ac(NFS4)	0	0	0	0	0	1.23	0	0	0	0	0.12	0.9
ns(NS)	0	0	0	0	0	0	0	0	0	0	0	0
Di wo(CS)	0	0	0	0	0	0	0	0	0	0	0	0
Di en(MS)	1.27	4.1	3.43	2.4	1.83	0	1.21	0.83	0.09	0.58	0	0
Di fs(FS)	0.5	2.75	2.34	1.66	1.27	0	0.93	0.64	0.07	0.44	0	0
Hy en(MS)	0.78	1.04	0.82	0.54	0.4	0	0.15	0.1	0.01	0.07	0	0
Hy fs(FS)	12.05	45.9	50.25	55.21	60.77	65.63	40.91	19.44	10.44	10.72	11.94	13.45
Ol fo(M2S)	18.6	17.31	17.5	17.85	19.11	16	6.82	3.19	1.75	1.75	2.48	2.39
Ol fa(F2S)	0.02	0	0	0	0	0	31.2	55.43	63.79	66.81	60.93	58.66
mt(FF)	0.04	0	0	0	0	0	5.74	10.04	11.83	12.07	13.99	11.49
he(F)	2.79	2.48	2.9	2.11	1.86	1.59	1.46	1.62	1.68	1.67	1.95	5.21
il(FT)	0	0	0	0	0	0	0	0	0	0	0	0
ap(CP)	7.08	0.58	0.51	0.46	0.65	0.51	0.25	0.23	0.24	0.23	0.21	0.35
Total	0.09	0.05	0.09	0.09	0.04	0.02	0.02	0.02	0	0.02	0	0.02
	100	100	100	100	100	100	100	100	100	100	100	100
opx	30.65	63.21	67.75	73.06	79.88	81.63	47.73	22.63	12.19	12.47	14.42	15.84
cpx	2.55	7.89	6.59	4.6	3.5	0	2.29	1.57	0.17	1.09	0	0
plag	56.79	22.11	19.44	17.36	12.46	14.6	11.3	8.46	10.11	5.63	8.39	7.54
sulphur	0.15	0.314	0.397	0.147	0.012	0.034	0.044	0.033	0.036	0.024	0.017	1.064

CIPW NORM DATA

Rock Unit Sample Depth (m)	U. MHZBG SH176UP38 620.50	U. MHZBG SH176UP39 639.10	U. MHZBG SH176UP40 647.60	U. MHZBG SH176UP41 662.34	U. MHZBG SH176UP42 673.34	U. MHZBG SH176UP43 696.61	U. MHZBG SH176UP44 716.60	L. MHZBG SH176UP45 741.04	L. MHZBG SH176UP46 751.42	L. MHZBG SH176UP47 775.52	L. MHZBG SH176UP48 791.06	L. MHZBG SH176UP49 807.04
SiO_2	39.25	39.32	39.77	38.36	38.30	36.22	39.46	37.24	38.46	35.94	35.62	36.80
TiO_2	0.13	0.15	0.16	0.15	0.16	0.13	0.13	0.15	0.15	0.15	0.18	0.13
Al_2O_3	2.69	2.65	2.71	2.86	2.70	2.36	2.51	2.89	3.22	3.60	3.23	2.42
Fe_2O_3	11.18	10.71	10.51	10.94	10.84	9.07	10.55	12.99	10.54	12.40	12.54	11.58
MnO	0.12	0.09	0.10	0.10	0.11	0.17	0.10	0.09	0.15	0.11	0.16	0.10
MgO	35.52	34.35	36.01	34.83	35.29	28.81	34.18	33.18	33.73	32.54	33.14	35.07
CaO	1.20	1.63	1.47	1.50	1.51	2.71	1.36	1.21	1.56	1.06	1.60	0.86
Na_2O	0.01	0.01	0.01	0.01	0.01	0.00	0.01	0.01	0.01	0.00	0.01	0.01
K_2O	0.16	0.13	0.16	0.14	0.16	0.00	0.14	0.12	0.15	0.04	0.19	0.15
P_2O_5	0.01	0.01	0.01	0.01	0.01	0.01	0.01	0.00	0.01	<0.01	0.02	0.01
Cr_2O_3	0.88	1.22	1.74	2.51	2.09	1.31	1.27	1.80	1.69	5.57	3.74	2.71
NiO	0.32	0.32	0.34	0.30	0.34	0.28	0.36	0.51	0.32	0.65	0.61	0.42
V_2O_5	0.01	0.01	0.01	0.02	0.01	0.01	0.01	0.02	0.01	0.03	0.02	0.02
ZrO_2	0.01	0.01	0.01	0.01	0.01	0.01	0.01	0.01	0.01	<0.01	0.01	0.01
LOI	9.35	8.12	7.72	7.82	7.49	18.14	8.89	9.07	9.15	9.07	10.03	9.52
TOTAL	100.83	98.73	100.72	99.55	99.04	99.23	99.00	99.29	99.14	101.16	101.07	99.81
or (KAS6)	0	0	0	0	0	0	0	0	0	0	0	0
ab (NAS6)	1.05	0.86	1.04	0.93	1.06	0	0.94	0.81	1.01	0.28	1.3	1.02
an (CAS2)	0.09	0.09	0.09	0.1	0.09	0	0.1	0.1	0.1	0	0.1	0.1
lc(KAS4)	6.53	7.63	7.56	8.25	7.68	8.09	7.22	6.84	8.74	6.13	9.03	4.83
ne(NAS2)	0	0	0	0	0	0	0	0	0	0	0	0
C(A)	0	0	0	0	0	0	0	0	0	0	0	0
ac(NFS4)	0.37	0	0	0	0	0	0	0.61	0.25	1.89	0.16	0.8
ns(NS)	0	0	0	0	0	0	0	0	0	0	0	0
Di wo(CS)	0	0	0	0	0	0	0	0	0	0	0	0
Di en(MS)	0	0.58	0.17	0.02	0.28	3.66	0.15	0	0	0	0	0
Di fs(FS)	0	0.44	0.13	0.02	0.21	2.74	0.11	0	0	0	0	0
Hy en(MS)	0	0.08	0.02	0	0.04	0.54	0.02	0	0	0	0	0
Hy fs(FS)	17.43	19.32	17.25	15.18	13.76	23.15	22.07	19.3	18.16	18.99	12.88	14.34
Ol fo(M2S)	3.43	3.72	3.09	2.93	2.61	4.58	4.18	3.53	3.52	3.61	1.96	2.71
Ol fa(F2S)	56.65	53.67	57.15	57.92	59.54	45.31	52.1	52.56	54.38	53.04	57.88	60.4
mt(FF)	12.3	11.4	11.3	12.34	12.48	9.89	10.89	10.62	11.64	11.13	9.72	12.6
he(F)	1.84	1.86	1.84	1.96	1.87	1.71	1.93	5.31	1.86	4.59	6.53	2.9
il(FT)	0	0	0	0	0	0	0	0	0	0	0	0
ap(CP)	0.27	0.32	0.33	0.32	0.34	0.31	0.28	0.32	0.32	0.33	0.39	0.28
Total	0.02	0.02	0.02	0.02	0.02	0.03	0.02	0	0.02	0	0.05	0.03
	100	100	100	100	100	100	100	100	100	100	100	100
opx	20.86	23.04	20.34	18.11	16.37	27.73	26.25	22.83	21.68	22.6	14.84	17.05
cpx	0	1.1	0.32	0.04	0.53	6.94	0.28	0	0	0	0	0
plag	7.67	8.58	8.69	9.28	8.83	8.09	8.26	7.75	9.85	6.41	10.43	5.95
sulphur	0.027	0.05	0.066	0.062	0.035	0.018	0.066	1.077	0.08	0.904	1.498	0.425

CIPW NORM DATA

Rock Unit Sample Depth (m)	L. MHZBG SH176UP50 828.32	PCR SH176UP51 854.06	PCR SH176UP52 890.56	PCR SH176UP53 905.16	LHZBG SH176UP54 922.05	LHZBG SH176UP55 931.50	LHZBG SH176UP56 974.61	LHZBG SH176UP57 974.67	BGAB SH176UP58 985.33	Basal top SH176UP59 987.55	BGAB Chill SH176UP60 990.29
SiO_2	36.39	35.12	38.70	35.40	38.27	38.51	43.80	35.41	44.05	47.39	50.65
TiO_2	0.16	0.21	0.25	0.48	0.18	0.44	0.82	0.47	0.81	0.97	1.64
Al_2O_3	3.72	4.62	4.85	10.84	3.77	5.27	6.79	3.73	6.82	13.27	14.04
Fe_2O_3	12.60	8.58	10.59	16.30	13.57	13.88	17.47	27.20	17.49	16.74	11.93
MnO	0.11	0.11	0.18	0.23	0.18	0.16	0.17	0.15	0.17	0.14	0.17
MgO	33.43	33.42	29.29	13.45	29.94	24.65	16.85	21.69	17.01	5.59	5.12
CaO	1.06	1.75	3.10	2.70	6.89	9.83	6.84	3.39	6.84	8.09	7.25
Na_2O	0.01	0.01	0.00	0.01	0.01	0.01	0.20	0.01	0.19	2.73	3.39
K_2O	0.03	0.29	0.15	0.05	0.22	0.69	1.77	0.16	1.78	1.62	2.35
P_2O_5	<0.01	0.03	0.02	0.01	<0.01	0.05	0.08	0.03	0.08	0.07	0.17
Cr_2O_3	6.19	4.77	5.11	19.70	0.15	0.88	0.07	0.04	0.07	0.01	0.00
NiO	0.66	0.30	0.25	0.19	0.26	0.28	0.46	0.57	0.46	0.54	0.01
V_2O_5	0.03	0.04	0.05	0.08	0.01	0.02	0.03	0.02	0.03	0.03	0.04
ZrO_2	<0.01	0.00	0.00	0.00	0.01	0.01	0.01	<0.01	0.03	0.01	0.02
LOI	7.03	8.23	8.15	1.24	7.50	5.80	3.83	7.16	3.83	2.51	1.60
TOTAL	101.43	97.48	100.69	100.68	100.93	100.47	99.18	100.02	99.66	99.71	98.36
or (KAS6)	0	0	0	0	0	0	0	0	0	0.14	8.83
ab (NAS6)	0.2	2.04	1.02	0.37	1.29	0	11.05	1.03	11.06	9.92	7.18
an (CAS2)	0.1	0.1	0	0.11	0	0	1.78	0.09	1.69	23.88	12.24
lc(KAS4)	6.01	10.12	14.66	16.79	10.3	13.13	13.06	10.46	13.1	19.81	22.08
ne(NAS2)	0	0	0	0	0.09	3.42	0	0	0	0	0
C(A)	0	0	0	0	0.05	0.05	0	0	0	0	0
ac(NFS4)	1.99	1.39	0	7.39	0	0	0	0	0	0	0
ns(NS)	0	0	0	0	0	0	0	0	0	0	0
Di wo(CS)	0	0	0	0	0	0	0	0	0	0	0
Di en(MS)	0	0	1.2	0	11.04	16.17	9.29	3.17	9.21	8.9	2.84
Di fs(FS)	0	0	0.92	0	8.44	12.04	6.36	2.18	6.09	5.15	1.65
Hy en(MS)	0	0	0.14	0	1.42	2.51	2.18	0.73	2.44	3.33	1.06
Hy fs(FS)	16.71	11.54	24.75	41.92	0	0	21.68	22.75	19.63	9.31	25.2
Ol fo(M2S)	3.36	1.25	3.87	25.65	0	0	7.43	7.65	7.87	6.01	16.21
Ol fa(F2S)	55.16	61.43	40.86	0.27	50.41	37.72	11.48	23.7	13.25	0	0
mt(FF)	12.24	7.36	7.05	0.19	9.38	8.69	4.34	8.79	5.86	0	0
he(F)	3.88	4.22	4.94	6.14	7.21	7.09	9.53	18.41	8.02	11.48	1.64
il(FT)	0	0	0	0	0	0	0	0	0	0	0
ap(CP)	0.35	0.47	0.55	1.15	0.37	0.89	1.64	0.97	1.62	1.91	0.93
Total	0	0.08	0.05	0.03	0	0.12	0.18	0.07	0.18	0.16	0.16
	100	100	100	100	100	101.83	100	100	100	100	100
opx	20.07	12.79	28.62	67.57	0	0	29.11	30.4	27.5	15.32	41.41
cpx	0	0	2.26	0	20.9	30.72	17.83	6.08	17.74	17.38	5.55
plag	6.31	12.26	15.68	17.27	11.59	13.13	25.89	11.58	25.85	53.61	41.5
sulphur	0.676	0.934	1.056	1.003	1.744	1.718	2.786	4.864	2.139	3.465	0.076

ICP-MS DATA NORMALIZED

NORMALIZED DATA TO CHONDRITE

Rock Unit		UGAB	UGAB	GN	GN	GN	GN	GN	GN	GN	PXT	PXT	PXT
Sample		SH176 UP1	SH176 UP5	SH176 UP8	SH176 UP11	SH176 UP15	SH176 UP19	SH176 UP22	SH176 UP23	SH176 UP25	SH176 UP26	SH176 UP28	SH176 UP31
Depth (m)	Chondrite	135.41	181.09	216.22	246.52	303.17	375.42	409.04	432.11	458.36	459.75	481.48	516.08
Sc	5.92	3.69	3.39	1.64	3.17	4.32	1.54	3.37	4.23	4.06	4.97	4.36	2.99
Se	21	0.01	0.00	0.00	0.00	0.05	0.00	0.01	0.00	0.01	0.03	0.06	0.01
Rb	2.3	40.47	34.08	0.38	3.50	23.99	12.50	9.02	7.14	7.04	7.41	5.04	3.73
Sr	7.25	15.99	31.44	24.16	31.47	23.07	25.59	43.27	33.26	23.08	12.11	12.26	6.92
Y	1.57	11.12	8.07	19.21	22.92	12.17	5.71	3.94	6.00	4.15	4.61	3.92	2.12
Zr	3.82	30.09	21.14	71.71	35.15	32.30	14.47	11.81	14.90	9.12	10.37	8.29	5.07
Nb	0.024	30.88	23.43	77.62	71.70	34.90	24.25	13.81	11.64	8.91	9.11	7.76	3.14
Mo	0.09	3.03	0.35	0.29	0.59	1.14	1.02	0.51	0.65	0.41	0.45	0.78	0.35
Sb	0.014	12.60	10.65	10.39	8.72	3.13	1.51	0.60	1.07	0.63	0.72	1.10	0.43
Cs	0.019	78.19	8.75	0.38	1.08	22.70	15.15	16.20	13.83	13.99	8.04	7.33	4.89
Ba	0.000241	116.13	134.19	30.36	87.46	137.36	72.43	50.42	63.96	66.42	47.42	40.15	35.40
La	0.0237	90.48	63.47	243.35	148.61	96.30	53.06	31.12	36.05	29.80	29.89	23.89	11.83
Ce	0.0613	72.71	49.21	170.20	127.24	78.68	43.14	24.90	29.78	23.99	24.15	19.80	9.65
Pr	0.00928	52.72	35.24	113.98	106.35	60.04	32.15	18.49	23.03	18.22	17.71	15.32	7.44
Nd	0.0457	41.86	27.67	86.76	95.17	50.12	26.38	15.47	19.52	14.86	15.05	12.84	6.28
Sm	0.0148	25.34	16.75	47.23	63.24	30.58	15.29	9.55	12.76	8.96	8.77	8.07	4.15
Eu	0.00563	14.68	11.15	27.85	36.06	22.78	16.01	13.03	12.29	7.11	6.92	6.17	3.07
Gd	0.0199	18.09	12.11	31.18	42.53	21.36	10.58	6.59	9.27	6.38	6.59	6.06	2.77
Tb	0.00361	15.20	10.32	25.03	34.05	17.09	8.26	5.32	7.84	5.43	5.91	5.20	2.42
Dy	0.0246	14.39	9.64	22.41	30.07	15.43	7.33	4.85	7.34	4.90	5.30	4.93	2.34
Ho	0.00546	13.01	8.74	20.23	24.96	13.94	6.39	4.30	6.69	4.60	5.12	4.46	2.34
Er	0.016	13.18	8.83	20.17	24.02	13.36	6.34	4.25	6.62	4.45	5.02	4.43	2.59
Tm	0.00247	12.42	8.60	19.11	21.03	12.36	5.98	4.01	6.19	4.35	4.82	4.20	2.46
Yb	0.0161	12.66	8.49	20.16	20.75	12.99	6.13	4.19	6.36	4.50	5.31	4.65	2.70
Lu	0.00246	12.25	8.38	20.82	18.38	12.43	5.93	4.12	6.04	4.45	5.28	4.36	2.70
Hf	0.0103	29.18	20.87	76.14	49.35	30.62	14.84	11.54	13.87	8.66	9.85	8.11	4.59
Th	0.0029	359.36	236.74	339.59	251.68	206.07	110.29	50.86	71.76	45.61	59.61	48.21	28.47
Ta	0.00136	83.95	66.75	120.32	114.15	68.41	50.32	34.63	30.48	24.88	23.62	25.39	10.62
Pb	0.247	7.22	1.57	0.93	4.23	4.07	1.88	1.42	1.72	1.14	0.90	2.60	0.98
U	0.0007	803.90	354.86	522.33	349.06	342.50	158.47	86.04	129.68	61.74	70.99	115.07	52.25
K	550	11293.44	17516.17	405.78	3146.68	11712.01	5578.61	4533.03	4072.13	4032.95	4908.59	2581.85	1865.43
Ti	440	3367.39	2511.91	4434.80	8579.08	2947.74	12514.20	17226.99	2041.90	1619.31	22399.12	1602.46	1600.67
[Th/La]n		3.97	3.73	1.40	1.69	2.14	2.08	1.63	1.99	1.53	1.99	2.02	2.41
[Sm/Ta]n		0.30	0.25	0.39	0.55	0.45	0.30	0.28	0.42	0.36	0.37	0.32	0.39

SELECTED NORMALIZED DATA TO PRIMITIVE MANTLE

	PRIMITIVE MANTLE													B1	B3
Ba	6.89	41	47	11	31	48	25	18	22	23	17	14	12	51.39	26.55
Rb	0.635	147	123	1	13	87	45	33	26	25	27	18	14	58.36	17.55
Th	0.085	123	81	116	86	70	38	17	24	16	20	16	10	38.34	9.94
K	250	45	70	2	13	47	22	18	16	16	20	10	7	28.23	11.29
Nb	0.713	10	8	26	24	12	8	5	4	3	3	3	1	6.01	2.65
La	0.687	31	22	84	51	33	18	11	12	10	10	8	4	24.82	11.70
Ce	1.775	25	17	59	44	27	15	9	10	8	8	7	3	19.08	9.27
Sr	21.1	5	11	8	11	8	9	15	11	8	4	4	2	8.42	15.88
Nd	1.354	14	9	29	32	17	9	5	7	5	5	4	2	10.96	6.43
Zr	11.2	10	7	24	12	11	5	4	5	3	4	3	2	5.89	2.77
Sm	0.444	8	6	16	21	10	5	3	4	3	3	3	1	6.01	4.67
Ti	1300	3	2	3	7	2	10	13	2	1	17	1	1	1.43	2.12
Eu	0.168	5	4	9	12	8	5	4	4	2	2	2	1	4.81	5.45
Yb	0.493	4	3	7	7	4	2	1	2	1	2	2	1	2.17	2.42
Lu	0.074	4	3	7	6	4	2	1	2	1	2	1	1	2.30	2.49

(Chondrite values from McDonough and Sun ,1995)
(Primitive mantle values from Sun and McDonough, 1989)
(B1 and B3 values from Curl, 2001)

ICP-MS DATA NORMALIZED

NORMALIZED DATA TO CHONDRITE

Rock Unit		PXT	Upper MHZBG	Upper MHZBG	Upper MHZBG	Lower MHZBG	PCR	PCR	LHZBG	LHZBG	BGAB	BGAB
Sample		SH176 UP32	SH176 UP33	SH176 UP35	SH176 UP40	SH176 UP49	SH176 UP51	SH176 UP52	SH176 UP54	SH176 UP57	SH176 UP59	SH176 UP60
Depth (m)	Chondrite	527.04	532.17	567.14	647.6	807.04	854.06	890.56	922.05	979.67	987.55	990.29
Sc	5.92	2.15	0.86	1.19	1.26	1.23	1.17	1.73	1.87	2.05	3.24	3.42
Se	21	0.06	0.00	0.05	0.04	0.08	0.15	0.07	0.17	0.77	0.35	0.00
Rb	2.3	2.60	0.07	2.37	3.12	4.94	5.34	3.25	3.15	2.67	20.72	30.90
Sr	7.25	6.97	8.98	5.52	1.58	2.11	2.39	2.72	4.84	1.86	62.55	53.78
Y	1.57	1.85	1.22	1.33	2.06	3.08	2.44	3.50	2.92	3.44	10.08	14.59
Zr	3.82	3.53	3.95	2.56	5.98	8.26	3.95	8.34	7.51	10.83	24.06	42.99
Nb	0.024	3.81	3.79	2.54	5.11	8.29	5.00	8.79	9.03	10.12	19.66	43.78
Mo	0.09	0.44	0.21	0.27	0.63	0.65	0.57	0.49	0.31	0.59	1.12	0.89
Sb	0.014	0.55	76.05	0.22	0.37	1.99	1.90	30.76	7.31	15.76	3.98	6.88
Cs	0.019	3.50	0.74	3.50	5.21	5.86	10.99	8.55	6.26	6.32	8.09	9.35
Ba	0.000241	21.39	1.41	28.63	11.94	19.35	14.70	7.37	16.10	12.05	133.31	373.06
La	0.0237	11.01	8.20	8.61	14.56	19.55	20.19	19.99	19.40	17.46	53.51	87.77
Ce	0.0613	8.87	5.83	6.84	11.78	17.76	16.06	18.00	16.64	15.70	47.30	76.59
Pr	0.00928	6.75	4.57	5.14	9.00	14.04	12.16	14.15	12.35	13.16	40.32	63.43
Nd	0.0457	5.58	3.79	4.39	7.41	11.59	9.69	12.09	9.63	11.84	36.19	57.22
Sm	0.0148	3.57	2.48	2.77	4.47	7.55	5.94	7.60	5.91	8.45	25.65	38.05
Eu	0.00563	3.02	4.19	2.53	3.07	3.94	4.85	4.29	4.94	4.51	21.65	30.27
Gd	0.0199	2.64	1.69	2.08	3.23	5.19	4.10	5.38	4.22	5.97	18.13	27.80
Tb	0.00361	2.34	1.50	1.72	2.83	4.29	3.39	4.53	3.56	5.01	14.92	22.15
Dy	0.0246	2.25	1.37	1.63	2.45	3.83	3.07	4.33	3.38	4.47	13.28	19.13
Ho	0.00546	2.09	1.35	1.46	2.20	3.36	2.66	3.78	3.25	3.79	11.29	16.36
Er	0.016	2.15	1.36	1.47	2.20	3.26	2.70	3.67	3.28	3.80	10.65	15.60
Tm	0.00247	2.07	1.31	1.29	2.10	3.21	2.64	3.26	2.94	3.37	9.32	13.62
Yb	0.0161	2.26	1.37	1.49	2.22	3.22	2.77	3.51	3.38	3.36	9.52	13.78
Lu	0.00246	2.29	1.47	1.48	2.28	3.39	2.78	3.26	3.20	3.23	9.05	13.09
Hf	0.0103	3.46	3.67	2.41	5.30	7.77	3.66	7.87	7.22	9.68	22.87	39.45
Th	0.0029	25.02	17.85	13.81	24.98	65.30	25.29	39.05	24.67	27.57	54.89	102.33
Ta	0.00136	18.91	13.49	15.03	18.08	30.45	23.76	21.98	20.00	24.52	35.79	69.75
Pb	0.247	0.62	0.80	2.06	0.61	0.97	0.47	0.55	1.65	0.76	6.36	1.91
U	0.0007	66.96	22.02	15.00	37.72	70.09	24.70	34.67	43.44	31.46	62.67	120.18
K	550	1395.57	806.24	1077.37	1303.75	1261.87	2410.76	1237.75	1786.07	1315.29	13449.68	19513.09
Ti	440	788.94	653.87	684.15	963.34	806.54	1279.99	1485.38	1055.18	2810.88	5830.86	9846.31
[Th/La]n		2.27	2.18	1.60	1.72	3.34	1.25	1.95	1.27	1.58	1.03	1.17
[Sm/Ta]n		0.19	0.18	0.18	0.25	0.25	0.25	0.35	0.30	0.34	0.72	0.55

SELECTED NORMALIZED DATA TO PRIMITIVE MANTLE

	PRIMITIVE MANTLE											
Ba	6.89	7	0	10	4	7	5	3	6	4	47	130
Rb	0.635	9	0	9	11	18	19	12	11	10	75	112
Th	0.085	9	6	5	9	22	9	13	8	9	19	35
K	250	6	3	4	5	5	10	5	7	5	54	78
Nb	0.713	1	1	1	2	3	2	3	3	3	7	15
La	0.687	4	3	3	5	7	7	7	7	6	18	30
Ce	1.775	3	2	2	4	6	6	6	6	5	16	26
Sr	21.1	2	3	2	1	1	1	1	2	1	21	18
Nd	1.354	2	1	1	2	4	3	4	3	4	12	19
Zr	11.2	1	1	1	2	3	1	3	3	4	8	15
Sm	0.444	1	1	1	1	3	2	3	2	3	9	13
Ti	1300	1	1	1	1	1	1	1	1	2	4	8
Eu	0.168	1	1	1	1	1	2	1	2	2	7	10
Yb	0.493	1	0	0	1	1	1	1	1	1	3	4
Lu	0.074	1	0	0	1	1	1	1	1	1	3	4

(Chondrite values from McDonough and Sun ,1995)
(Primitive mantle values from Sun and McDonough, 1989)
(B1 and B3 values from Curl, 2001)

PGE NORMALIZED

Whole rock PGE analyses of borehole SH176, together with normalized data for primitive mantle

Rock Unit	top chill	UGAB	UGAB	UGAB	UGAB	UGAB	UGAB	GN	GN	GN	GN	GN	GN	GN	GN	GN	GN
Sample	SH176 UP1	SH176 UP2	SH176 UP3	SH176 UP4	SH176 UP5	SH176 UP6	SH176 UP7	SH176 UP8	SH176 UP9	SH176 UP10	SH176 UP11	SH176 UP12	SH176 UP13	SH176 UP14	SH176 UP15	SH176 UP16	SH176 UP17
Depth	135.41	137.45	152.25	163.33	181.09	192.25	202.29	216.22	217.28	229.21	246.52	264.52	278.54	286.4	303.17	313.12	329.19
Ni (ppm)	105	101	75	73	175	239	204	3	5	6	11	11	14	12	138	14	15
Os (ppb)	<0.6	<0.4	<0.4	<0.3	<0.5	0.5	<0.6	<0.4	<0.5	<0.7	<0.3	<0.4	<0.6	<0.3	<0.3	0.5	<0.6
Ir (ppb)	0.083	0.053	0.057	0.020	0.100	0.113	0.110	0.008	0.009	0.010	0.019	0.012	0.160	0.010	0.060	0.020	0.020
Ru (ppb)	5	5	<2	<4	4	<1	<2	<2	<2	<3	<2	<1	<4	<2	3	<4	<4
Rh (ppb)	0.8	0.7	1.1	0.8	1.0	1.2	1.3	<0.3	<0.3	<0.5	<0.4	<0.4	<0.7	<0.7	0.6	0.2	0.2
Pt (ppb)	32	7	4	4	11	5	12	<3	4	<2	2	1	23	<2	<8	<2	33
Pd (ppb)	8	10	11	10	6	5	10	<3	<5	<6	1	<2	2	<4	7	<2	<2
Au (ppb)	2.67	2.39	6.76	3.83	5.34	3.24	3.28	1.37	1.53	4.94	1.69	0.87	3.06	2.66	1.04	2.63	3.55
Cu (ppm)	114	21	47	67	7	44	59	13	25	16	13	7	14	13	39	30	29
Re (ppm)	0.17	0.21	<0.24	<0.25	<0.21	<0.21	<0.22	0.28	0.20	<0.23	0.38	<0.22	0.12	<0.14	<0.19	<0.14	0.12
Se (ppm)	109	21	61	74	6	50	57	11	24	17	17	10	16	13	47	43	37
NORMALIZED TO PRIMITIVE MANTLE																	
Ni (ppb)	0.0525	0.0505	0.0375	0.0365	0.0875	0.1195	0.1020	0.0015	0.0025	0.0030	0.0055	0.0055	0.0070	0.0060	0.0690	0.0070	0.0075
Os (ppm)	-	-	-	-	-	0.1389	-	-	-	-	-	-	-	-	-	0.1399	-
Ir (ppb)	0.0243	0.0157	0.0168	0.0059	0.0294	0.0333	0.0324	0.0024	0.0027	0.0029	0.0056	0.0036	0.0471	0.0029	0.0176	0.0059	0.0059
Ru (ppb)	0.9558	1.0485			0.7475	-	-	-	0.4000	-	-	-	-	-	0.6921	-	-
Rh (ppb)	0.8687	0.7368	1.1579	0.8421	1.0526	1.2632	1.3684	-	-	-	-	-	-	-	0.6316	0.2105	0.1958
Pt (ppb)	4.5278	0.9357	0.5171	0.5494	1.5957	0.7129	1.6461	-	0.6143	-	0.2556	0.1555	3.3271	-	-	-	4.7129
Pd (ppb)	2.0723	2.5000	2.7500	2.5000	1.5000	1.2500	2.5000	0.5000	1.0000	1.2500	0.2500	0.2500	0.5942	0.7500	1.7500	0.2500	0.2500
Au (ppb)	2.6952	2.4153	6.8331	3.8658	5.3921	3.2740	3.3156	1.3847	1.5469	4.9870	1.7048	0.8802	3.0906	2.6891	1.0524	2.6565	3.5888
Cu (ppb)	4.0714	0.7500	1.6786	2.3929	0.2500	1.5714	2.1071	0.4643	0.8929	0.5714	0.4643	0.2500	0.5000	0.4643	1.3929	1.0714	1.0357
|Ni/Ir|n	2.1636	3.2214	2.2368	6.2050	2.9750	3.5892	3.1527	0.6375	0.9239	1.0200	0.9791	1.5081	0.1488	2.0400	3.9100	1.1900	1.2750
|Cu/Pd|n	1.9647	0.3000	0.6104	0.9571	0.1667	1.2571	0.8429	0.9286	0.8929	0.4571	1.8571	1.0000	0.8415	0.6190	0.7959	4.2857	4.1429

Normalization factors from Barnes and Maier, 1999

Rock Unit	GN	GN	GN	GN	PX in GN	GN	GN	GN Base	PXT	PXT	PXT	PXT	PXT	PXT	PXT	U.MHZBG	U.MHZBG
Sample	SH176 UP18	SH176 UP19	SH176 UP20	SH176 UP21	SH176 UP22	SH176 UP23	SH176 UP24	SH176 UP25	SH176 UP26	SH176 UP27	SH176 UP28	SH176 UP29	SH176 UP30	SH176 UP31	SH176 UP32	SH176 UP33	SH176 UP34
Depth	358.33	375.42	382.48	402.64	409.04	432.11	450.44	458.36	459.75	467.3	481.48	492.04	507.15	516.08	527.04	532.17	542.66
Ni (ppm)	14	31	30	33	51	94	150	637	481	846	906	677	718	720	1615	1857	2512
Os (ppb)	0.4	<0.5	<0.5	<0.5	<0.5	<0.3	<0.3	<0.4	<0.6	<0.7	1.8	<0.2	0.8	1.7	2.6	2.4	9.7
Ir (ppb)	0.018	0.023	0.019	0.058	0.038	0.036	0.037	0.057	0.053	0.050	2.012	0.550	0.619	1.348	2.238	2.410	9.441
Ru (ppb)	<4	<3	<2	<2	<2	1	<2	<2	<3	<4	5	<8	3	16	23	8	32
Rh (ppb)	<0.4	<0.2	<0.2	<0.2	<0.1	<0.2	0.3	<0.3	<0.4	0.2	5.2	3.3	1.9	2.4	3.1	1.1	4.9
Pt (ppb)	<1	<1	1	1	2	1	1	3	3	3	46	18	91	21	13	25	25
Pd (ppb)	<3	<5	<2	<3	1	1	<2	<3	<3	6	82	53	5	7	<8	4	6
Au (ppb)	1.34	1.29	0.88	0.80	0.40	0.56	1.13	1.48	1.60	4.09	11.12	5.90	1.58	1.97	3.03	1.86	2.06
Re (ppm)	<0.17	0.10	0.19	0.11	0.40	0.40	0.13	1.79	0.80	1.92	1.38	1.60	<0.13	<0.65	<0.60	<0.76	0.23
Cu (ppm)	21	13	33	37	53	62	22	315	164	387	278	115	9	49	35	21	25
Se (ppm)	29	21	43	48	70	69	27	307	170	340	266	133	56	55	40	23	26
NORMALIZED TO PRIMITIVE MANTLE																	
Ni (ppb)	0.0070	0.0155	0.0015	0.0165	0.0255	0.0470	0.0075	0.3185	0.2405	0.4230	0.4530	0.3385	0.3590	0.3600	0.8075	0.9285	2.6060
Os (ppm)	0.1172	-	-	-	-	-	-	-	-	-	0.5419	-	0.2261	0.4975	0.7537	0.6921	2.8454
Ir (ppb)	0.0054	0.0068	0.0055	0.0169	0.0111	0.0106	0.0110	0.0168	0.0155	0.0146	0.5916	0.1618	0.1821	0.3965	0.6582	0.7088	2.7767
Ru (ppb)	-	-	-	-	-	0.2610	-	-	-	-	0.9386	-	0.6560	3.2284	4.5712	1.6023	6.3612
Rh (ppb)	-	-	-	-	-	-	0.3158	-	-	0.2105	5.4737	3.4492	2.0222	2.5659	3.2421	1.1158	5.1579
Pt (ppb)	-	-	0.1455	0.1524	0.2163	0.1671	0.2079	0.4274	0.3834	0.3834	6.5167	2.5714	13.0100	2.9953	1.8917	3.5237	3.6127
Pd (ppb)	0.5000	1.0000	0.2500	0.5000	0.2500	0.2500	0.2500	0.5000	0.5000	1.5000	20.4175	13.1750	1.1750	1.6500	1.7500	1.0250	1.5000
Au (ppb)	1.3522	1.3062	0.8937	0.8058	0.3997	0.5662	1.1422	1.4984	1.6193	4.1308	11.2290	5.9582	1.5987	1.9891	3.0617	1.8794	2.0821
Cu (ppb)	0.7500	0.4643	1.1786	1.3214	1.8929	2.2143	0.7857	11.2500	5.8571	13.8214	9.9286	4.1071	0.3214	1.7500	1.2500	0.7500	0.8929
|Ni/Ir|n	1.2935	2.2814	0.2713	0.9740	2.2876	4.4389	0.6836	18.9318	15.5456	28.8795	0.7657	2.0925	1.9713	0.9079	1.2269	1.3099	0.9385
|Cu/Pd|n	1.5000	0.4643	4.7143	2.6429	7.5714	8.8571	3.1429	22.5000	11.7143	9.2143	0.4863	0.3117	0.2736	1.0606	0.7143	0.7317	0.5952

Primitive Mantle (from Barnes and Maier (1999)

Ni (ppm)	Os (ppm)	Ir (ppb)	Ru (ppb)	Rh (ppb)	Pt (ppb)	Pd (ppb)	Au (ppb)	Cu (ppm)
2000	3.4	3.4	5	0.95	7	4	0.99	28

PGE NORMALIZED

Rock Unit	U.MHZBG	U.MHZBG	U.MHZBG	U.MHZBG	U.MHZBG	U.MHZBG	U.MHZBG	U.MHZBG	U.MHZBG	U.MHZBG	L. MHZBG	L. MHZBG	L. MHZBG
Sample	SH176 UP35	SH176 UP36	SH176 UP37	SH176 UP38	SH176 UP39	SH176 UP40	SH176 UP41	SH176 UP42	SH176 UP43	SH176 UP44	SH176 UP45	SH176 UP46	SH176 UP47
Depth	567.14	584.22	603.6	620.5	639.1	647.6	662.34	673.34	696.61	716.6	741.04	751.42	775.52
Ni (ppm)	2583	2551	3593	2515	2647	2668	2322	2484	1799	2889	4091	2431	5206
Os (ppb)	19.9	5.0	30.0	2.3	6.0	7.1	7.5	4.6	4.8	3.6	8.5	3.6	25.6
Ir (ppb)	18.286	5.658	15.072	1.824	5.410	5.740	5.280	4.360	3.680	3.160	6.940	3.210	18.310
Ru (ppb)	55	18	87	12	23	22	24	18	<12	17	40	15	107
Rh (ppb)	15.9	1.1	13.9	1.4	8.3	10.0	6.1	7.3	5.3	7.9	9.4	5.3	21.9
Pt (ppb)	116	9	71	7	41	164	16	102	59	97	79	50	170
Pd (ppb)	16	<3	120	4	69	49	33	49	<28	79	117	27	278
Au (ppb)	4.69	1.55	12.79	1.69	4.43	16.48	1.69	7.12	5.90	9.19	19.35	3.62	31.44
Cu (ppm)	14	11	740	6	27	48	26	38	10	54	858	76	560
Re (ppm)	<0.30	0.26	7.91	<0.2	0.24	0.21	0.59	0.44	<0.93	0.34	6.45	1.05	8.58
Se (ppm)	117	44	835	72	33	47	25	41	7	83	852	71	590
NORMALIZED TO PRIMITIVE MANTLE													
Ni (ppb)	1.2815	1.2755	1.7965	1.2575	1.3235	1.3340	1.1610	1.2420	0.8995	1.4445	2.0455	1.2155	2.6030
Os (ppm)	5.8424	1.4652	8.8292	0.6793	1.7588	2.0962	2.1991	1.3471	1.4000	1.0529	2.5029	1.0588	7.5294
Ir (ppb)	5.3782	1.6642	4.4328	0.5366	1.5912	1.6881	1.5529	1.2824	1.0824	0.9294	2.0412	0.9441	5.3853
Ru (ppb)	10.9064	3.6334	17.4394	2.3588	4.6720	4.3931	4.7776	3.6100	-	3.3900	7.9180	3.0480	21.3600
Rh (ppb)	16.7684	1.1579	14.6316	1.4737	8.7368	10.5263	6.3684	7.6316	5.6105	8.3474	9.8842	5.5579	23.0316
Pt (ppb)	16.5614	1.2335	10.1303	1.0477	5.9229	23.3914	2.2229	14.5129	8.4200	13.7894	11.2611	7.2000	24.3000
Pd (ppb)	4.0000	0.5000	30.0000	1.0000	17.2500	12.2500	8.2500	12.2500	6.7500	19.7500	29.2500	6.7500	69.5000
Au (ppb)	4.7408	1.5667	12.9198	1.7115	4.4758	16.6439	1.7043	7.1869	5.9631	9.2852	19.5476	3.6566	31.7545
Cu (ppb)	0.5000	0.3929	26.4286	0.2143	0.9643	1.7143	0.9286	1.3571	0.3571	1.9286	30.6429	2.7143	20.0000
[Ni/Ir]n	0.2383	0.7664	0.4053	2.3436	0.8318	0.7902	0.7476	0.9685	0.8311	1.5542	1.0021	1.2874	0.4834
[Cu/Pd]n	0.1250	0.7857	0.8810	0.2143	0.0559	0.1399	0.1126	0.1108	0.0529	0.0976	1.0476	0.4021	0.2878

Normalization factors from Barnes and Maier, 1999

Rock Unit	L. MHZBG	L. MHZBG	PCR	PCR	PCR	LHZBG	LHZBG	LHZBG	LHZBG	LHZBG	BGAB	Basal top	BGAB Chill
Sample	SH176 UP48	SH176 UP49	SH176 UP50	SH176 UP51	SH176 UP52	SH176 UP53	SH176 UP54	SH176 UP55	SH176 UP56	SH176 UP57	SH176 UP58	SH176 UP59	SH176 UP60
Depth	791.06	807.04	828.32	854.06	890.56	905.16	922.05	931.5	974.61	979.61	985.33	987.55	990.29
Ni (ppm)	4490	4388	4027	3848	2701	3407	1920	2073	11815	4331	3126	3997	73
Os (ppb)	18.1	11.2	13.5	17.9	94.4	49.7	15.9	9.5	N/D	2.2	20.4	14.9	<0.5
Ir (ppb)	12.179	8.766	10.600	13.300	22.011	38.487	8.130	7.996	N/D	2.920	30.250	40.653	0.180
Ru (ppb)	66	32	54	90	38	183	25	11	N/D	<4.8	13	13	<2
Rh (ppb)	28.4	17.7	17.4	21.3	33.3	49.4	26.1	19.6	N/D	1.9	25.7	27.3	0.4
Pt (ppb)	205	112	114	123	691	316	197	210	N/D	428	404	341	3
Pd (ppb)	409	222	201	265	466	410	501	478	N/D	868	526	399	4
Au (ppb)	30.16	19.16	15.36	13.29	24.19	33.93	36.38	15.12	N/D	156.68	170.74	77.96	1.00
Re (ppm)	8.73	6.33	8.11	8.38	5.56	6.11	2.04	3.56	N/D	1.08	6.09	13.54	0.84
Cu (ppm)	955	685	464	490	509	505	736	1133	2199	3271	6262	6961	171
Se (ppm)	1012	673	553	546	542	782	746	1139	2497	3481	6007	6956	186
NORMALIZED TO PRIMITIVE MANTLE													
Ni (ppb)	2.2450	2.1940	2.0135	1.9240	1.3505	1.7035	0.9600	1.0365	5.9075	2.1655	1.5630	1.9985	0.0365
Os (ppm)	5.3224	3.2865	3.9603	5.2647	27.7531	14.6047	4.6765	2.7835	-	0.6412	6.0000	4.3706	
Ir (ppb)	3.5821	2.5783	3.1176	3.9118	6.4737	11.3196	2.3912	2.3518	-	0.8588	8.8971	11.9566	0.0529
Ru (ppb)	13.2000	6.3317	10.7220	18.0758	7.6980	36.5800	5.0000	2.1242	-		2.6240	2.6323	
Rh (ppb)	29.9368	18.6316	18.3053	22.3789	35.0526	52.0000	27.4737	20.6316	-	2.0000	27.0526	28.7368	0.4211
Pt (ppb)	29.3329	15.9286	16.3429	17.5571	98.6874	45.2023	28.0714	30.0613	-	61.1014	57.6571	48.7579	0.3857
Pd (ppb)	102.2500	55.5000	50.2500	66.2500	116.5000	102.5000	125.2500	119.5000	-	217.0000	131.5000	99.7500	1.0000
Au (ppb)	30.4674	19.3511	15.5163	13.4221	24.4374	34.2763	36.7455	15.2739	-	158.2667	172.4636	78.7475	1.0074
Cu (ppb)	34.1071	24.4643	16.5714	17.5000	18.1786	18.0357	26.2857	40.4643	78.5357	116.8214	223.6429	248.6071	6.1071
[Ni/Ir]n	0.6267	0.8509	0.6458	0.4918	0.2086	0.1505	0.4015	0.4407	-	2.5215	0.1757	0.1671	0.6894
[Cu/Pd]n	0.3336	0.4408	0.3298	0.2642	0.1560	0.1760	0.2099	0.3386	-	0.5383	1.7007	2.4923	6.1071

Primitive Mantle (from Barnes and Maier (1999)

Ni (ppm)	Os (ppm)	Ir (ppb)	Ru (ppb)	Rh (ppb)	Pt (ppb)	Pd (ppb)	Au (ppb)	Cu (ppm)
2000	3.4	3.4	5	0.95	7	4	0.99	28

APPENDIX IV

CALCULATION OF (F)

VALUES FOR Ni, Cu AND PGE CORRECTED FOR SELECTED SAMPLES

CALCULATION OF (F) FOR SELECTED SAMPLES

Sample	Zr (ppm)	Trapped melt (%)	S (wt%)	S Calc	Ol% in Sample Est	Ni in Olivine (Measured)	Ni in Ol (Calculated)	B1 Ni Conc	Ni (TM)	Comb Ni in Sil wt%	Ni wt%	Ni Calc	Cu (ppm)	B1 Cu Conc (ppm)	Cu (TM)	Cu Calc	Fe(s)	F
SH176UP31	29.64	38.49	0.03	0.05	15	3454.58	518.19	328	126.25	0.06	0.07	0.01	0.01	59	0.0023	0.0021	0.04	1149.08
SH176UP32	25.83	33.54	0.04	0.07	40	3394.75	1357.90	328	110.01	0.15	0.16	0.01	0.00	59	0.0020	0.0013	0.05	893.89
SH176UP33	25.57	33.21	0.03	0.05	60	2907.33	1744.40	328	108.93	0.19	0.19	0.00	0.00	59	0.0020	0.0002	0.05	1197.60
SH176UP34	19.22	24.96	0.04	0.05	70	3225.00	2257.50	328	81.88	0.23	0.25	0.02	0.00	59	0.0015	0.0007	0.04	1094.66
SH176UP35	21.98	28.55	0.02	0.04	70	3493.60	2445.52	328	93.63	0.25	0.26	0.00	0.01	59	0.0017	0.0066	0.03	1560.93
SH176UP36	24.82	32.24	0.02	0.03	70	3382.00	2367.40	328	105.74	0.25	0.26	0.01	0.00	59	0.0019	0.0017	0.02	2282.05
SH176UP37	26.09	33.88	1.06	1.62	65	2035.33	1322.97	328	111.13	0.14	0.36	0.22	0.08	59	0.0020	0.0537	1.36	36.81
SH176UP38	28.09	36.48	0.03	0.04	60	3547.75	2128.65	328	119.66	0.22	0.25	0.03	0.01	59	0.0022	0.0033	0.01	1429.70
SH176UP39	31.10	40.39	0.05	0.08	60	3582.71	2149.63	328	132.48	0.23	0.26	0.04	0.00	59	0.0024	0.0006	0.04	789.43
SH176UP40	30.14	39.14	0.07	0.10	60	3617.67	2170.60	328	128.37	0.23	0.27	0.04	0.00	59	0.0023	0.0015	0.06	596.73
SH176UP41	28.94	37.58	0.06	0.09	60	3320.67	1992.40	328	123.27	0.21	0.23	0.02	0.00	59	0.0022	0.0002	0.07	637.92
SH176UP42	28.56	37.09	0.04	0.05	65	3593.00	2335.45	328	121.66	0.25	0.25	0.00	0.00	59	0.0022	0.0013	0.05	1122.21
SH176UP43	23.65	30.71	0.02	0.03	45	3522.88	1585.29	328	100.73	0.17	0.18	0.01	0.00	59	0.0018	-0.0007	0.02	2216.33
SH176UP44	27.60	35.85	0.07	0.10	65	3452.75	2244.29	328	117.59	0.24	0.29	0.05	0.01	59	0.0021	0.0041	0.04	592.05
SH176UP45	29.10	37.80	1.08	1.64	65	3251.67	2113.58	328	123.97	0.22	0.41	0.19	0.09	59	0.0022	0.0547	1.40	36.37
SH176UP46	28.38	36.86	0.08	0.12	60	1929.67	1157.80	328	120.90	0.13	0.24	0.12	0.01	59	0.0022	0.0032	0.00	490.62
SH176UP47	20.03	26.02	0.90	1.38	65	2213.00	1438.45	328	85.33	0.15	0.52	0.37	0.06	59	0.0015	0.0379	0.97	43.40
SH176UP48	38.37	49.83	1.50	2.29	55	2292.67	1260.97	328	163.44	0.14	0.45	0.31	0.10	59	0.0029	0.0648	1.92	26.19
SH176UP49	40.14	52.13	0.43	0.65	50	2317.33	1158.67	328	170.97	0.13	0.44	0.31	0.07	59	0.0031	0.0424	0.30	91.25
SH176UP50	29.29	38.04	0.68	1.03	50	1931.50	965.75	328	124.78	0.11	0.40	0.29	0.06	59	0.0022	0.0350	0.70	57.93
SH176UP51	28.04	36.42	0.93	1.43	50	1689.50	844.75	328	119.46	0.10	0.38	0.29	0.05	59	0.0021	0.0346	1.10	42.05
SH176UP52	50.87	66.06	1.06	1.61	35	1511.42	529.00	328	216.69	0.07	0.27	0.20	0.05	59	0.0039	0.0331	1.38	37.24
SH176UP53	52.57	68.28	1.00	1.53	30	1333.33	400.00	328	223.95	0.06	0.34	0.28	0.08	59	0.0040	0.0489	1.20	39.06
SH176UP54	36.25	47.08	1.74	2.66	20	1621.50	324.30	328	154.41	0.05	0.19	0.14	0.07	59	0.0028	0.0474	2.47	22.57
SH176UP55	69.90	90.78	1.72	2.62	10	1909.67	190.97	328	297.77	0.05	0.21	0.16	0.11	59	0.0054	0.0715	2.39	22.84
SH176UP56	21.25	27.60	2.79	4.25	15	1333.33	200.00	328	90.53	0.03	1.18	1.15	0.25	59	0.0016	0.1635	2.94	14.04
SH176UP57	54.64	70.96	4.86	7.43	10	1333.33	133.33	328	232.75	0.04	0.43	0.40	0.35	59	0.0042	0.2267	6.80	8.06

VALUES FOR Ni, Cu AND PGE CORRECTED FOR SULPHIDES

Sample	Ni Sul (wt%)	Cu Sul (wt%)	Cu/Ni	Ir (sil) (ppb)	Ir (SUL)	Ru (sil) (ppb)	Ru [SUL]	Rh (sil) (ppb)	Rh (SUL)	Pt (sil) (ppb)	Pt (SUL)	Pd (sil) (ppb)	Pd (SUL)	Au (sil) (ppb)	Au [SUL]
B1 DATA				*0.35*		*3.00*		*1.40*		*17.00*		*12.00*		*3.05*	
SH176UP31	8.66	3.74	0.43	1.35	1394.38	16.14	17221.42	2.44	2181.78	20.97	16573.96	6.60	2276.39	1.97	913.77
SH176UP32	13.16	1.79	0.14	2.24	1895.40	22.86	19531.30	3.08	2333.42	13.24	6739.82			3.03	1795.01
SH176UP33	0.46	0.38	0.83	2.41	2747.02	8.01	8401.33	1.06	712.65	24.67	22778.86	4.10	137.53	1.86	1015.22
SH176UP34	18.94	1.22	0.06	9.44	10238.71	31.81	33997.05	4.90	4981.25	25.29	23036.96	6.00	3288.65	2.06	1422.93
SH176UP35	6.86	15.65	2.28	18.29	28386.96	54.53	83783.88	15.93	24241.70	115.93	173382.86	16.00	19627.60	4.69	5966.97
SH176UP36	17.82	5.77	0.32	5.66	12655.25	18.17	39251.13	1.10	1480.29	8.63	7197.85			1.55	1295.60
SH176UP37	7.95	3.00	0.38	15.07	550.45	87.20	3172.50	13.90	494.23	70.91	2398.40	120.00	4267.79	12.79	432.81
SH176UP38	38.13	7.20	0.19	1.82	2425.65	11.79	15297.28	1.40	1271.38	7.33	1618.43	4.00	-540.04	1.69	831.69
SH176UP39	28.81	0.75	0.03	5.41	4159.19	23.36	17484.41	8.30	6105.83	41.46	27308.99	69.00	50644.07	4.43	2525.43
SH176UP40	22.03	1.40	0.06	5.74	3343.19	21.97	12406.88	10.00	5640.33	163.74	93738.12	49.00	26437.18	16.48	9120.29
SH176UP41	13.17	0.16	0.01	5.28	3284.32	23.89	14519.47	6.05	3523.79	15.56	5850.45	33.00	18174.54	1.69	345.15
SH176UP42	3.02	2.19	0.72	4.36	4747.16	18.05	19007.21	7.25	7553.30	101.59	106929.43	49.00	49993.47	7.12	6714.99
SH176UP43	25.00	-2.38	-0.10	3.68	7917.87			5.33	10860.15	58.94	119059.68			5.90	11008.16
SH176UP44	31.21	3.69	0.12	3.16	1796.59	16.95	9398.51	7.93	4397.81	96.53	53539.82	79.00	44225.01	9.19	4794.95
SH176UP45	6.74	3.02	0.45	6.94	247.57	39.59	1398.48	9.39	322.23	78.83	2632.93	117.00	4089.82	19.35	661.83
SH176UP46	56.55	2.39	0.04	3.21	1511.60	15.24	6934.54	5.28	2337.30	50.40	21652.95	27.00	11076.62	3.62	1224.46
SH176UP47	15.98	2.49	0.16	18.31	790.75	106.80	4601.55	21.88	933.85	170.10	7190.88	278.00	11930.51	31.44	1330.02
SH176UP48	8.03	2.57	0.32	12.18	314.34	66.00	1689.08	28.44	726.44	205.33	5154.80	409.00	10553.18	30.16	750.02
SH176UP49	27.91	5.86	0.21	8.77	783.29	31.66	2746.17	17.70	1548.55	111.50	9365.87	222.00	19686.95	19.16	1603.08
SH176UP50	17.01	3.07	0.18	10.60	606.30	53.61	3039.31	17.39	976.49	114.40	6252.13	201.00	11378.73	15.36	822.60
SH176UP51	12.13	2.21	0.18	13.30	553.91	90.38	3754.51	21.26	872.55	122.90	4907.61	265.00	10959.53	13.29	512.05
SH176UP52	7.28	1.87	0.26	22.01	810.95	38.49	1359.38	33.30	1205.49	690.81	25304.21	466.00	17056.33	24.19	825.80
SH176UP53	10.87	2.90	0.27	38.49	1494.13	182.90	7064.93	49.40	1892.46	316.42	11907.28	410.00	15696.49	33.93	1244.25
SH176UP54	3.25	1.62	0.50	8.13	179.74	25.00	532.26	26.10	574.08	196.50	4253.50	501.00	11177.76	36.38	788.48
SH176UP55	3.62	2.48	0.68	8.00	175.37	10.62	180.37	19.60	418.63	210.43	4453.61	478.00	10668.47	15.12	282.12

PGE B1 DATA FROM DAVIES AND TREDOUX (1985)

APPENDIX V

TEXT VERSION OF BOREHOLE LOG BY R.D. HORNSEY (1999)

Category SURF_DD
Borehole SH176
Logged by R. D. Hornsey (1999)

UNIT CODE	DEPTH	DESCRIPTION
OVB	0.00 - 15.05	----- OVERBURDEN; fragments of weathered shale. Timeball Hill Formation
OVB	25.29 - 25.51	----- SHEAR ZONE; sheared; silicified; fine-grained; light brown; non-susceptible; pervasive alteration, minor shearing. Timeball Hill Formation
OVB	27.17 - 27.56	----- SHEAR ZONE; sheared; silicified; fine-grained; light brown; non-susceptible; pervasive alteration. Timeball Hill Formation
OVB	29.94 - 30.25	----- SHALE; veined; silicified; fine-grained; light brown; non-susceptible; Leached. Timeball Hill Formation
OVB	30.81 - 31.25	----- FRACTURED ZONE; fractured; silicified; pegmatitic; dark grey white; non-susceptible; hard; angular shale fragments in vuggy quartz. Some haematitic zones. Timeball Hill Formation
OVB	33.51 - 33.55	----- QUARTZ VEIN; pegmatitic; light grey; non-susceptible; hard; vuggy; milky quartz. Altered shale halo. Uitkomst Suite.
OVB	46.70 - 46.49	----- DIABASE; homogeneous; medium-grained; dark grey white; non-susceptible; hard; sill, decomposed at contacts. Uitkomst Suite
OVB	51.64 - 53.17	----- DIABASE; homogeneous; medium-grained; dark grey white; non-susceptible; hard; sill, decomposed at contacts. Uitkomst Suite
OVB	95.08 - 107.46	----- DIABASE; homogeneous; medium-grained; dark grey white; non-susceptible; hard; chilled margins, occassional. taxitic zones. Sill. Uitkomst Suite
OVB	107.46 - 112.97	----- HORNFELS; homogeneous; metamorphosed; fine-grained; dark grey; susceptible; 1-5% sulphides; pyrrhotite - disseminated - clusters - stringers; hard; bedding parallel to mineralization, with occassional. Cross-cutting veinlets. Timeball Hill
OVB	112.97 - 120.14	----- DIABASE; homogeneous; fine-grained; dark grey; non-susceptible; hard; sill. Uitkomst Suite
OVB	120.14 - 134.15	----- HORNFELS; homogeneous; metamorphosed; fine-grained; dark grey; susceptible; <1% sulphides; pyrrhotite - disseminated - clusters - stringers; hard; rare palimpsest sedimentary structures. Timeball Hill Formation.
TOP CHILL	134.15 - 136.65	----- GABBRO; homogeneous; aphanitic; dark grey; non-susceptible; hard; chilled margin to Uitkomst Complex. Amygdaloidal, magmatic deformation features.
TOP CHILL	136.65 - 144.30	----- GABBRO; homogeneous; aphanitic; dark grey; non-susceptible; hard; quenched zone, acicular pyroxene crystals to top, euhedral plagioclase laths lower down. Uitkomst Suite.
UGAB	144.30 - 149.51	----- DIABASE; homogeneous; medium grained; dark grey white; non-susceptible; hard; sill? Chilled margins, similar looking to gabbroic host rock. Uitkomst Suite
UGAB	149.51 - 154.00	----- GABBRO; homogeneous; medium-grained; dark grey white; non-susceptible; hard; euhedral plagioclase laths in fine grained pyroxene matrix. Uitkomst Suite.
UGAB	153.04 - 153.27	----- DOLERITE; homogeneous; aphanitic; dark grey; non-susceptible; hard; dyke? Contains gabbroic xenoliths. Uitkomst Suite.
UGAB	154.00 - 170.91	----- GABBRO; homogeneous; medium-grained; dark grey white; non-susceptible; hard; euhedral plagioclase laths, taxitic, occassional finer grained quench zones. Uitkomst Suite.
UGAB	164.40 - 164.45	----- QUARTZ CARBONATE VEIN; pegmatitic; light grey; non-susceptible; hard; quartz/dolmomite vein, with alteration halo. Uitkomst Suite.
UGAB	170.91 - 180.87	----- PYROXENITE; homogeneous; fine-grained; dark grey; non-susceptible; hard, pyroxenitic zone. Uitkomst Suite
UGAB	180.87 - 207.80	----- GABBRO; medium grained; dark grey white; non-susceptible; hard; pyroxenitic. Uitkomst Suite
UGAB	207.80 - 213.23	----- GABBRO; medium grained; dark grey white; non-susceptible; hard; contact zone with magmatic breccation and cross-cutting diorite veins. Uitkomst Suite
UGAB	123.23 - 234.60	----- NORITE; homogenous; medium grained; light grey; non-susceptible; hard; diorite, with pegmatitic zones. Intrusive into gabbroic roof chill zone. Uitkomst Suite.
GN	248.93 - 251.09	----- NORITE; layered; medium-grained; speckled grey; non-susceptible; hard; Diorite, minor coarse-grained pegmatitic zones. Uitkomst Suite.
GN	253.74 - 253.86	----- PEGMATITE; coarse-grained; light grey; non-susceptible; hard; quartz/feldspar pegmatite vein. Uitkomst Suite.

UNIT CODE	DEPTH	DESCRIPTION
GN	254.36 - 255.27	NORITE; layered; medium-grained; speckled grey; non-susceptible; hard; diorite, minor pyroxene in quartz/feldspar matrix. Uitkomst Suite.
GN	234.60 - 280.10	NORITE; layered, fine-grained; dark grey white; non-susceptible; hard; Acicular pxt, minor quartz. occassional pegmatitic zones with granophyric texture. Uitkomst
GN	280.10 - 294.71	NORITE; medium-grained; speckled grey; non-susceptible; hard; taxitic diorite with anherdal amphibole - alteration pyroxene in quartz/feldspar matrix. Pegmatite zones at base. Uitkomst Suite.
GN	294.71 - 294.80	PYROXENITE; homogeneous; fine-grained; grey green; non-susceptible; hard, melanorite/feldspathic pyroxenite. Uitkomst Suite
GN	294.80 - 295.41	PEGMATITE; pegmatitic; light grey; non-susceptible; hard; quartz/feldspar pegmatite with patchy rounded pyoxenitic aggregations. Uitkomst Suite.
GN	295.41 - 305.98	PYROXENITE; layered; medium-grained; grey green; non-susceptible; hard, melanorite, slightly sheared, minor thin granophyric layers. Uitkomst Suite
GN	305.98 - 308.25	NORITE; medium-grained; light green grey; non-susceptible; hard; diorite, granophyric texture in some zones, anhedral amphibole-alt pyroxene. Uitkomst
GN	317.54 - 317.66	PEGMATITE; pegmatitic; dark grey white; non-susceptible; hard; Granophyric texture. Uitkomst Suite.
GN	318.01 - 318.17	PEGMATITE; pegmatitic; dark grey white; non-susceptible; hard; irregular body, granophyric texture. Uitkomst Suite.
GN	308.25 - 343.97	NORITE; homogenous; medium-grained; grey green; non-susceptible hard; Gabbronorite, magnetite, orthopyroxene, fine-grained clinopyroxene. occassional melanocratic zones. Uitkomst Suite.
GN	325.95 - 326.41	NORITE; layered; fine-grained; dark grey white; non-susceptible; hard; Streaky interlayers of melanorite and granophyric textured diorite. Uitkomst Suite.
GN	333.79 - 333.87	QUARTZ CARBONATE VEIN; fine-grained; light grey; non-susceptible; hard; with sheared contacts. Uitkomst Suite.
GN	343.97 - 344.63	ANORTHOSITE; layered; fine-grained; light grey; non-susceptible; hard; streaky pyroxene layering. Uitkomst Suite.
GN	344.63 - 347.51	DIABASE; homogeneous; fine-grained; dark grey white; non-susceptible; hard; chilled top and bottom contacts steep top contact 30deg. (sill). Uitkomst Suite
GN	347.48 - 347.51	DOLERITE; homogeneous; aphanitic; dark grey; non-susceptible; hard; sill. Uitkomst Suite.
GN	347.90 - 347.92	DOLERITE; homogeneous; aphanitic; dark grey; non-susceptible; hard; sill. Uitkomst Suite.
GN	349.67 - 352.54	DIABASE; homogenous; fine-grained; dark grey white; non-susceptible; hard; chilled top and bottom contacts (sill). Uitkomst Suite.
GN	353.13 - 356.47	DIABASE; homogenous; fine-grained; dark grey white; non-susceptible; hard; sill with chilled contacts and phenocrysts. Uitkomst Suite.
GN	347.12 - 375.31	NORITE; layered; medium-grained; dark grey white; non-susceptible; hard; minor shearing with layered leuco norite. Uitkomst Suite.
GN	375.31 - 376.35	PYROXENITE; homogeneous; fine-grained; brown; non-susceptible; hard, pyroxenitic layer. Uitkomst Suite
GN	376.35 - 387.00	NORITE; homogeneous; medium-grained; dark grey white; non-susceptible; <1% sulphides; pyrite - cluster; hard; taxitic gabbronorite with some leuco norite layers. Uitkomst Suite.
GN	387.00 - 398.30	NORITE; layered; medium-grained; dark grey white; non-susceptible; <1% sulphides; pyrite - clusters; hard; taxitic; with numerous leuco layers and zones of magnetite. Uitkomst Suite.
GN	393.50 - 393.84	ANORTHOSITE; layered; fine-grained; yellowish grey; weakly susceptible; hard; streaky pyroxene in yellowish anorthosite. Uitkomst Suite.
GN	394.36 - 395.20	ANORTHOSITE; layered; fine-grained; yellowish grey; weakly susceptible; hard; streaky pyroxene with less anorthosite. Uitkomst Suite.
GN	398.30 - 398.92	ANORTHOSITE; layered; fine-grained; light grey; non-susceptible; hard; leuco norite with layers of pyroxene. Uitkomst Suite.
GN	404.84 - 405.37	ANORTHOSITE; layered; medium-grained; dark grey white; weakly susceptible; hard; representative of a leuco layering. Uitkomst Suite.

UNIT CODE	DEPTH	DESCRIPTION
GN	398.92 - 425.63	NORITE; layered; medium-grained; brown; non-susceptible; hard; compositional layering occasionally taxitic. Uitkomst Suite.
GN	421.01 - 421.37	ANORTHOSITE; layered; medium-grained; light grey; non-susceptible; hard; some pyroxene layers. Uitkomst Suite.
GN	425.63 - 428.15	ANORTHOSITE; layered; medium-grained; white; non-susceptible; hard; more pyroxenitic towards base. Uitkomst Suite.
GN	428.15 - 440.94	NORITE; homogeneous; medium-grained; dark grey white; non-susceptible; hard; with minor anorthositic layering. Uitkomst Suite.
GN	436.86 - 436.90	ANORTHOSITE; layered; medium-grained; light grey; non-susceptible; hard. Uitkomst Suite.
GN	438.38 - 438.45	ANORTHOSITE; layered; fine-grained; light grey; non-susceptible; hard; with pyroxene accumulations. Uitkomst Suite.
GN	439.27 - 439.23	ANORTHOSITE; layered; fine-grained; light grey; non-susceptible; hard; pyroxene layering. Uitkomst Suite.
GN	441.18 - 441.35	NORITE; homogeneous; medium-grained; dark grey white; non-susceptible; hard. Uitkomst Suite.
GN	440.94 - 442.97	DOLERITE; homogeneous; fine-grained; dark green; non-susceptible; hard; sill. Uitkomst Suite.
GN	442.97 - 459.00	NORITE; layered; medium-grained; dark grey white; non-susceptible; hard; fabric 35deg. Uitkomst Suite
PXT	484.91 - 484.93	SHEAR ZONE; sheared; talc alteration; fine-grained; light grey; non-susceptible;
PXT	459.00 - 519.48	PYROXENITE; homogeneous; medium-grained; dark grey; weakly susceptible; <1 % sulphides; pyrite-disseminated; hard; minor talc alteration at shear zones. Uitkomst Suite
PXT	496.03 - 496.05	SHEAR ZONE; sheared; talc alteration; fine-grained; light grey; non-susceptible;
PXT	519.48 - 529.40	PYROXENITE; homogeneous; serpentinized; medium-grained; dark grey; susceptible; hard, with <2% feldspar (<1 mm) peridotitic. Uitkomst Suite
MHZBG	529.40 - 555.10	PERIDOTITE; homogeneous; serpentinized; medium-grained; dark grey brown; susceptible; medium; poikilitic texture. Uitkomst Suite
MHZBG	544.28 - 545.16	DIABASE; homogeneous; slightly altered; fine-grained; light grey; non-susceptible; hard; chilled top and bottom contacts (sill). Uitkomst Suite
MHZBG	555.10 - 557.16	DIABASE; homogeneous; medium-grained; dark grey; non-susceptible; hard; chilled to and bottom contacts (sill) Uitkomst Suite.
MHZBG	558.80 - 559.43	PYROXENITE; homogeneous; medium-grained; dark green grey; non-susceptible; hard. Uitkomst Suite
MHZBG	557.16 - 564.05	PERIDOTITE; homogeneous; serpentinized; fine-grained; dark grey brown; weakly susceptible; hard; with ghost poikilitic textures. Uitkomst Suite
MHZBG	564.05 - 569.61	PERIDOTITE; homogeneous; serpentinized; medium-grained; dark grey; susceptible; hard; poikilitic textures. Uitkomst Suite
MHZBG	569.61 - 569.92	CHROMITITIC PYROXENITE; homogeneous; serpentinized; fine-grained; dark grey; weakly susceptible; medium. Uitkomst Suite
MHZBG	569.92 - 592.50	PYROXENITE; homogeneous; serpentinized; fine-grained; dark grey; weakly susceptible; hard, serpentine in thin veins chromitite occasionally concentrated in zones. Uitkomst Suite
MHZBG	590.29 - 590.41	SHEAR ZONE; sheared; talc alteration; fine-grained; light grey; non-susceptible;
MHZBG	592.50 - 602.65	PERIDOTITE; homogeneous; serpentinized; medium-grained; dark grey; susceptible; hard; poikilitic texture with chromitite at 594.35m. Uitkomst Suite
MHZBG	602.65 - 602.73	CHROMITITIC PYROXENITE; layered; medium-grained; dark grey; weakly susceptible; hard. Uitkomst Suite.
MHZBG	602.73 - 603.98	PERIDOTITE; layered; serpentinized; medium-grained; dark grey; susceptible; 1-5% sulphides; pyrrhotite-disseminated - net; hard. Uitkomst Suite.
MHZBG	603.98 - 604.05	CHROMITITIC PYROXENITE; layered; fine-grained; dark grey; weakly susceptible; <1% sulphides; pyrrhotite-disseminated; hard. Uitkomst Suite.
MHZBG	604.05 - 604.21	QUARTZ CARBONATE VEIN; sheared; carbonitisation; medium-grained; white; weakly susceptible; soft; with minor serpentinite layers. Uitkomst Suite.
MHZBG	604.21 - 639.45	PERIDOTITE; homogeneous; serpentinized; medium-grained; dark grey brown; susceptible; medium; poikilitic texture and picrolite filled shear at 616.9 m. Shear fabric 30 deg. Uitkomst Suite

UNIT CODE	DEPTH	DESCRIPTION
MHZBG	639.92 - 640.47	SHEAR ZONE; sheared; carbonitisation; fine-grained; dark grey white; weakly susceptible; medium. Uitkomst Suite
MHZBG	639.45 - 641.41	PYROXENITE; homogeneous; serpentinized; fine-grained; dark green; weakly susceptible; hard. Uitkomst Suite
MHZBG	641.41 - 651.19	PERIDOTITE; homogeneous; serpentinized; medium-grained; dark grey; susceptible;<1 % sulphides; pyrite-disseminated; pyrrhotite; hard; poikilitic texture and sulphides concentrated towards base. Uitkomst Suite
MHZBG	651.19 - 652.00	SCHIST; homogeneous; talc alteration; fine-grained; black; non-susceptible; soft. Uitkomst Suite.
MHZBG	652.00 - 655.40	DIABASE; veined; slightly altered; medium grained; dark grey brown; non-susceptible; medium; chilled top and bottom contacts (sill). Uitkomst Suite.
MHZBG	655.40 - 663.19	PERIDOTITE; homogeneous; serpentinized; medium-grained; dark grey; susceptible;<1 % sulphides; pyrite-disseminated; pyrrhotite; hard; disseminated sulphides throughout. Uitkomst Suite
MHZBG	663.19 - 665.16	DIABASE; homogeneous; carbonatisation; medium-grained; green; non-susceptible; hard; chilled contacts (sill) Uitkomst Suite.
MHZBG	665.16 - 667.34	PERIDOTITE; homogeneous; serpentinized; fine-grained; dark grey; susceptible;<1 % sulphides; pyrite-disseminated; pyrrhotite; hard; poikilitic
MHZBG	667.34 - 668.74	PYROXENITE; homogeneous; fine-grained; dark grey; weakly susceptible; hard. Uitkomst Suite
MHZBG	668.74 - 669.13	PYROXENITE; veined; carbonitisation; fine-grained; dark green; weakly susceptible; hard. Uitkomst Suite
MHZBG	669.13 - 670.28	PYROXENITE; homogeneous; fine-grained; dark green; weakly susceptible; hard, minor carbonate filled veins. Uitkomst Suite
MHZBG	670.28 - 676.54	PERIDOTITE; homogeneous; serpentinized; fine-grained; dark grey; susceptible;<1 % sulphides; pyrite-disseminated; pyrrhotite; hard; poikilitic
MHZBG	676.54 - 677.22	PYROXENITE; homogeneous; serpentinized; fine-grained; dark green; weakly susceptible; hard. Uitkomst Suite
MHZBG	677.22 - 677.59	SHEAR ZONE; sheared; fine-grained; light green grey; weakly susceptible; hard; mylonitic. Uitkomst Suite
MHZBG	677.59 - 679.43	PYROXENITE; homogeneous; talc alteration; medium-grained; dark green; weakly susceptible; soft. Uitkomst Suite
MHZBG	679.43 - 679.73	SHEAR ZONE; sheared; talc alteration; fine-grained; dark grey white; weakly susceptible; soft. Uitkomst Suite
MHZBG	679.73 - 683.66	DIABASE; veined; medium-grained; brown; non-susceptible; hard; faulted contacts (sill). Uitkomst Suite.
MHZBG	683.66 - 694.04	DIABASE; veined; medium-grained; light green; non-susceptible; hard; chilled bottom contact (sill). Uitkomst Suite.
MHZBG	688.78 - 689.11	QUARTZ VEIN; veined; medium-grained; white; non-susceptible; hard. Uitkomst Suite
MHZBG	689.36 - 692.10	QUARTZ VEIN; veined; medium-grained; white; non-susceptible; hard. Uitkomst Suite
MHZBG	694.36 - 695.17	DIABASE; homogeneous; medium-grained; green; non-susceptible; hard; piece of diabase core may not be in correct position. Uitkomst Suite.
MHZBG	694.04 - 698.32	PYROXENITE; veined; talc alteration; fine-grained; grey; non-susceptible. Uitkomst Suite
MHZBG	698.32 - 689.59	QUARTZ CARBONATE VEIN; homogeneous; carbonitisation; coarse-grained; white; non-susceptible; hard. Uitkomst Suite.
MHZBG	698.59 - 703.48	DIABASE; homogeneous; carbonatisation; medium-grained; dark green; non-susceptible; minor carbonate filled veins. Uitkomst Suite.
MHZBG	703.48 - 704.25	SCHIST; homogeneous; talc alteration; fine-grained; black; non-susceptible; soft. Uitkomst Suite.
MHZBG	704.25 - 706.00	PYROXENITE; homogeneous; carbonatisation; fine-grained; dark green; weakly susceptible; hard, with occasional picrolite filled veins. Uitkomst Suite
MHZBG	706.00 - 717.20	PERIDOTITE; homogeneous; serpentinized; medium-grained; dark grey; susceptible; <1 % sulphides; pyrrhotite-disseminated; pyrite; hard. Uitkomst Suite.
MHZBG	717.20 - 721.26	PYROXENITE; homogeneous; talc alteration; medium-grained; dark grey; non-susceptible; <1 % sulphides; pyrrhotite-disseminated; soft. Uitkomst Suite

UNIT CODE	DEPTH	DESCRIPTION
MHZBG	721.26 - 721.32	MASSIVE CHROMITITE; homogeneous; fine-grained; black; non-susceptible. Uitkomst Suite
MHZBG	721.32 - 721.35	QUARTZ CARBONATE VEIN; homogeneous; fine-grained; white; non-susceptible; hard. Uitkomst Suite.
MHZBG	721.35 - 727.34	DIABASE; homogeneous; medium-grained; dark grey white; non-susceptible; hard; chilled contacts (sill) Uitkomst Suite.
MHZBG	727.34 - 727.48	SCHIST; sheared; talc alteration; fine-grained; grey; non-susceptible; soft. Uitkomst Suite.
MHZBG	727.48 - 728.80	PYROXENITE; layered; medium-grained; grey; weakly susceptible; hard. Uitkomst Suite
MHZBG	728.80 - 755.10	PERIDOTITE; homogeneous; serpentinized; medium-grained; black; susceptible; 1-5 % sulphides; pyrrhotite-disseminated; pyrite-net; hard; poikilitic texture with occasional finer grained zones. Minor picrolite. Uitkomst Suite.
MHZBG	755.10 - 757.00	SCHIST; homogeneous; talc alteration; medium-grained; dark grey; non-susceptible; soft; with remnant olivine and ghost pokilitic structures. Uitkomst Suite.
MHZBG	757.00 - 763.47	SCHIST; sheared; talc alteration; fine-grained; grey; non-susceptible; soft; minor carbonate in veins. Uitkomst Suite.
MHZBG	763.47 - 767.56	PYROXENITE; homogeneous; medium-grained; black; non-susceptible; hard. Uitkomst Suite
MHZBG	767.56 - 770.00	PYROXENITE; homogeneous; talc alteration; medium-grained; dark grey; non-susceptible; <1 % sulphides; pyrrhotite-disseminated; poikilitic texture. Uitkomst Suite
PCR	770.00 - 779.65	PERIDOTITE; homogeneous; serpentinized; medium-grained; black; susceptible; 1-5 % sulphides; pyrrhotite-disseminated; pyrite-net; hard; thin Cr seams at 777.19, 778.2, 778.51, minor picrolite filled veins and poikilitic. Uitkomst Suite.
PCR	779.65 - 787.20	DIABASE; homogeneous; carbonatisation; medium-grained; dark green; non-susceptible; hard; chilled top and bottom contacts (sill). Uitkomst Suite.
PCR	784.70 - 785.24	QUARTZ CARBONATE VEIN; veined; carbonitisation; medium-grained; white; non-susceptible; hard. Uitkomst Suite.
PCR	787.20 - 787.30	CHROMITITIC PYROXENITE; laminated; carbonitisation; fine-grained; dark grey white; non-susceptible. Uitkomst Suite
PCR	787.30 - 789.89	PERIDOTITE; homogeneous; serpentinized; fine-grained; dark grey; susceptible; 1-5 % sulphides; pyrrhotite-disseminated; pyrite-net; hard. Uitkomst Suite.
PCR	789.89 - 789.95	MASSIVE CHROMITITE; homogeneous; fine-grained; dark grey; non-susceptible; hard. Uitkomst Suite
PCR	789.85 - 816.04	PERIDOTITE; homogeneous; serpentinized; fine-grained; dark grey; susceptible; 1-5 % sulphides; pyrrhotite-disseminated; pyrite-net; hard; with occasional thin Cr seams. Uitkomst Suite.
PCR	816.04 - 816.26	DIABASE; homogeneous; medium-grained; green; non-susceptible; hard. Uitkomst Suite.
PCR	816.26 - 817.12	PYROXENITE; homogeneous; coarse-grained; dark grey; weakly susceptible; 1-5% sulphides; pyrrhotite-disseminated; hard. Uitkomst Suite
PCR	817.12 - 817.65	PYROXENITE; homogeneous; coarse-grained; light green; weakly susceptible; <1% sulphides; pyrrhotite-disseminated; hard. Uitkomst Suite
PCR	817.65 - 818.28	DOLERITE; homogeneous; fine-grained; light grey; non-susceptible; hard. Uitkomst Suite.
PCR	818.28 - 823.72	PEGMATITE; homogeneous; pegmatite; white; non-susceptible; hard; abundant feldspar. Uitkomst Suite.
PCR	823.72 - 824.10	DOLERITE; sheared; slightly altered; fine-grained; dark grey brown; non-susceptible; hard. Uitkomst Suite.
PCR	824.10 - 824.33	SHEAR ZONE; sheared; carbonitisation; fine-grained; white; non-susceptible. Uitkomst Suite.
PCR	824.65 - 824.69	SHEAR ZONE; sheared; carbonitisation; fine-grained; white; non-susceptible. Uitkomst Suite.

UNIT CODE	DEPTH	DESCRIPTION
PCR	825.78 - 825.84	SHEAR ZONE; sheared; carbonitisation; fine-grained; white; non-susceptible. Uitkomst Suite.
PCR	824.33 - 833.20	PERIDOTITE; homogeneous; serpentinized; fine-grained; dark grey; susceptible; 1-5 % sulphides; pyrrhotite-disseminated; pyrite-net; hard; with occasional thin Cr seams. Uitkomst Suite.
PCR	833.20 - 838.73	DIABASE; homogeneous; medium-grained; dark grey white; non-susceptible; <1% sulphides; pyrrhotite-blebby; hard; chilled contacts (sill) with sulphides concentrated in veins. Uitkomst Suite.
PCR	838.73 - 843.23	PERIDOTITE; homogeneous; medium-grained; dark grey brown; susceptible; <1% sulphides; pyrrhotite-blebby-disseminated; hard. Uitkomst Suite
PCR	843.23 - 847.92	DIABASE; homogeneous; medium-grained; dark grey white; non-susceptible; hard; chilled contacts (sill). Uitkomst Suite.
PCR	847.92 - 851.10	PERIDOTITE; homogeneous; serpentinized; medium-grained; dark grey brown; susceptible; 1-5 % sulphides; pyrrhotite-disseminated; hard. Uitkomst Suite.
PCR	851.10 - 851.46	CHROMITITIC PYROXENITE; homogeneous; serpentinized; medium-grained; dark grey; susceptible; <1% sulphides; pyrrhotite-disseminated; hard. Uitkomst
PCR	851.46 - 852.68	PYROXENITE; homogeneous; medium-grained; dark grey; susceptible; 1-5% sulphides; pyrrhotite-disseminated; hard. Uitkomst Suite
PCR	852.68 - 853.25	CHROMITITIC PYROXENITE; layered; fine-grained; dark grey; weakly susceptible; <1% sulphides; pyrrhotite-disseminated; pyrite; hard. Uitkomst Suite.
PCR	853.25 - 855.10	PYROXENITE; homogeneous; medium-grained; dark grey; susceptible; 1-5% sulphides; pyrrhotite-disseminated; hard. Uitkomst Suite
PCR	855.10 - 858.61	CHROMITITIC PYROXENITE; layered; medium-grained; dark grey; weakly susceptible; 1 - 5% sulphides; pyrrhotite-disseminated; pyrite-blebby; hard; minor carbonate filled veins. Uitkomst Suite.
PCR	858.61 - 859.30	CHROMITITIC PYROXENITE; homogeneous; fine-grained; dark grey brown; weakly susceptible; <1% sulphides; pyrrhotite-blebby; pyrite; hard; minor carbonate filled veins. Uitkomst Suite.
PCR	859.30 - 862.20	CHROMITITIC PYROXENITE; homogeneous; talc alteration; medium-grained; dark grey; weakly susceptible; 1-5% sulphides; pyrrhotite-blebby; pyrite-disseminated. Uitkomst Suite.
PCR	862.20 - 865.00	PYROXENITE; homogeneous; talc alteration; coarse-grained; dark grey; weakly susceptible; <1% sulphides; pyrrhotite-blebby; pyrite; hard. Uitkomst Suite
PCR	865.00 - 867.25	PYROXENITE; homogeneous; fine-grained; dark grey; non-susceptible; <1% sulphides; pyrrhotite-blebby; pyrite; hard. Uitkomst Suite
PCR	867.25 - 868.58	PYROXENITE; homogeneous; fine-grained; dark green; non-susceptible; <1% sulphides; pyrrhotite-blebby; pyrite; hard.. Uitkomst Suite
PCR	868.58 - 887.78	DIABASE; homogeneous; medium-grained; dark grey white; non-susceptible; hard; chilled contacts (sill) Uitkomst Suite
PCR	887.78 - 910.50	CHROMITITIC PYROXENITE; layered; talc alteration; medium-grained; dark grey; weakly susceptible; <1% sulphides; pyrite-blebby; pyrrhotite-disseminated; hard. Uitkomst Suite.
PCR	910.80 - 911.90	CHROMITITIC PYROXENITE; sheared; talc alteration; fine-grained; dark grey white; non-susceptible; <1% sulphides; pyrite-blebby; pyrrhotite stringer; soft. Uitkomst Suite.
PCR	910.50 - 918.00	CHROMITITIC PYROXENITE; layered; talc alteration; fine-grained; dark grey; weakly susceptible; <1% sulphides; pyrite-blebby; pyrrhotite; hard; strongly magnetic in places. Uitkomst Suite.
PCR	918.00 - 918.54	PYROXENITE; homogeneous; fine-grained; light grey; non-susceptible; hard, <1% sulphides; pyrite-blebby; pyrrhotite; hard. Uitkomst Suite
PCR	918.54 - 921.15	CHROMITITIC PYROXENITE; homogeneous; serpentinized; medium-grained; dark grey brown; susceptible; 1-5% sulphides; pyrite-blebby; pyrrhotite-disseminated; hard; minor carbonate filled veins with occasional picrolite development. Uitkomst Suite.
PCR	921.15 - 922.72	PYROXENITE; homogeneous; serpentinized; medium-grained; dark grey brown; susceptible; 1-5% sulphides; pyrite-blebby; pyrrhotite; hard, could still be classed as PCR. Uitkomst Suite

NIT CODE	DEPTH	DESCRIPTION
CR	922.72 - 926.00	PYROXENITE; homogeneous; coarse-grained; dark grey brown; susceptible; 1-5% sulphides; pyrite-blebby-pods; hard. Uitkomst Suite
CR	926.00 - 927.65	PYROXENITE; homogeneous; serpentinized; medium-grained; dark grey brown; susceptible; 1-5% sulphides; pyrite-blebby; pyrrhotite; hard, sulphides concentrated towards top of unit. Uitkomst Suite
CR	927.65 - 928.83	PYROXENITE; homogeneous; epidotised; coarse-grained; light green; weakly susceptible; <1% sulphides; pyrite-blebby; hard, xenolith. Uitkomst Suite
CR	928.83 - 932.34	PYROXENITE; homogeneous; serpentinized; medium-grained; dark green; susceptible; 1-5% sulphides; pyrite-blebby; pyrrhotite; hard, moderate picrolitic development with occasional Cr seams. Uitkomst Suite
CR	931.25 - 931.31	DOLERITE; homogeneous; fine-grained; light grey; non-susceptible; hard; sill. Uitkomst Suite.
CR	932.34 - 933.80	PYROXENITE; xenolith; slightly altered; medium-grained; light green; weakly susceptible;1-5% sulphides; pyrite-blebby; pyrrhotite; hard, dark pyroxene development towards base. Uitkomst Suite
PCR	933.80 - 934.16	PYROXENITE; homogeneous; serpentinized; medium-grained; dark grey brown; susceptible; 1-5% sulphides; pyrite-blebby-disseminated; hard, ghost poikilitic texture (peridotitic). Uitkomst Suite
PCR	934.33 - 934.39	PYROXENITE; homogeneous; serpentinized; fine-grained; dark grey brown; susceptible; <1% sulphides; pyrite-disseminated; pyrrhotite; hard. Uitkomst Suite
PCR	934.50 - 934.63	PYROXENITE; homogeneous; serpentinized; fine-grained; dark grey brown; susceptible; <1% sulphides; pyrite-disseminated; pyrrhotite; hard. Uitkomst Suite
PCR	934.16 - 937.28	QUARTZITE; xenolith; epidotisation; medium-grained; light green grey; non-susceptible; 1-5 % sulphides; pyrite-blebby; hard; with minor pyroxene zones at top. Uitkomst Suite.
PCR	937.28 - 937.52	PEGMATITE; homogeneous; epidotisation; pegmatitic; light green; non-susceptible; <1% sulphides; pyrite blebby; hard. Uitkomst Suite.
PCR	937.52 - 938.58	MASSIVE SULPHIDE; homogeneous; epidotisation; medium-grained; yellow; non-susceptible; >50 % sulphides; pyrite-massive sulphide; hard. Uitkomst Suite.
PCR	937.58 - 938.65	QUARTZITE; xenolith; epidotisation; medium-grained; light green grey; non-susecptable; 1-5 % sulphides; pyrite-blebby; hard; slightly pyroxenitic in places. Uitkomst Suite.
PCR	938.65 - 938.86	PYROXENITE; homogeneous; coarse-grained; grey green; susceptible; 25-50% sulphides; pyrrhotite-disseminated; pyrite-net; hard; coarse grained sulphides. Uitkomst Suite
PCR	938.86 - 940.05	PEGMATITE; homogeneous; epidotisation; medium-grained; light green; weakly susceptible; <1% sulphides; pyrite blebby; medium. Uitkomst Suite.
PCR	940.05 - 940.62	PYROXENITE; sheared; epidotisation; fine-grained; yellow; weakly susceptible; <1% sulphides; pyrite-disseminated. Uitkomst Suite
PCR	940.62 - 941.07	QUARTZITE; laminated; fine sand; light grey; non-susceptible; hard; bottom contact irregular. Uitkomst Suite.
PCR	941.07 - 966.80	DIABASE; homogeneous; medium-grained; dark grey white; non-susceptible; hard; chilled bottom contact with irregular top contact (sill). Uitkomst Suite
PCR	966.80 - 967.00	QUARTZITE; homogeneous; fine-grained; light grey; non-susceptible; <1% sulphides; pyrite-blebby; pyrrhotite; hard. Uitkomst Suite.
PCR	967.00 - 968.00	PYROXENITE; homogeneous; epidotisation; medium-grained; grey; susceptible; 1-5 % sulphides; pyrite-blebby-disseminated; hard. Uitkomst Suite
PCR	968.00 - 969.93	SKARN; homogeneous; epidotisation; medium-grained; grey; non-susceptible; 1-5% sulphides; pyrrhotite-blebby; po. Uitkomst Complex.
PCR	969.93 - 970.36	QUARTZITE; homogeneous; carbonitisation; fine sand; light grey; non-susceptible; <1 % sulphides; pyrite-blebby; hard. Uitkomst Suite.
PCR	970.36 - 970.55	QUARTZITE; homogeneous; epidotisation; medium sand; light green; non-susceptible; 5-10%; pyrite - blebby; hard. Uitkomst Suite
PCR	970.55 - 970.95	PYROXENITE; homogeneous; serpentinized; medium-grained; dark grey brown; susceptible;25-50% sulphides; pyrrhotite-blebby; pyrite-net; hard. Uitkomst Suite
PCR	970.95 - 971.38	QUARTZITE; laminated; fine sand; light grey; non-susceptible; hard; <1 % sulphides; pyrite-disseminated; hard. Uitkomst Suite.

UNIT CODE	DEPTH	DESCRIPTION
PCR	971.38 - 971.83	PYROXENITE; homogeneous; serpentinized; fine-grained; dark grey; susceptible; 1-5% sulphides; pyrite-disseminated; pyrrhotite; hard; serpentinized towards base with quartz xenoliths in core of unit. Uitkomst Suite
PCR	971.83 - 973.35	QUARTZITE; laminated; fine sand; light grey; non-susceptible; hard; <1 % sulphides; pyrite-disseminated; hard. Uitkomst Suite.
LHZBG	973.35 - 974.13	WHERLITE; homogeneous; medium-grained; dark grey brown; susceptible; >50% sulphides; pyrrhotite-net; pyrite; hard. Uitkomst Suite.
LHZBG	974.20 - 974.26	WEHRLITE; homogeneous; medium-grained; dark grey brown; susceptible; >50% sulphides; pyrrhotite-massive sulphide -net; hard. Uitkomst Suite.
LHZBG	974.13 - 974.60	QUARTZITE; homogeneous; fine sand; light grey; non-susceptible; 1-5% sulphides; pyrrhotite-net-massive sulphide; hard; pyrrhotite rich wehrlite in core of unit. Uitkomst Suite.
LHZBG	974.60 - 975.30	WEHRLITE; homogeneous; medium-grained; dark grey brown; susceptible; 20 - 50% sulphides; pyrrhotite-net; pyrite; hard. Uitkomst Suite.
LHZBG	975.38 - 975.46	QUARTZITE; homogeneous; fine grained; light grey; non-susceptible; hard. Uitkomst Suite.
LHZBG	975.30 - 975.55	PERIDOTITE; homogeneous; fine-grained; dark grey brown; susceptible; 1-5% sulphides; pyrrhotite-blebby; pyrite - net; hard. Uitkomst Suite
LHZBG	975.55 - 975.92	PERIDOTITE; sheared; medium-grained; dark grey; susceptible; 5-10% sulphides; pyrrhotite-net; pyrite blebby; hard. Uitkomst Suite.
LHZBG	975.92 - 976.18	WEHRLITE; homogeneous; medium-grained; dark grey brown; susceptible; >50% sulphides; pyrrhotite-net; pyrite; hard. Uitkomst Suite.
LHZBG	976.18 - 976.25	QUARTZITE; fractured; metamorphosed; fine-grained; light green grey; non-susceptible; hard; chloritic veining. Uitkomst Suite.
LHZBG	976.25 - 976.41	PYROXENITE; homogeneous; serpentinized; medium-grained; dark grey;susceptible;1-5% sulphides; pyrrhotite-blebby; pyrite - net; hard. Uitkomst
LHZBG	976.41 - 977.13	WEHRLITE; serpentinized; medium-grained; dark grey brown; susceptible; 10 - 25% sulphides; pyrrhotite-net; pyrite; hard. Uitkomst Suite.
LHZBG	977.13 - 978.41	QUARTZITE; layered; metamorphosed; fine-grained; light green grey; non-susceptible; <1% sulphides; pyrite-wisps; chalcopyrite-blebby; hard; minor fractures with sulphide Veining. Uitkomst Suite.
LHZBG	978.41 - 979.37	PERIDOTITE; layered; serpentinized; medium grained; dark grey; susceptible; <1% sulphides; pyrrhotite-disseminated; pyrite; hard; quartzose to top. Uitkomst
LHZBG	979.03 - 979.11	DOLOMITE; homogeneous; metamorphosed; fine-grained; grey; non-susceptible; hard; altered siliceous dolomite. Uitkomst Suite.
LHZBG	979.37 - 980.36	PERIDOTITE; serpentinized; medium-grained; dark grey; susceptible; 1-5% sulphides; pyrrhotite-net; pyrite-clusters; taxitic, with patchy wehrlitic zones. Uitkomst Suite
LHZBG	980.36 - 987.55	PERIDOTITE; layered; serpentinized; medium-grained; dark grey; susceptible; <1% sulphides; pyrrhotite-disseminated; pyrite; hard; minor troctolitic layers. Uitkomst Suite.
LHZBG	984.82 - 984.87	PEGMATITE; pegmatitic; light grey; non-susceptible; hard; quartzose pegmatite. Uitkomst Suite.
BGAB	987.55 - 990.95	GABBRO; homogeneous; serpentinized; fine-grained; dark grey white; weakly susceptible; 1-5% sulphides; pyrrhotite-disseminated; chalcopyrite-clusters; pyrite; hard; mineralized mainly on top. Well developed basal chill. Uitkomst Suite
BGAB	990.70 - 990.80	QUARTZ VEIN; pegmatitc; white; non susceptible; hard. Uitkomst Suite
BGAB	990.95 - 992.39	SHEAR ZONE; sheared; carbonitisation; fine-grained; white; non-susceptible. Uitkomst Suite.
BGAB	992.39 - 992.67	QUARTZ VEIN; pegmatitc; white; non susceptible; hard; milky quartz. With fragments of sheared country rock. Uitkomst Suite
BGAB	992.67 - 995.83	SHEAR ZONE; sheared; carbonitisation; fine-grained; white; non-susceptible. Uitkomst Suite.
COUNTRY	995.83 - 1016.05	DIABASE; veined; amphibolitization; fine-grained; dark grey brown; non-susceptible; hard; pervasively altered. Godwan Lava flow.
COUNTRY	1016.05 - 1016.9	SHEAR ZONE; mylonitized; amphibolitization; medium-grained; grey green; non-susceptible; pervasive shear fabric. Reverse movement. Godwan Formation
COUNTRY	1016.94 - 1017.0	QUARTZITE; homogeneous; amphibolitization; fine-grained; grey-green; non-susceptible; hard; calcareous quartz. Malmani Subgroup.